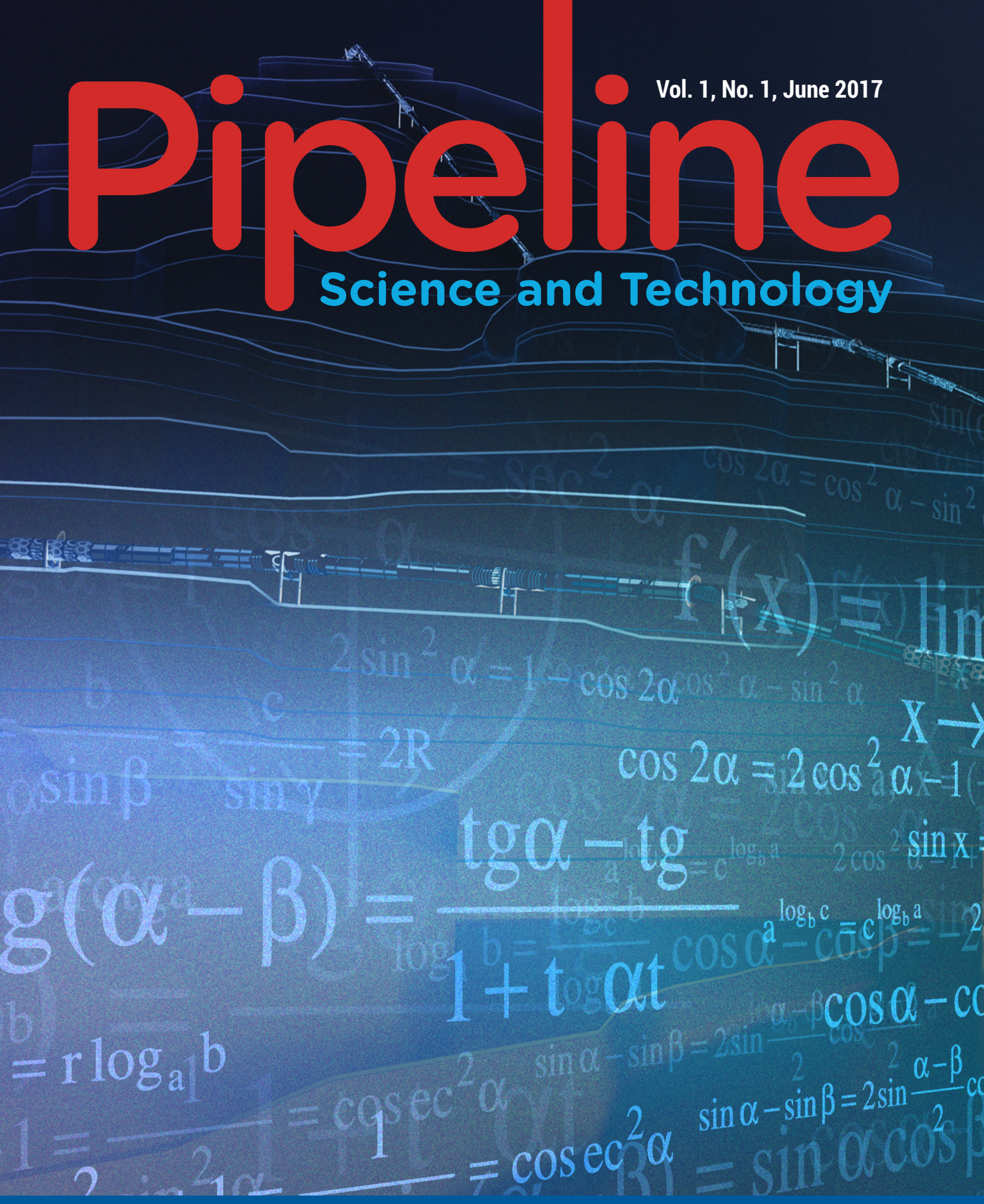

Pipeline

Science and Technology

Vol. 1, No. 1, June 2017

PIPELINE
SCIENCE AND TECHNOLOGY

published by
Pipeline Transport Institute
Technical Productions (London) Ltd
ISSN 2514-541X

Founder, Pipeline Science and Technology

Dr Yury V. Lisin, General Director, Pipeline Transport Institute, Moscow, Russian Federation

Chairman of the Editorial Board and Editor-in-Chief

Dr Anatoly E. Soschenko, Head, Department of Innovation Development and R&D, Transneft, Moscow, Russian Federation

Editorial Board Members

Dr Samer M. Adeeb, Southwest Petroleum University China, Chengdu, China
Dr Samuel Ariaratnam, Ira A. Fulton Schools of Engineering, Arizona State University, Tucson, AZ, USA
Dr Anatoly N. Dmitrievsky, Oil and Gas Research Institute, Moscow, Russian Federation
Nikolay N. Gorban, Caspian Pipeline Consortium JSC, Moscow, Russian Federation
Erik Green, Total E&P Russie, France
Dr Mohammed Hadj-Meliani, Hassiba Benbouali Unibersity, Chlef, Algeria
Dr Galina Ilieva, Shipbuilding Faculty, Technical University-Varna, Varna, Bulgaria
Cliff Jonhson, PRCI, Falls Church, VA, USA
Dr Saravanan Karuppanan, Mechanical Engineering Department, Petronas Universiti Teknologi, Malaysia
Dr Anatoly M. Korolyonok, Pipeline Network Design, Construction and Operation Faculty, Gubkin Russian State University of Oil and Gas, Moscow, Russian Federation
Dr Jyant Kumar, Indian Institute of Science, Bangalore, India
Dr Yuanhua Lin, School of Materials Science and Engineering, Southwest Petroleum University, Chengdu, China
Dr Nikolay A. Makhutov, Center for Steel and Welding, Strength Analysis, Pipeline Transport Institute, Moscow, Russian Federation
Dr Yerbol S. Makhmotov, KazTransOil JSC, Astana, Kazakhstan
Dr Yury G. Matvienko, Department of Strength, Survivability and Safety of Machines, Mechanical Engineering Research Institute, RAS, Moscow, Russian Federation
Dr Atef Mohany, Faculty of Engineering and Applied Science, University of Ontario Institute of Technology, Ontario, Canada
Dr Olga P. Molchanova, Faculty of Economics, Lomonosov Moscow State University, Moscow, Russian Federation
Dr Georgy V. Nesyn, Service for Efficiency Assessment of Hydraulic Resistance Methods, Pipeline Transport Institute, Moscow, Russian Federation
Dr Fabrizio Paolacci, University of Rome III, Rome, Italy
Dr Dimitrios G. Pavlou, University of Stavanger, Sravanger, Norway
Dr Guy Pluvinage, Polytechnic University of Tirana (Albania), Metz, France
Dr Pathmanathan Rajeev, Swinburne University of Technology, Melbourne, Vic., Australia
Berik K. Sayahov, KazTransOil JSC, Astana, Kazakhstan
Pavel Y. Serikov, Department of Economics, Transneft, Moscow, Russian Federation
Dr Sergei S. Sherbakov, Belarus State University, Minsk, Belarus
Dr Vladimir B. Sigitov, Institute of Polymeric Materials and Technologies, Almaty, Kazakhstan
Dr Leonid A. Sosnovskiy, Tribofatigue Ltd, Gomel, Belarus
Dr Lakhdar Taleb, Department of Mechanics, INSA, Rouen, France
Dr Pingbo Tang, Ira A. Fulton Schools of Engineering, Arizona State University, Tucson, AZ, USA
John Tiratsoo, Technical Productions (London) Ltd, Beaconsfield, UK
Dr Moran Wang, Multiscale Interfacial Transport, Tsinghua University, Beijing, China
Dr Shugen Xu, College of Chemical Engineering, China University of Petroleum, Qingdao, China
Dr Jie Zhang, School of Mechatronic Engineering, Southwest Petroleum University, Chengdu, China
Dr Vladimir V. Zholobov, Department of Mathematical Modelling of Oil Trunk Pipeline Operation, Pipeline Transport Institute, Moscow, Russian Federation

Pipeline Science and Technology

Volume 1, No 1, June 2017

Contents

Pipeline Science and Technology: A message of welcome from Yury V. Lisin 3

Pipeline Science and Technology: A message of welcome from John Tiratsoo 4

A comprehensive analysis of pipeline safety factors and of the basic mechanical properties of pipe steels ... 5
Y. V. Lisin, N.A. Makhutov, D.A. Neganov, and V.M. Varshitskiy

Listing of forthcoming industry events 16

Improvement of fthe ailure-assessment diagrams used to check the harmfulness of pipe defects 17
G.Pluvinage

Listing of forthcoming industry events 16, 24, 48, 64, 80

Flap pressure and arrest length considerations in propagating shear failure 25
Dr B.N. Leis and Dr A. Cosham

Design challenges of steel pipelines in unsteady flow conditions 41
Prof. D.G. Pavlou

Structural analysis of of vertical storage tanks using new approaches to determine their safe operational life 49
D.A. Neganov

A study of the impact of low ambient temperatures on weld technology and the properties of welded joints in trunk pipelines 57
N.G. Goncharov, O.I. Kolesnikov, A.A. Yushin, and O.I. Filippov

Geomechanical modelling of construction conditions for trunk pipeline underwater crossings 65
D.R. Vafin, D.A. Shatalov, and Z.Z. Sharafutdinov

Pipeline Science and Technology

Administrative information

1. Disclaimer: While every effort is made to check the accuracy of the contributions published in Pipeline Science and Technology, the publishers do not accept responsibility for the views expressed which, although made in good faith, are those of the authors alone.

2. Copyright and photocopying: © 2017 Pipeline Transport Institute, Moscow, Russian Federation, and Technical Productions (London) Ltd, Beacsonsfield, UK. All rights reserved. No part of this publication may be reproduced, stored or transmitted in any form or by any means without the prior permission in writing from the copyright holder. Authorization to photocopy items for internal and personal use is granted by the copyright holder for libraries and other users registered with their local reproduction rights organization. This consent does not extend to other kinds of copying such as copying for general distribution, for advertising and promotional purposes, for creating new collective works, or for resale. Special requests should be addressed to Pipeline Transport Institute, Moscow, Russian Federation, or to the editor.

3. Publisher: Pipeline Science and Technology is published by Pipeline Transport Institute, Moscow, Russian Federation, in association with Technical Productions (London) Ltd, Beaconsfield, UK:

Pipeline Transport Institute (PTI, LLC) , 47 A Sevastopolskiy prospekt, Moscow 117186, Russian Federation
tel: +7 (495) 950-82-95 ext.2234

Technical Productions (London) Ltd, PO Box 21, Beaconsfield HP9 1NS, UK
tel: +44 1494 675139

Editor in chief (Russian Federation): Anatoly E. Soschenko (*soschenkoae@gmail.com*)
Managing editor (Russian Federation): Valentin Komaritsa (*komaritsavn@niitnn.transneft.ru*)
Leading editorial assistant (Russian Federation): Victoria Malinina (*malininavn@niitnn.transneft.ru*)
Pruduction editor (UK): John Tiratsoo (*jtiratsoo@gs-press.com*)

4. ISSN 2514-541X

Pipeline Science and Technology

A message of welcome from

Yury V. Lisin
General Director,
Pipeline Transport Institute (PTI, LLC)

Dear Colleagues,

Sharing knowledge and experience is an extremely important aspect of the effective functioning of such a complex system as the world pipeline network, the length of which is measured in millions of kilometres.

The analysis of the current status of the pipeline science, expert assessment, and a well-informed outlook for the future – these are the goals we set ourselves when developing the idea of the new international publication titled Pipeline Science and Technology, which I am now pleased to introduce for your attention.

I sincerely hope that the new journal will help us all keep pace with the pipeline industry's exciting developments as well as providing an opportunity encourage contributions from across the industry and, in particular, broadening the horizons of young professionals.

The search for innovative solutions should not be limited to one company. I hope the journal will serve as a reliable communication platform for the entire pipeline-engineering community. Publication of papers by both Russian and invited authors from elsewhere will enable scientists to comprehensively assess problems, develop joint solutions, and consequently influence the development of new pipeline transport technologies, particularly in terms of increasing reliability and safety, as well as the efficiency, of operations.

I wish the new publication success and many years of benefit for the whole community of scientists and engineers involved with pipeline transport! Let's meet on the pages of the Pipeline Science and Technology.

Pipeline Science and Technology

A message of welcome from

John Tiratsoo
Managing Director, Technical Productions (London) Ltd

Valued Colleagues,

The introduction by the Pipeline Transport Institute of the new journal Pipeline Science and Technology is of great significance. As the world's hydrocarbons' pipelines grow older – and it is estimated that 60% of the network exceeds 40 years in age – the responsibility of the industry to maintain safety and integrity, while at the same time ensuring cost-effective and optimal operation, increases, almost exponentially. The necessity of sharing knowledge and best practices, and the requirement to codify and increase competencies, similarly increases.

We hope that Pipeline Science and Technology will provide an important opportunity for sharing the latest research and scientific analyses surrounding these pressing issues. The new quarterly journal will publish peer-reviewed papers moderated by its Editorial Board in English, so that as many as possible in the international pipeline industry will be able to benefit from its contents.

I am honoured to be part of the team that will bring Pipeline Science and Technology to its readers, and I look forward very much to implementing the aims that Dr Lisin has defined. With him, I warmly welcome the new journal to the international industry, and I sincerely hope that this new opportunity for knowledge sharing will prove successful and valued.

A comprehensive analysis of pipeline safety factors and of the basic mechanical properties of pipe steels

by Y.V. Lisin, N.A. Makhutov, D.A. Neganov, and V.M. Varshitskiy*

Pipeline Transport Institute, Moscow, Russian Federation

THIS PAPER PRESENTS an analysis of standard strength calculations for pipelines using allowable stresses and limit states, based on the quantitative determination of safety factors according to yield strength and ultimate strength and developed from decades of practice both in Russia and abroad. A new scientific background for design analysis and substantiation for safety factors is presented, quantitatively taking into account all basic operational, technological, and construction factors, including the effects of ageing, the degradation of pipe steels and pipes, and the formation and development of dangerous damage and defects (caused by corrosion and by erosion).

Key words: engineering stresses, allowable stresses, safety factor, reliability factor, strength theory, loading mode, durability, service life, ageing, crack growth resistance, survivability.

IN THE SECOND HALF of the 20th century and the beginning of the 21st, both in Russia and abroad, extensive systems were created for pipeline transport of hydrocarbons, including trunk and field oil, gas, and other products pipelines. One of the largest pipeline systems is currently in operation in Russia (Table 1) has a total length of more than 500,000 km.

For many decades, the engineering, construction and operation of pipelines was based predominantly on strength criteria [1-3]. In turn these criteria – in the form of the GOST state standard (applicable across the CIS), the OST industry standard, the SNiP construction regulations and rules, the RD guidelines, the TR technical regulations, the FNiP federal standards and rules, and the MR procedural recommendations – were based on:

- classical strength theories (1: maximum normal stresses σ_{max}; 2: maximum strain e_{max}; 3: maximum tangential stress τ_{max}, 4: maximum distortion energy V_{max});
- analysis of calculated operational nominal stresses σ_n^{op} using material strength, rod, plate and shell theories;
- the use in calculations of allowable stress $[\sigma]$ or ultimate resistance R_u;
- the basic mechanical properties of pipe steel, which determine its resistance to plastic strain, rupture, and buckling.

Currently, the conditions for pipeline strength can be expressed in a generalised form (Fig.1) by the relationship [1-4]:

$$\sigma_{n\max}^{op} = F_\sigma\left\{p, N, M_p, M_k, \delta, D, E, R_b, \mu\right\} \le [\sigma] = \frac{\sigma_{\lim}}{n_\sigma}$$

$$\sigma_{\lim} \le F_0\left\{\sigma_{\max}, \varepsilon_{\max}, \tau_{\max}, V_{\max}\right\} = \left(\sigma_y, \sigma_u, \sigma_{bck}\right) \quad (1)$$

where:

$\sigma_n^{op}{}_{max}$ is the maximum calculated nominal stress for the most

*Corresponding author's contact details:
Email: varshitskiivm@niitnn.transneft.ru

System type	Function	Length, km x 10^3
Trunk pipelines	Gas pipelines	180.2
	Oil pipelines	55.3
	Pipelines for other products including: – ammonia pipelines – ligh-fraction hydrocarbon pipelines	22.2 1.4 4.3
	Total	**257.7**
Field pipelines	General	250.0
Total		**507.7**

Table 1. Types, contents, and lengths of pipeline systems.

dangerous operational conditions (taking into account internal and external pressure p, axial force N, bending moment M_b and torsional moment M_t at a dangerous cross-section and dangerous point);

σ_{lim} is the dangerous (limit) stress, as defined by data from tensile (compression) testing of standard samples at the stages of initial yielding (with yield strength σ_y), of reaching its strength limit (with ultimate strength σ_u) or at the start of buckling (critical stress σ_{bck});

$N = N_x$, the longitudinal force along the x-axis
M_{by}, M_{bz}, bending moments about the y- and z-axes
$M_t = M_x$, the torsional moment about the x-axis
n_σ = safety factor (≥ 1)
δ = pipe wall thickness
D = pipeline diameter (external, internal, or average)
E = Young's modulus
μ = Poisson's ratio
R_b = radius of the pipeline axis bend

The engineering definition of stresses $\sigma_{n\ max}^{op}$ as the function F_s in Equn 1 is the initial independent aim of solving boundary-value problems: the analysis of nominal stress-strain states in complex operative modes of structural and operational loading at all stages in the lifecycle of pipes and pipelines.

The following parameters are used as dangerous stresses σ_{lim} in Equn 1, according to the static tensile stress-strain curve of a smooth standard sample (Fig.2) in the range $\sigma - e$ (without taking into account the reduction in cross-section area, and the increase in sample length) [4-6]:

- In the yield zone: yield strength σ_y as the ultimate resistance to elastic strain — the proportionality limit σ_{pr}, the physical yield strength σ_y at the yield plateau, the offset yield strength, which corresponds to the attainment of a given plastic strain (e.g. 0.2% — $\sigma_{0.2}$) or of a given elasto-plastic strain (e.g. 0.5% — $\sigma_{0.5}$ or 1% — $\sigma_{1.0}$);

- In the zone of limiting stresses: the strength limit — ultimate strength σ_u as the maximum engineering stress at the stage of loss of plastic strain uniformity and necking during tension.

The design plastic (e_p = 0.2%) and elasto-plastic (e = 0.5% and e = 1%) strains for modern pipe steels are substantially less than the elongation δ_f at rupture. In connection with this, for pipe steels $\sigma_{pr} \leq \sigma_y \leq \sigma_{0.2} \leq \sigma_{0.5} \leq \sigma_{1.0}$.

The insertion into the calculation by Equn 1 of stresses σ_{dan} in the form of the above-mentioned characteristics allows the mechanical properties in three dangerous limit states to be excluded:

- the beginning of yielding and the formation of plastic strains (σ_{pr}, σ_y, $\sigma_{0.2}$, $\sigma_{0.5}$, $\sigma_{1.0}$)
- rupture after reaching the ultimate strength (σ_u)
- general buckling after reaching the critical stress

This demanded the use of three safety factors n_σ:

- according to the yield strength n_y
- according to the ultimate strength n_u
- according to the critical stresses at buckling n_{bck}

Then in accordance with Equn 1, the allowable stress [σ] should be minimal:

$$[\sigma] = \min\left\{\frac{\sigma_y}{n_y}, \frac{\sigma_u, \sigma_{pr}}{n_u}\right\} \quad (2)$$

Since in the first two limit states $\sigma_y \leq \sigma_u$ for pipe steels work-hardening in the elasto-plastic range, then the factors are $n_y \leq n_u$. In the third limit state, two design cases are possible:

- $\sigma_{bck} \leq \sigma_u$, and therefore $n_{bck} \leq n_u$
- $\sigma_{bck} \leq \sigma_y$, and therefore $n_{bck} \leq n_y$

In order that calculations of pipeline strength in limit states comply with national regulations, using design resistances R_y (plastic strain development not allowed) and R_m (rupture not allowed), the allowable stresses for strength calculation in a circular direction constitute:

$$[\sigma] = \min\left\{\frac{\sigma_y m}{0.9K_f}, \frac{\sigma_u m}{nK_1K_f}\right\} \quad (3a)$$

where:

m is the service conditions factor
K_f is the functional safety factor
K_1 is the material safety factor
n is the load safety factor

The allowable stresses for calculating the stress-strain behaviour of the material in the longitudinal direction for buried pipelines are:

$$[\sigma] = \frac{\sigma_y m}{0.9K_f} \quad (3b)$$

and for above-ground pipelines:

$$[\sigma] = \frac{\sigma_y m}{K_2K_f} \quad (3c)$$

where K_2 is the material safety factor.

When calculating the strain capacity, reduced stresses are determined, as opposed to allowable stresses. Where there are compressional longitudinal stresses, the stress intensity is taken as the reduced stresses, and where there are longitudinal tensile stresses, longitudinal stresses are used.

For linear sections of buried pipeline, and sections elastically bent during construction, and where longitudinal and lateral pipeline displacement, subsidence, and soil heaving are absent, the longitudinal stresses can be determined

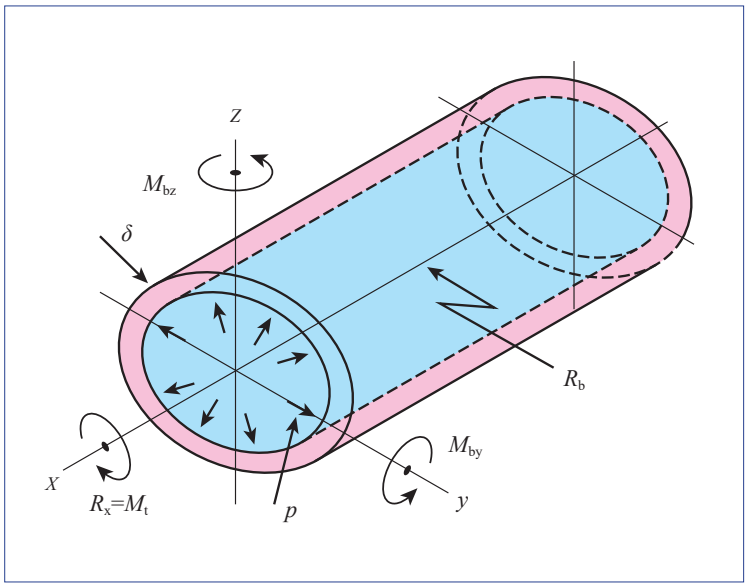

Fig.1. Pipeline loading during operation.

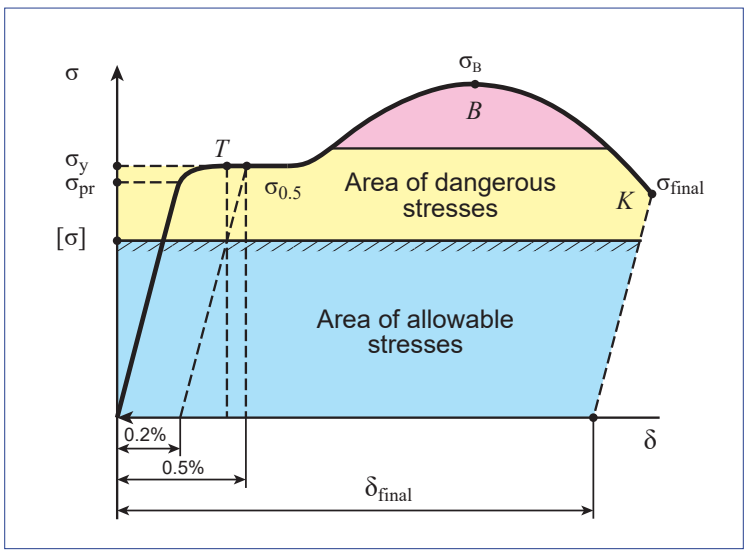

Fig.2. Static tensile stress-strain curve of a standard sample.

by taking into account elasto-plastic straining.

From Equns 2 and 3a, it follows that factors n_y and n_u for calculations of allowable stresses are linked to factors m, n, K_1, K_f in Equn 3a for calculations by the limit states:

$$n_y = \frac{0.9K_f}{m}, n_u = \frac{nK_1K_f}{m} \quad (4)$$

By definition, the safety factors n_y and n_u, and the stability factor n_t from Equns 2-4, reflect the role of uncertainities, inaccuracies, lack of knowledge, and responsibility in pipeline systems.

On the basis of strength and stability calculations using Equn 1 and with the use of Equns 2 and 3, for a pipeline with given p, N, M_b, M_t, R_u, and D, the largest wall thickness δ is selected based on the minimum ratio of yield strength σ_y and ultimate strength σ_u to n_y or n_u with the subsequent correlation of stability by σ_{fin} and n_{fin}.

Equation 2 determines the area of allowable stresses given pipeline strength calculations (Fig.1). The corresponding factor values are cited in regulations [2] (Table 2).

Trends in the improvement of calculation methods and the management of mechanical properties in pipe steels

Over the long-term period which has been examined, the predominant trends in the development of pipeline transport, both in Russia and abroad, taking into account Equns 1-4 were – and remain at present (Fig.3) – the following three tendencies [4-6]:

- the increase of pipeline diameters D (from 250-300 mm to 1200-1400 mm) and pressure p (from 20-25 atm to 140-160 atm)
- the enhancement of mechanical properties of pipe steels: yield strength σ_y (from 200-250 MPa to 600-800 MPa) and ultimate strength σ_B (from 400-450 MPa to 700-900 MPa)
- the lowering of safety factors n_y (from 1.8-3.2 to 1.2-1.5) and n_u (from 2.4-3.5 to 1.6-1.8).

During the first stages of pipeline system development (1930-1960), unalloyed carbon steels (with carbon content 0.22-0.35 %) were predominantly used with the safety factors n_y and n_u the highest of those indicated above, and with the parameters p, D, σ_y and σ_u at their lowest. In these conditions, the determining factors in calculating pipeline wall thickness δ were found to be the factors n_y and yield strength σ_y, which gave lower values of allowable stresses $[\sigma]$ according to Equns 2 and 3.

The understanding established in those years about the decisive role of increasing the yield strength σ_y in pipe steels led to metallurgists, technologists, and constructors trying by all means and methods available to reduce pipeline material consumption by increasing the yield strength σ_y (by alloying the steels, thermomechanical processing of plates and pipes while simultaneously lowering the design factor n_y). The same approach was characteristic in the development of general mechanical engineering, energy systems, the petrochemical industry, transport, and construction.

As development of these systems accelerated from the 1960s on, low-alloyed steels, low-carbon low-alloyed steels, and low-alloyed heat-treated steels were successively adopted.

This pursuit, which was not supported by the necessary scientific evidence, had by the period 1960-1970 already led to the following problems:

- substantially increased damage rate in structures such as boilers and high-pressure and high-temperature pipelines in thermal power engineering, as well as load-bearing structures in civil and industrial engineering;

- extensive brittle fractures and buckling in trunk pipelines.

A generalized analysis of the damage and ruptures at various facilities (including those working under high pressure) demonstrated that material science, engineering, and technological solutions, connected with increasing σ_y and reducing n_y, were insufficient for preventing large-scale incidents. It became clear that within the framework of established engineering practice, calculations geared towards establishing independent safety factors n_y and n_u and basic strength characteristics σ_y and σ_u were accompanied by danger to the functioning of the pipeline system.

One of the main problems was the comprehensive interconnected analysis of determining parameters of the safety margins n_s, n_y, and n_u, and the mechanical properties σ_y and σ_u in Equns 1-4. According to Equns 2 and 3, the minimum allowable stresses [σ] give a limiting quantitative correlation between these parameters:

$$n_y = n_u \{\sigma_y/\sigma_u\} \qquad (5)$$

The reduction in the values of the safety factors n_y and n_u requires taking into account the ratio σ_y/σ_u which, in accordance with Fig.1, characterizes the degree (or modulus) of pipe steel work hardening in the elasto-plastic domain beyond the yield strength σ_y. For the majority of pipe steels actually in use, the ratio σ_y/σ_u increases due to predominant growth of σ_y, while σ_y and $_u$ increase in the steels that are improved by available strengthening methods (Fig.4).

In the nomenclature and types of previously used pipe carbon steels with lowered yield strength (Figs 1 and 2) σ_y (less than 300 MPa) and the ratio σ_y/σ_u (less than 0.6), the traditional calculations for yield strength σ_y with a safety factor n_y have fundamental value. Where there is subsequent growth of yield strengths σ_y and reduction of the safety factor n_y, the calculations for ultimate strength σ_u with safety factor n_u become the determining factors in accordance with Equn 5.

Parameter	Symbol	Value
Conditions of use factor	m	Table 1 Construction Regulations and Rules 2.05.06-85*
Material resistance factor	K_1	Table 9 Construction Regulations and Rules 2.05.06-85*
Material resistance factor	K_2	Table 10 Construction Regulations and Rules 2.05.06-85*
Function reliability factor	K_f	Table 11 Construction Regulations and Rules 2.05.06-85*

Table 2. Standard design values.

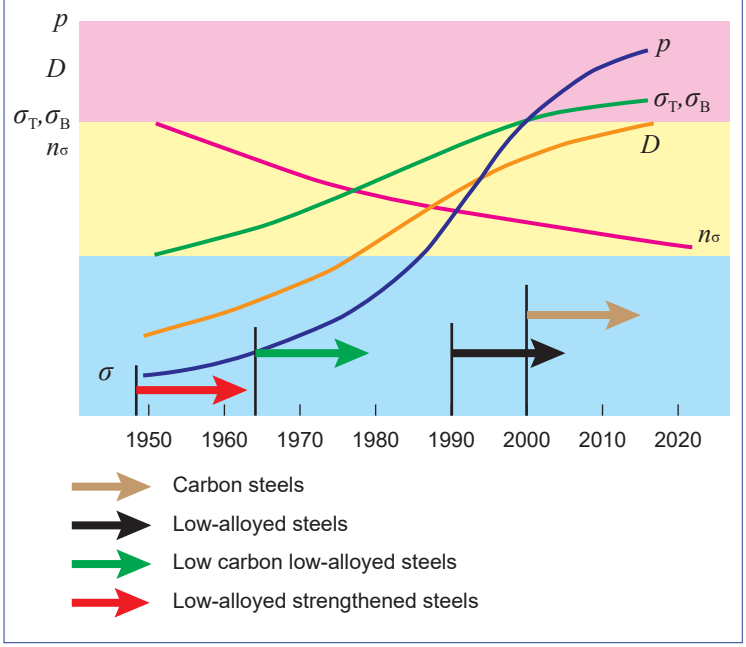

Fig. 3. Changes in pipeline design parameters.

However, in this case, the problem remains, not explicitly expressed in Equn 5, that there is an increased risk of buckling and uncontrolled dangerous transition to large plastic strains according to Equn 2, due to the decreased degree of steel work-hardening with the simultaneous increase of σ_y and σ_y/σ_u. This finding, in the context of the modern understanding of strength calculations [1, 4-7], demanded a step-by-step transition from calculations in stresses σ to calculations in strains *e*. This approach has already obtained not only scientific validation [7-9], but also practical application in the strength

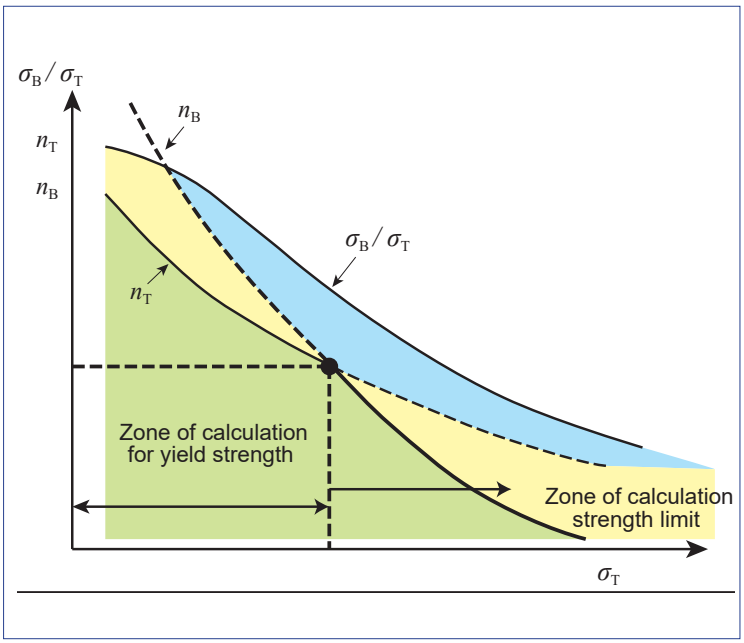

Fig.4. The link between safety factors and mechanical properties in pipe steels.

standards and codes for nuclear reactors [9-11] and space rocket systems [12].

Current problems of substantiating pipeline system strength

At present, four strategic challenges are being tackled in the Russian trunkline oil transportation system:

- the design and construction of new pipelines for the transportation of liquid and gaseous hydrocarbons (including offshore, and in the climatic conditions of Siberia and the Far North);
- the extension of active pipeline operation within the limits of modern standards' requirements for strength and durability (for service life) of pipe steels;
- the solution to issues in conducting comprehensive technical assessment and repair/rehabilitation work on pipelines damaged beyond regulatory limits for allowable defects, in order to extend their safe operation within specified time limits;
- the withdrawal from operation of facilities where specified operational time limits have been exceeded and dangerous critical and irreparable defects have occurred.

The solutions to these challenges must comply with modern requirements as set down in federal legislation for establishing and guaranteeing industrial safety according to risk criteria, and also with industrial regulations and rules for validating strength, durability, and reliability.

The challenges to establishing and guaranteeing industrial safety in pipeline systems according to strength, service life, and risk criteria, in accordance with Federal law No. 116-F3, are being resolved under the co-ordinating and defining role of Rostechnadzor (the Federal Environmental, Industrial and Nuclear Supervision Service of Russia) with the participation of:

- RAS (Russian Academy of Sciences)
- PJSC Transneft
- PJSC Gazprom
- PJSC Rosneft
- the Russian Union of Oil and Gas Builders
- leading academic institutes (IMASH, IMET, IPNG [Mechanical Engineering Research Institute; Institute of Metallurgy and Material Science; Oil and Gas Research Institute])
- leading research and industry scientific institutes and higher-education institutions (Transneft R&D, LLC, and VNIIGAZ [Scientific & Research Institute of Natural Gases and Gas Technologies – Gazprom]
- Oil and Gas Universities in Moscow, Ufa, Tyumen
- associations of expert organisations (NPS Riskom, NUTs Kachestvo, RONKTD [The Russian Society for Non-Destructive Testing and Technical Diagnostics], RNOAR [The Russian Scientific Society for Risk Analysis]).

The basic trends in scientific research

and developments in this direction are reflected in proceedings of the Industrial Safety Forums I and II [13].

Research to resolve the challenges of forming and developing industry regulations and rules for validating pipeline strength, durability, service life, and reliability is centred in the leading scientific institutes of the national pipeline transportation system – Pipeline Transport Institute and VNIIGAZ.

In industry regulations [14-16] the following assumptions are made:

- the technological inheritance of the manufacturing processes is not explicitly taken into account — including obtaining the primary metal, and making steel plates and pipes in mills and plants;
- the mechanical properties of pipe steels are assumed to be unchanging (including limits σ_y and σ_u) during pipe transportation, and pipeline construction and operation;
- both safety margins n_s in Equn 1 and safety factors n_y and n_u in Equns 2, 4, 5 are assumed to be unchanged for all stages of the pipeline's life cycle;
- degradation of pipes and pipelines is mainly as a result of the reduction of wall thickness due to corrosion (general and local) and erosion;
- most important for lowering the material consumption is the increase of nominal operational stresses $\sigma_{n\ max}^{op}$, of yield and ultimate strength limits, and decrease in safety factors n_y and n_u in accordance with Equn 1.

The standard approach by the Pipeline Transport Institute [14] has an important further development in comparison with [2, 3, 15, 16]: pipeline strength and durability are evaluated not only according to nominal stresses $\sigma_{n\ max}^{op}$, but also according to local strains e_{max}^{op} $_c$ in the stress-concentration zones which are formed during construction and operation factors (weld joints, defects, corrosion). This forms a standard calculation of pipeline strength by [14] answering both to modern strain criteria [7, 8] and to regulations applied in the nuclear energy and space rocket industries [10-12].

Basic directions of development in pipeline strength regulations

Taking into account the above, the direction of computational-experimental analysis of pipeline strength will involve a direct quantitative calculation of degradation and ageing time of pipe steels at various temperatures t and numbers of cycles N, which lead to alteration in the basic design characteristics — yield strength sσ_y and ultimate strength σ_u:

$$\left\{\sigma_\tau\left(\tau,t,\sigma,e,N\right),\sigma_y\left(\tau,t,\sigma,e,N\right)\right\} = \left\{\sigma_\tau,\sigma_y\right\}\times F_c\left\{\tau,t,\sigma,e,N\right\}$$

where: σ_y (τ, t, σ, e, N), σ_u (τ, t, σ, e, N) are kinetically changing yield and ultimate strength limits for the given time τ, temperature t, stress σ, and strain e;

F_c {τ, t, σ, e, N} are generalized functions describing the changes in basic mechanical properties under the impact of temperature, time, stress, cyclic, and strain factors at all stages of pipeline life-cycle.

The functional F_c {τ, t, σ, e, N} with parameters τ, t, σ, e, N, in fact reflects degradation and ageing processes in pipe steels during sheet and pipe production and transportation, as well as during pipeline construction, testing, and operation.

Despite the enormous quantity of research in manufacturers' laboratories, scientific institutes, design, construction, and operational organizations, and powerful industry research centres in Russia and abroad, there has as yet been no success in obtaining and substantiating this functional F_c with its corresponding parameters. Prerequisites for forming a system of initial equations for functional F_c are found in [5, 9, 12, 16, 17, 18].

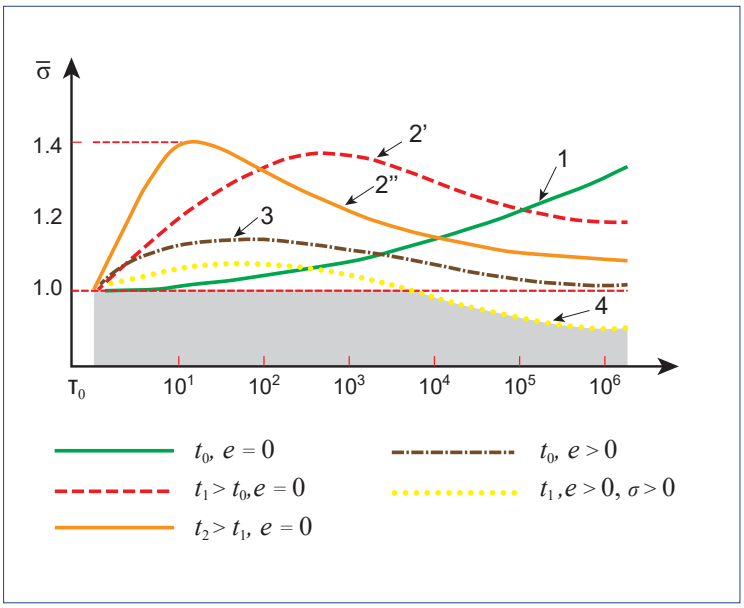

Fig.5. Pipe steel ageing processes.

The knowledge base that has been developed thus far regarding ageing and degradation processes in carbon and low-alloyed steels in time τ can be summarized with the following basic points (Fig.5):

- natural ageing (curve 1) of steels in their initial state ($e = \sigma = 0$) at room temperature t_0 is characterized by slow growth in yield strength σ_y, reaching values of 1.1-1.25 at τ of order 30-40 years; at that the ratio of yield strength σ_y (τ) to ultimate strength is reduced;`
- thermal ageing (curves 2I, 2II) of steels in their initial state ($e = \sigma = 0$) at increased temperatures t_1 and t_2 ($t_1 > t_0$; $t_2 > t_1$) leads to accelerated growth in yield strength σ_y (τ, t) at the initial stages of ageing treatment (up to 10^3 -10^4 hours) with its subsequent reduction (steel overageing);
- strain ageing (curve 3) of cold-worked steels where $e > 0$ even at room temperature t_0 gives less change in σ_y (τ, e) than natural ageing;
- dynamic ageing (curve 4) for increased temperatures in a plastic strained state ($e > 0$) under stresses ($\sigma > 0$) may initially be accompanied by insignificant growth, but will subsequently see a fall in yield strength σ_y (τ, t, e, σ) and ultimate strength σ_u (τ, t, e, σ) with a reduction in the degree of pipe steel hardening in the plastic domain.

In all types of ageing (curves 1-4), the ratio of yield strength σ_y to ultimate strength σ_u increases (owing to a lesser change in the ultimate strength σ_u in comparison with the yield strength σ_y).

In standard calculations of strength [10], areas where yield strength σ_y (τ, t, e, σ) is increased due to ageing should not be taken into account, as this goes into the safety margin. In revised and standard calculations of pipeline strength, the following points should be taken into consideration [5-10, 17-19]:

- in all ageing and degradation conditions, continuous change in values σ_y and σ_u according to Equn 6;
- the effects of degradation in mechanical properties include a decrease in relative yield strength

$$\bar{\sigma}_y = \frac{\bar{\sigma}_y}{\sigma_u}; \bar{\sigma}_y \{\tau, t, e, \sigma, N\} \le 1$$

- the reduction in plasticity (δ_{final} in Fig.2) and fracture toughness which accompanies ageing and degradation.

Based on Equns 2-5 and taking into account Figs 2-5:

$$n_y = \frac{\sigma_y(\tau, t, \sigma, e, N)}{\sigma^{op}_{n\,max}} \qquad (6)$$

$$\frac{n_y}{n_u} = \frac{\sigma_y(\tau, t, \sigma, e, N)}{\sigma_u(\tau, t, \sigma, e, N)} \qquad (7)$$

Equations 6 and 7 imply that safety factors n_y and n_u depend on pipe steel ageing and degradation processes and on time τ, temperature t, cyclic factor N and on stress-strain state ($\sigma - e$). This is not explicitly reflected in national [1-3] and foreign [12-14] regulations, and must be considered for future development of pipeline strength regulations.

In [2-6, 14, 15], the experimental analysis

was performed for the changes over time of the mechanical properties of pipe steel — first and foremost, for yield strength σ_y and ultimate strength σ_u according to tensile test results for samples machined from pipes in their initial state and after long-term operation. The time varied from $t_0 \cong 5 \times 10^{-2}$ to 3×10^5 hours; operating temperature t from -45°C to +50°C; stress σ from 0.6 s_y to 1.0 σ_y; and strain e from 0.8×10^{-3} to 3×10^{-3}.

Averaged data from these tests showed that reduction in yield strength s_y (τ, t, e, σ) over operating time from initial at t_0 to maximum at $\tau = 3 \times 10^5$ hours made up 10-15% of yield strengths s_y. The ratio of yield strength to ultimate strength also increased by 1.15-1.2. This means that the margin n_y for yield strength σ_y may be reduced by 1.1-1.17, while the margin n_u for ultimate strength σ_u may be reduced by 1.20-1.25. This corresponds to generalized experimental data from Transneft R&D, LLC, obtained by testing laboratory samples from real operational pipes.

Together with this, it is important to bear in mind that the bulk of damage to pipelines is connected with the defects on the surface layers of the pipes due to corrosion, erosion, and mechanical effects. Standard tensile testing of samples (whose surface layers are removed during preparation) does not permit an evaluation to be made of the effect this type of damage has on strength characteristics σ_y and σ_u. Other experiments are being carried out with this aim in mind. For example, cyclic bend testing on samples of full-scale thickness with non-machined surfaces showed a reduction of 15-18% in fatigue strength on the basis of $N = 10^5$-10^6 cycles [19]. This must affect the above-mentioned reduction in safety factors n_y and n_u (up to 10-15%).

One significant factor for the indicated margins n_y and n_u is the degradation of pipelines as a consequence of reduction in wall thickness δ in time τ due to corrosion and erosion, included in Equn 1 in order to determine nominal maximum operational stresses $\sigma^{op}_{max\ c}$. As laboratory experiments show, as well as observations of real metal-loss processes during operation due to these mechanisms, the rate of corrosion and erosion reduction in wall thickness $d\delta/d\tau$ can be from 0.05-0.1 to 0.3 mm/year. Where the thickness of the walls is from 10 to 30 mm, the reduction in margins can reach 10-30 %.

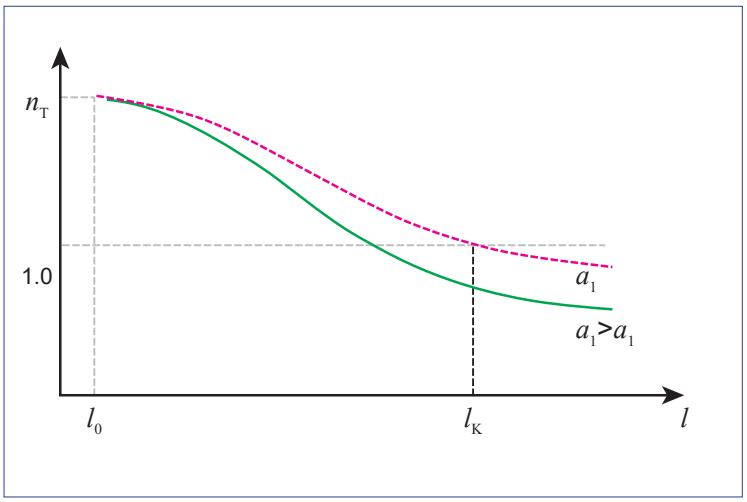

Fig.6. The impact of flaws (a type of crack) on safety factors.

Pipe steel ageing and pipe degradation during operation can thus, given an unfortunate combination of all the damaging factors indicated above, lead to a substantial reduction in margins n_y and n_u, and structural failure according to Equns 1, 6, and 7. The number of such cases in real operation [4-6, 17] in the period 1970-2015 gradually decreased from 1.2-1.0 to 0.12-0.15 fractures in 1000 km/yr.

Crack growth resistance and survivability are and will continue to be key issues in the analysis of pipeline strength, where the initiation and propagation of cracks with technological and operational origins are observed [4-7, 13, 20, 21]. In strength calculations for pipelines with cracks, depth l and length a are used in equations and criteria for linear and non-linear fracture mechanics [4-8, 13-16]. Then the local stress-strain state at the tip of the crack is determined from the solution of the boundary-value problem, using numerical methods [14] with stresses $\sigma^{op}_{max\ c}$ and strains $e^{op}_{max\ c}$ thus determined:

$$\left\{\sigma^{op}_{\max K}, e^{op}_{\max K}\right\} = \sigma^{op}_{n\max} K_{\sigma\ell} \quad (8)$$

where

σ^{op}_{max} is the maximum nominal stress according to Equn 1

$K_{\sigma\ell}$ is the effective stress concentration factor in the crack zone.

The value of $K_{\sigma\ell}$ is defined using samples with cracks:

$$K_{\sigma\ell} = F_{\ell}\left\{D, \sigma, \ell, a, S_*\right\} \quad (9)$$

where:

$F_{\ell}\left\{D, \sigma, \ell, a, S_*\right\}$ is the function of the pipe geometry (D, δ) and crack geometry (ℓ, a);

S_* is the structural parameter of the material, as determined experimentally in tests of samples with cracks.

As $\sigma^{op}_{max\ c} > \sigma^{op}_{max}$ and $F_c\left\{D, \delta, \ell, a\right\} \geq 1$ the safety factors in Equn 6 for pipes with cracks, taking into account Equn 8, will be additionally reduced (Fig.6):

$$\left\{(n_r)_{\ell}, (n_u)_{\ell}\right\} = \frac{\left\{n_y, n_u\right\}}{F_c\left\{D, \delta, \ell, S_*, a\right\}} \quad (10)$$

In strength calculation for pipelines with flaws, two basic calculated flaws sizes are introduced:

- ℓ_0 – the initial size (depth) of the flaw, as determined by accepted flaw detection (NDT) methods (taking into account their resolution and sensitivity);
- ℓ_c – the critical size (depth) of the flaw, at which the safety margin n_y (or n_u) according to Equn 9 becomes less than unity.

In calculations of ℓ_c, cracks take elliptical $\frac{\ell}{a} \approx 1/3$ or extended $\frac{\ell}{a} \to \infty$ shapes. Usually surface fractures prove to be the most dangerous.

The second, and most widespread method of evaluating pipeline strength is the evaluation of margins $(n_y)l$, $(n_u)l$ by equations and criteria of linear and non-linear fracture mechanics [4, 8, 11, 20]. In this approach, stress intensity factors are determined with the calculation for given σ^{op}_{max} as in Equn 1 and $F_{\ell}\left\{D, \sigma, \ell, a, S_*\right\}$ in Equn 8:

$$K^{op}_{l} = \sigma^{op}_{n\max}\sqrt{\pi\ell}F_c\left\{D, \delta, \ell, a\right\} \quad (11)$$

When a sample or a pipe with a crack fractures, the critical value for stress intensity factor $K1_c$ is reached at the tip of the crack, in accordance with linear fracture mechanics. Thus, in survivability calculations for pipes with cracks, by analogy with Equn 2, the introduction of a margin for stress intensity factor comes to:

$$n_{final} = \frac{K_{lc}}{K^{op}_{l}} \quad (12)$$

Using values $K1_{op}$ and $K1_c$ and Equns 8 and 12, the following equation can be obtained:

$$\left\{(n_r)_{\ell}, (n_u)_{\ell}\right\} = \left\{n_y, n_u\right\}\frac{K_{lc}}{\left\{\sigma_y, \sigma_u\right\}\sqrt{\pi\ell}F_c} \quad (13)$$

The difference in factors from Equns 10 and 13 should be insignificant.

Where plastic strains arise, rather than the stress intensity factor values $K1$ and $K1_c$, the strain intensity factor values should be used.

A generalized analysis of strength, service life, reliability, survivability, and safety for complex technical systems for civilian and defence purposes can be found in the multi-volume series *The Safety of Russia* [20].

Conclusions

Standard pipeline strength calculations using allowable stresses and limit states, grounded in decades of national and international practice, are based on the quantitative calculation of safety factors n_y for yield strength σ_y, and n_u for the

ultimate strengths σ_u. These calculations remain relevant in the present day. The safety factors n_y and n_u, which were chosen based on overall experience in engineering, constructing, and operating pipelines, tend to decrease step-by-step as working parameters increase – first and foremost, pressure *P*, diameter *D*, and wall thickness δ increased, and pipe steel yield strength σ_y and ultimate strength σ_u grew.

Based on design and experimental work with significant depth and range, carried out in academic and leading industry institutes, a new scientific foundation is being laid for the design analysis and the verification of safety margins using the system of Equns 1-13, presupposing a quantitative account of all basic operational, technological, and construction factors, including the effects of ageing, degradation of pipe steels and pipe, and the formation and development of dangerous damage and flaws (including those caused by corrosion and erosion).

In scientific research and regulation developments carried out by the Pipeline Transport Institute, and VNIIGAZ, significant experimental material has been amassed, allowing safety factors n_y and n_u to be minimized on the basis of more reliable evidence, both for functioning pipeline systems and for those under construction or at the planning stage.

References

1. S.G.Radionova, Y.V.Lisin, H.A.Makhutov, P.A.Revel-Muroz, D.A.Neganov, N.E.Zorin, Scientific, technical, socio-economic and legal aspects of reliability of oil and oil products transportation, Science and technology of oil and oil products pipeline transportation, 6, (2016), 20-31.
2. SNiP 2.05.06-85. Main Pipelines.
3. RD-23.040.00.KTN-011-16. Oil and oil products – Trunk pipeline transport. Determination of the strength and durability of pipes and welded joints with defects.
4. I.I.Mazur, O.M. Ivantsov,Safety of pipeline systems, Moscow (Russian Federation): ITs ELIMA, (2004), 1104.
5. N.N.A.Makhutov, V.N.Permyakov, *et al*. Risk analysis and ensuring of safety of critical petrochemical industry facilities. Tyumen (Russian Federation): TyuGNGU, (2013), 560.
6. Y.V.Lisin, Pipes withstand pressure: how scientific studies improve the safety of the pipeline transport, Pipeline transportation of crude oil, 8, (2015), 4-14.
7. H.A.Makhutov. Strength and safety: fundamental and applied research. Novosibirsk (Russian Federation), Science, (2008), 528.
8. H.A.Makhutov, Deformation criteria of destruction and calculation of the structures elements strength, Moscow (Russian Federation), Mashinostroenie, (1981), 272.
9. The series: Study of stresses and strength of nuclear reactors, Moscow (Russian Federation), Science, 1-9, (1987-2009).
10. Norms for strength calculation of equipment and pipelines of nuclear power installations, Moscow (Russian Federation), Energoatomizdat, 1989, 525.
11. ASME Boiler and Pressure Vessel Code, (2015), Section III.
12. H.A.Makhutov, V.S.Rachuk, M.M. Gadenin, *et al.*, Strength and resource/ service life of LRE. H.A.Makhutov V.S.Razuk, editors, Moscow (Russian Federation), Science, (2011), 525.
13. Reports on Forum: dialogue I and II – Industrial safety is the responsibility of the State, Business and Society, Moscow (Russian Federation), Rostekhnadzor, (2015–2016).
14. RD-23.040.00-KTN-011-16 Oil and oil products Trunk pipeline transport. Determination of the strength and durability of pipes and welded joints with defects.
15. Gazprom JSC. Gazprom proprietary standard 2-2.1-249-2008. Documents regulations for the design, construction and operation of Gazprom JSC facilities. Main Gas Pipelines.
16. ASME B31.4. Pipeline transportation systems for liquid hydrocarbons and other liquids.
17. A.G.Gumerov, Oil pipelines ageing, Moscow (Russian Federation), Science, (1995).
18. The problem of steel pipelines ageing and service life: reports collection, V.N.Chuvildeev, editor, N. Novgorod (Russian Federation), NNGU, (2010), 560.
19. H.A.Makhutov, The problems of destruction, resource and safety of

technical systems, V.V.Moskvicheva, M.M.Gadenin, *et al.*, editors. Krasnoyarsk (Russian Federation), Association KODAS – RPE (Research and Production Enterprise) SIBERA, (1997), 520.
20. Safety Guide. Methods of risk assessment of accidents at hazardous production facilities, oil and gas refining and petro-gas-chemical industry, Moscow, RTN. 09, (2004), 38.
21. Russia's safety. Legal, socio-economic and scientific-technical aspects, Moscow (Russian Federation), MGOF Knowledge 1-50, (1998-2015).

Listing of forthcoming industry events

22nd World Petroleum Congress
9-13 July 2017
Istanbul, Turkey
22wpc.com
The 22nd World Petroleum Congress is the most attractive and reputable oil and gas industry event of the world, attracting more than 5,000 delegates and 600 exhibitors from 100 countries.

The International Fair INNOPROM
10 -13 July 2017
Ekaterinburg, Russian Federation
www.innoprom.com/en/
Russian's leading metalworking and welding trade fair. It unites the key sectors of industry – industry automation, power engineering technologies, machine building and components for mechanical engineering, metalworking.

Oil & Gas Africa
11-13 July 2017
CTICC, Cape Town
oilgasafrica.com
Oil & Gas Africa is dedicated to developing the mid-stream and downstream sectors across the continent and features leading industry experts sharing a platform to discuss the latest challenges, market developments and opportunities.

Oil & Gas Asia
11-13 July 2017
Kuala Lumpur, Malaysia
www.oilandgas-asia.com/home/homes
Oil and Gas Asia 2017 will showcase the most up to date technology, equipment and machinery in the fields of oil, gas and petrochemical engineering.

Gas Indonesia Summit (GIS)
12-14 July 2017
Jakarta, Indonesia
www.gasindosummit.com
Gas Indonesia Summit (GIS 2017) provides the perfect platform for companies to showcase their expertise and brands to a regional and international audience in an ever changing dynamic Indonesian gas market.

continued on p24

Improvement of the failure-assessment diagrams used to check the harmfulness of pipe defects

by G.Pluvinage

Fiabilité Mécanique, Conseils, Silly sur Nied, France

IN THIS PAPER, the principle of the failure-assessment diagram (FAD) is presented including the definitions of the failure-assessment curve and the assessment point. Classical FAD allows computing a safety factor associated with defect geometry and loading conditions. Extension to a probabilistic FAD (PFAD) is used to compute the failure probability. In order to reduce the conservatism associated with the 'crack-like defect' procedure, the use of notch-failure-assessment diagram (NFAD) takes advantage of the increase of fracture toughness by reducing the defect acuity. The domain-failure-assessment diagram (DFAD) are pertinent to associate the right fracture-mechanics' tool with the failure mechanism: brittle, ductile, or plastic collapse. The fatigue-assessment diagram (fAD) use the Wöhler curve as failure-assessment curve and is used to develop a maintenance policy by determining loading conditions to guarantee a life duration with a given probability.

Key words: failure-assessment diagram, safety factor, failure probability.

Failure-assessment diagram

The failure-assessment diagram (FAD) methodology replaces the three fracture-mechanic-parameter relationship (fracture toughness, defect size, and loading) by two parameters, in order to have a plane representation where the non-dimensional crack-driving force k_r and the non -dimensional applied stress L_r are the coordinates.

The non-dimensional crack-driving force is defined as the ratio of the applied stress-intensity factor, K_{app}, to the fracture toughness of the material, K_k:

$$k_r = \frac{K_{app}}{K_{Ic}} \qquad (1)$$

An improvement was made by introducing the J-integral or crack opening displacement as:

$$k_r = \sqrt{\frac{J_{app}}{J_{mat}}} \quad or \quad k_r = \sqrt{\frac{\delta_{app}}{\delta_{mat}}} \qquad (2)$$

where J_{app} and δ_{app} are the applied J-integral and crack-opening displacement and J_{mat} and δ_c are fracture toughness in terms of critical value of the J-integral or critical crack-opening displacement of the material.

The non-dimensional stress L_r is described as the ratio of the gross stress σ_g over flow stress, chosen as yield stress σ_y, ultimate stress σ_U; or classical flow stress $\sigma_0 = \left(\sigma_y + \sigma_{ul}\right)/2$:

$$L_r = \frac{\sigma_g}{\sigma_0} \qquad (3)$$

The FAD exhibits a failure curve relating the critical non-dimensional crack-driving force $k_{r,c}$ to the critical non-dimensional stress or loading parameter $L_{r,c}$. The curve $k_{r,c} = f(L_{r,c})$ is obtained from fracture-toughness data measured from specimens tested under high levels of stress triaxiality (deep crack associated with bending). Such conditions ensure conservative conditions. The local stress distribution ahead of the crack tip is assumed to

Author's contact details:
Email: pluvinage@cegetel.net

be plane strain with high constraint. However, for real structures, defect-tip constraint is reduced by small thickness, blunt defect, or tensile loading and real fracture toughness increases.

The failure-assessment curve $k_{r,c} = f(L_{r,c})$ delineates a fracture design curve according to the available codes, including SINTAP [1], R6 [2], and RCC-MR[3].

The failure curve for the basic level of the SINTAP procedure is given by Equn 7. The fracture toughness, yield strength, and ultimate strength of the material are required for this, as shown in Equns 4 and 5 (*below*).

The assessment point of a component can be highlighted by a point of coordinates k_r^* and L_r^*. If this point is inside the boundary lines of the diagram which is limited by the failure-assessment curve curve, the structure is safe (Fig.1); if not, failure occurs, and the assessment point is situated outside of the interpolation curve.

In the FAD, the assessment point is denoted A. Due to the definition of the parameter k_r and L_r, if the crack length remains constant during loading, the loading path is linear from the origin to B. Increasing loading until failure allow the failure-assessment curve at point B to be reached. As illustrated in Fig.1, the safety factor f_s is defined by the ratio of OB over OA, i.e.:

$$f_s = \text{OB/OA} \qquad (6)$$

According to the codes safety-factor consideration, the assessment point is positioned within the acceptable zone of the FAD and the structure fulfils the required conditions for practical engineering applications.

Notch -failure-assessment diagram

The classical fracture toughness K_{Ic} is determined from the cracked specimen and plane-strain conditions. The use of pre-cracked specimens is time consuming and also costly. For some brittle materials like ceramics, it is impossible to pre-crack the specimen due to sensitivity to crack propagation. Therefore, the use of notched specimens is preferable and cheaper. However, it has been seen than the fracture toughnesses measured with this kind of specimen is generally higher than those measured with cracked specimens, and called the notch-fracture toughness $K_{(\rho,c)}$. It has been seen [4] that $K_{(\rho,c)}$) increases linearly with the square root of the notch radius ρ:

$$K_{\rho,c} = K_{Ic} + \alpha\sqrt{\rho} \ \ for\ \rho > \rho_c \qquad (7)$$
$$K_{\rho,c} = K_{Ic} \ \ for\ \rho \le \rho_c$$

ρ_c is the critical radius. Due to the sensitivity of the fracture toughness with notch radius, it is necessary – when the defect is to be assessed by the FAD method –to modify Equn 1 and replace the fracture toughness K_{IC} by $K_{(\rho,c)}$:

$$k_r = \frac{K_\rho}{K_{\rho,c}} \qquad (8)$$

K_{ro} is the notch stress-intensity factor which governs the stress distribution at the notch tip at distance greater than the distance where the maximum stress

$$k_{r,c} = \frac{1}{\sqrt{1 + L_{r,c}^2/2}} \times \left[0.3 + 0.7\exp\left(-\mu L_{r,c}^6\right)\right] \ for\ 0 \le L_r \le 1$$
$$k_{r,c} = f\left(L_r = 1\right) \times L_r^{(N-1/2N)} \ for\ 1 \le L_r \le L_{r,\max} \qquad (4)$$
$$L_{r,\max} = 0.5\left[\sigma_y + \sigma_{ul}/\sigma_{ul}\right]$$

$$\mu = \min\left\{\left(0.001E/\sigma_y\right); 0.6\right\}$$
$$N = 0.31\left(1 - \left(\sigma_y/\sigma_{ul}\right)\right) \qquad (5)$$

occurs. The L_r parameter keeps the same definition. It can be seen that the failure-assessment curve is independent of the notch radius and is the same as that of the crack. Therefore, using these assumptions, the notch-failure-assessment diagram (NFAD) can be used to assess a non-crack-like defect with radius ρ. One notes that the uses of NFAD needs to obtain the critical notch radius and the notch sensitivity for each material.

In the following, the NFAD is used to compute the safety factor associated with a gouge in a pipe made from API X-52 pipe steel submitted to internal pressure. Here we consider three types of defect in the pipe with a diameter D = 219 mm and wall thickness t = 6.1 mm. The first is central semi-spherical crack-like defect (ss) with depth d (= $t/2$); the second is a central semi-elliptical defect (se) of length L ($d = t/2$, d/L = 0.1); and the third is a central long blunt notch (ln) of notch radius ρ ($d = t/2$, d/L = 0.1, ρ = 0.15 mm). The defect direction is longitudinal, and the service pressure is equal to 70 bar. The applied notch-stress-intensity factors have been obtained from the volumetric method [6] and reported in Table 1. The stress distribution at the notch tip was computed by a finite-element method and extracted from Ref.10.

Probabilistic-failure-assessment diagram

Engineers gradually realized the insufficiencies of a safety design, and this awakening brought about the development of the concept of reliability from a probabilistic angle. According to the probabilistic approach, a structure is considered sure if its probability of failure is lower than a conventional value, a value which depends on many factors such as the expected life of the structure, the consequences generated by its ruin, the risks of obsolescence, and certain economic criteria, such as the value of replacement, maintenance costs, etc. The safety factor is then defined as the ratio of the ultimate strength, which corresponds to the mean value of the strength

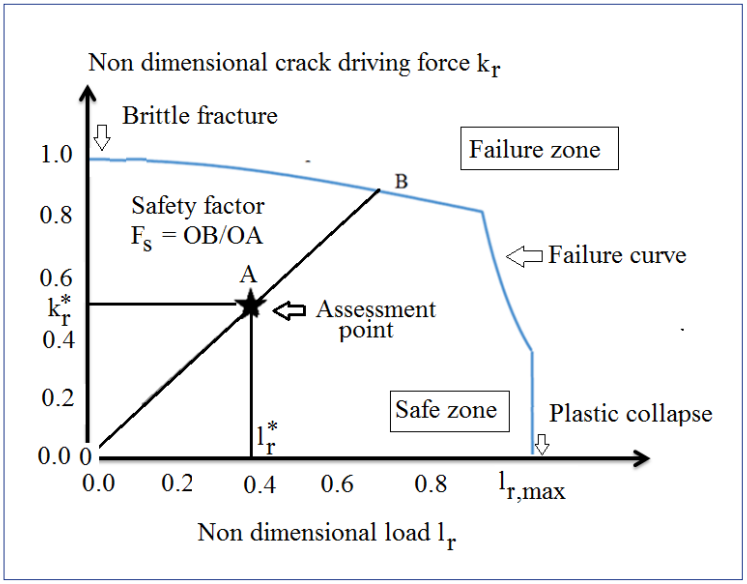

Fig.1.Typical FAD indicating safe and failure zones, and assessment point and safety factor.

distribution over the admissible stress. The admissible stress is the failure stress associated with a low and conventional probability of failure $P_{r,\,conv}$ ($P_{r,\,conv}$ =10^{-4} or 10^{-6} if there is risk to human life).

In a probabilistic approach, two iso-probability failure curves (P_r = 1 and P_r = 10^{-4} or10^{-6}) divide the FAD into three zones: the unsafe zone below the failure curve (P_r = 1); the safe zone with maintenance P^*_r >10^{-4} or 10^{-6}; and the safe zone without maintenance P_r <10^{-4} or P_r < 10^{-6}, see Fig.2. Any assessment point of the coordinates (L_r*-k_r*) is situated on an iso-probability curve P_r* and the safety factor keeps the same definition as for a deterministic FAD.

The criticality of the situation of a structure is evaluated with better accuracy by introducing the real scatter of the parameters defining the crack-extension force on the defect (load, defect size, fracture toughness). It is not based on an empirical and unique safety factor for all materials and situations, but on the

Defect type	$f_{s,T=0}$
(ss)	3.16
(se)	3.13
(ln)	3.04

Table 1. Safety factors for three types of defect (ss), (se), and (ln) at a service pressure of 70 bar.

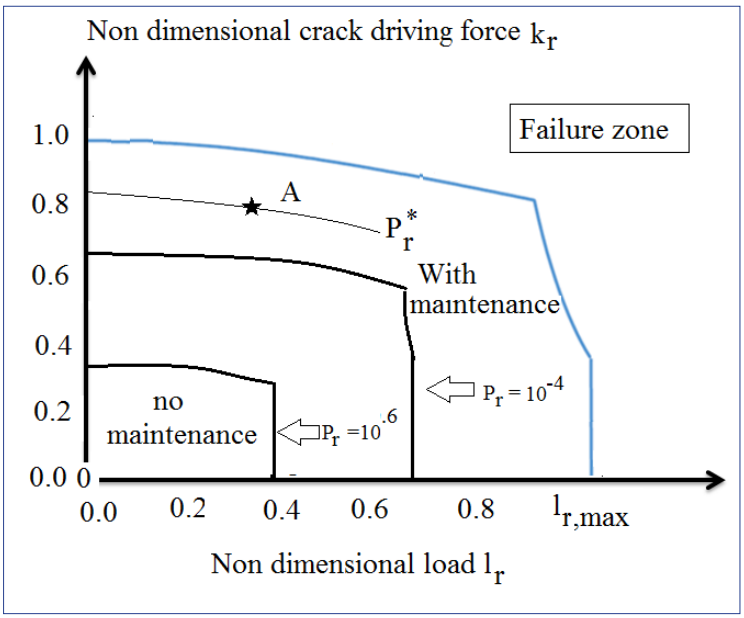

Fig.2. Typical probabilistic-failure-assessment diagram (PFAD).

acceptable risk from an economic and societal definition of the risk.

For conservative reasons, a defect which promotes pipe failure is assumed to be a semi-elliptical or semi-spherical surface crack of depth *a* and length 2*c*. For such a defect, the applied stress-intensity factor is given by the following relationship:

$$K_{app} = \frac{pR_m}{B}\sqrt{\pi a}F\left(\frac{R_i}{B};\frac{a}{B};\frac{2c}{a}\right) \quad (9)$$

where I is the internal pressure, R_m and R_i are respectively the mean internal radius, and *B* the thickness of the pipe wall; *F* is a geometry correction which is given in Ref.1.

The internal pressure in a gas pipe fluctuates continuously, and may vary depending on the rate of gas injection into the network and the service of delivery points downstream. Pipeline operators often cannot control these flows. To characterize the pressure of a gas pipeline, one must consider three factors:

- the maximum pressure applied
- the range of fluctuation of the pressure and the minimum pressure
- the rate of pressure change (change almost instantly in some cases, over several days in others).

These fluctuations are commonly expressed by the *R* ratio which is the ratio of the minimum pressure to the maximum. In this study, the *R* ratio has been given by the gas company and is equal to 4/7. The lower limit pressure is 40 bar and an upper limit pressure is about 70 bar. This ratio is kept constant when the maximum pressure fluctuates with a coefficient of variation of CV= 0.1. The fluctuations are normally distributed.

The Weibull distribution describes the scatter of fracture toughnesses, and the normal distribution describes the scatter of yield stress and ultimate strength. For conservative reason, a lower bound of the coefficient of variation has been used (CV = 0.1). A summary of the distribution, mean, and coefficient of variation, of the five parameters introduced in probabilistic fracture mechanics is given in Table 2.

Figure 3 gives the results of the failure probability given by these two methods for a given maximum pressure converted into circumferential stress $\sigma_{\theta\theta}$. Two security levels are associated: level 2 associated with a conventional failure probability

Table 2. Parameters introduced in the probabilistic fracture mechanics analysis of a gas pipe.

Parameters	Distribution	Coefficient of variation	Mean
Fracture toughness	Weibull	0.1	116 MPa/m
Yield stress	Normal	0.1	410 MPa
Ultimate strength	Normal	0.1	528 MPa
Defect size	Exponential	1	3 mm
Internal pressure	Normal	0.1	55 bar

of10^{-6} and risk to human life; and level 1 associated with a conventional failure probability 10^{-4} and no risk to human life. One note that, for the assessment point associated with a maximum service pressure of 70 bar or a circumferential stress of 125 MPa, the failure probability is less than 10^{-6} and the pipe with a surface defect is working in the security zone.

Domain-failure-assessment diagram

In FAD, the loading path is linear because the two non-dimensional parameters k_r and L_r are proportional to the applied gross stress σ_g. The angle between this loading path and the L_r axis is called the assessment angle θ. Two particular values of the assessment angle can be defined as θ_1 and θ_2: these two angles determine three failure domains in the NFAD diagram (Fig.3):

$\theta < \theta_1$	brittle fracture
$\theta_1 < \theta < \theta_2$	elastoplastic fracture
$\theta > \theta_2$	plastic collapse

Based on Federsen diagram [12] the limit of these three zones is defined conventionally as follows:

Zone I $0 < L_r < 0.62\ L_{r,y}$
Zone II $0.62\ L_{r,y} < L_r < 0.95\ L_{r,L}$
Zone III $0.95\ L_{r,max} < L_r < L_{r,max}$

where $L_{r,y}$ is associated with the yield pressure and $L_{r,max}$ is the maximum value of L_r. The values of θ_1 and θ_2 are $\theta_1 = 55°$ and $\theta_2 = 22°$.

The use of NFAD is particularly interesting for choosing the appropriate tool for assessing the risk of failure emanating from a pipe defect. Gouges and combined gouges and dents generally fail by elastoplastic fracture, but the use of limit analysis is also possible. Dents are generally assessed by limit analysis.

In the following the NFAD is coupled with a probabilistic approach in order to compute the distribution of the safety factor associated with a defect in a pipe subjected to internal pressure. The pipe exhibits a radial semi-elliptical defect with a notch angle Ψ = 0° and notch radius of ρ = 0.25 mm. The notch-stress-intensity factor was calculated by introducing the circumferential maximum stress given in Table 3 and the geometry of the defect. The value of the notch-stress-intensity factor obtained is low compared to the notch fracture toughness, and consequently we are in elastic loading conditions. For this reason, and due to the fact that the notch is sharp and the notch angle is zero, the notch-stress-intensity factor is close to the crack-stress-intensity factor. The pipe is subjected to internal pressure which delivers a hoop stress of 41.8 MPa; the

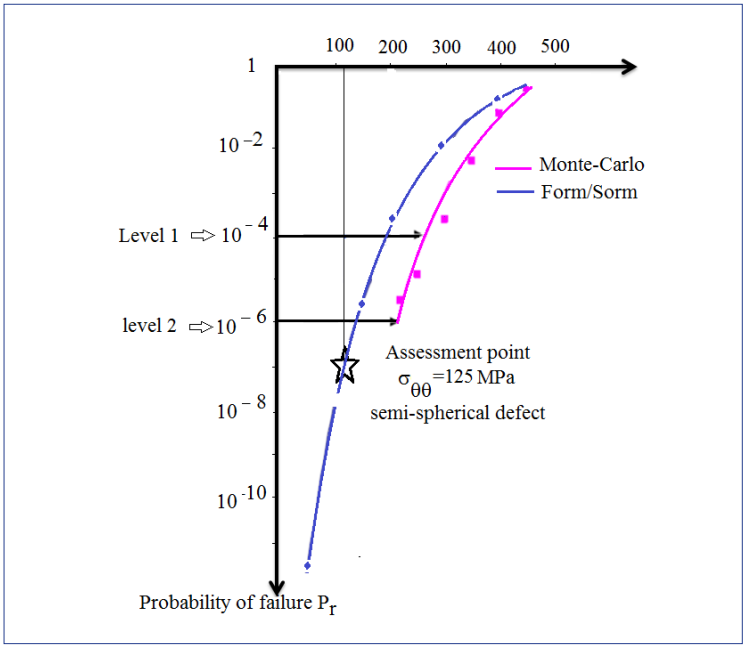

Fig.3. Evolution of the failure probability of a pipe with a semi-spherical surface defect with circumferential stress [6].

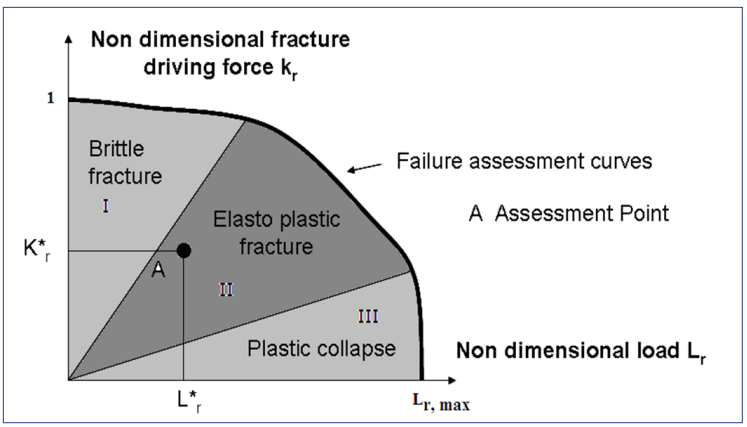

Fig.4. Domain-failure-assessment diagram with three fracture domains.

Mechanical properties	Yield strength (MPa)	Ultimate strength (MPa)	Circumferential stress (MPa)	Fracture toughness (MPa/m)	Defect
Mean	410	528	41.8	116	2 mm
CV	0.1	0.1	0.4	0.1	
σ	41	52.8	18.44	11.6	
Distribution	Normal	Normal	Normal	Weibull	Exponential

Table 3. Mechanical properties of pipe steel and distributions used.

pipe steel is API 5L X-52, and the data are presented in Table 3.

Within the chosen procedure, the following parameters are treated as random parameters and introduced into the notch-failure-assessment diagram:

- notch fracture toughness $K_{r,c}$
- yield strength R_e
- ultimate tensile strength s_{ult}
- defect depth a
- maximum pressure p_{max}

These random parameters are treated as not being correlated with one another. Fracture toughness is assumed as Weibull's distribution. Yield strength ultimate, and tensile strength and internal pressure can be mainly assumed as a normal distribution. For the defect, depth a is assumed to follow an exponential distribution. The exponential distribution generally governs the defect-size analysis.

The assessment points lie in the plastic collapse zone. Another way to define the safety factor is to consider that we have plastic collapse only for $\theta = 0$ and the defined associated safety factor f_s^*. We have examined the evolution of the safety factor with the angle θ, and it has been shown that the angle is in the range 0-7° for steel. All data are in a narrow scatter band of range $(\mu \pm 3\sigma)$ and in the region of plastic collapse. For this reason the safety factor f_s^*computed from the ultimate pressure done by code ASME B31G is also reported. The mean values and standard deviations for the safety factor of the three materials are reported in Table 4.

Table 4. Mean values and standard deviations for the safety factor of the three materials.

Mean	f_s^*	Standard deviation	Coefficient of variation
10.4	8.92	1.58	0.12

Conclusions

The FAD is a universal tool to appraise the harmfulness of a pipe defect for any kind of failure, from brittle fracture to plastic collapse. This harmfulness is analysed through the comparison of the safety factor associated with pipe geometry and service loading conditions, and a conventional safety factor. This can be done in a deterministic or a probabilistic way. In this case, the probability of failure is comparable to a conventional and admissible probability of failure.

The use of the domain-failure-assessment diagram allows choice of the best fracture-mechanics' tool according to the position of the assessment point in the domain, or the value of the assessment angle. It can be linear-elastic fracture mechanics, elasto-plastic fracture mechanics, or limit anlysis.

For non-conservative reasons, it is not necessary to treat any type of pipe defect as a crack-like defect, but with their real parameters. Therefore, the use of the notch-failure-assessment diagram introduces a supplementary reduction of the conservatism.

References

1. SINTAP: Structural Integrity Assessment Procedure, Final Report E-U project

BE95-1462 Brite Euram Programme Brussels, (1999).
2. R.P.Harrisson, I.Milne, L.Loosmore, Aassessment of the integrity of structures containing defects, Central Electricity Generating Board Report R/H R6 Revision 1 , Leatherthead, UK, (1977).
3. RCC-MRx 2015 - EN Design and Construction Rules for mechanical components of nuclear installations: high-temperature, research and fusion reactors, AFCEN, Paris (2015).
4. G.Pluvinage, Fracture and fatigue emanating from stress concentrators, Kluwer Academic Publishers, Dordretch Netherlands, (2003).
5. H.Adib-Ramezani, J.Jeong, G.Pluvinage, Structural integrity evaluation of X52 gas pipes subjected to external corrosion defects using the SINTAP procedure, Int. J. Pressure Vessels and Piping 1, (13), (2006).
6. S.Jallouf, Lj.Milović, G.Pluvinage, A.Carmasol, S.Sedmak, Determination of safety margin and reliability factor of boiler tube with surface crack, Structural Integrity and Life, 5, (3) (2005), 131–142.
7. C.E.Feddersen, Evaluation and prediction of residual strength of center cracked tension panels, ASTM STP 486, (1970) 50-62.
8. G.Pluvinage, C.Schmitt, Probabilistic approach of safety factor from failure assessment diagram. In: S.Kadry, A.El Hami A, Eds, Numerical methods for reliability and safety assessment. Multiscale and multiphysics systems, (2014), 549–577. ISBN: 978-3-319-07166-4.
9. T.W. Anderson, D.A.Darling, A test of goodness-of-fit, J. Am. Stat. Assoc, 49, (1954), 765-769.

Listing of forthcoming industry events *(continued from p16)*

International Pipeline Geotechnical Conference
25-26 July 2017
Lima, Peru
www.asme.org/events/ipg
The ASME 2017 International Pipeline Geotechnical Conference (IPG2017) is an international event to promote knowledge sharing, technological progress and international cooperation for advancing the management of natural forces impacting pipelines with the intent of protecting the public, environment, energy infrastructure assets and ensure safe and reliable operations.

ASCE Pipelines Conference
6-9 August 2017
Phoenix, AZ, USA
www.pipelinesconference.org
Premier industry event covering the most current state-of-the-art engineering technologies for pipeline and utilities infrastructure.

INDOAIM 2017 Conference & Exhibition
10-11 August 2017
Daerah Khusus Ibukota Jakarta, Indonesia
indoaim.com
INDOAIM 2017 Conference & Exhibition comes up with more engaging themes and topics focusing on the critical issues facing the global oil and gas industry via new discussion on strategies to achieve cost savings, reduce risk and extend the life of aging assets.

Pacific Oil Conference
5-7 September 2017
Los Angeles, CA, USA
www.petroshow.com
The POC is an engaging event offering multiple ways to network with others in the industry, attend valuable education sessions from business professionals and meet with vendors offering the products and services you need.

SPE Offshore Europe
5-8 September 2017
Aberdeen, UK
www.offshore-europe.co.uk
SPE Offshore Europe is recognised by offshore E&P professionals as Europe's leading E&P event.

Oil Sands Trade Show & Conference
12-13 September 2017
Fort McMurray, AB, Canada
oilsandstradeshow.com
The Oil Sands Trade Show and Conference focuses on promoting the latest technologies, innovations and business efficiencies in the areas of facility operations, maintenance, shutdown/turnarounds, mining, upgrading, health & safety, and environmental strategies.

continued on p48

Flap pressure and arrest length considerations in propagating shear failure

by Dr B.N. Leis*[1] and Dr A. Cosham[2]

1 B.N .Leis Consultant, Inc., Worthington, OH, USA

2 Ninth Planet Engineering Ltd, Newcastle upon Tyne, UK

PROPAGATING SHEAR FAILURE refers to the rapid axial growth of a split along a hydrocarbon transmission pipeline transporting a gas or a liquid with a high vapour pressure. Growth of the split continues if its speed exceeds that of the decompression front; otherwise arrest occurs, with the balance between these speeds dependent on the fluid's properties, the linepipe's size, the flow and fracture properties, and the backfill conditions.

Interest in propagating fractures was motivated by in-service failures in the 1950s and 60s. Linepipe steels of the 1960s and before offered little resistance to propagating failure which, when it occurred, ran in a brittle mode. While steels were soon developed that overcame such brittle fracture, it became clear by way of full-scale experiments simulating service conditions that a propagating failure could run in a shear mode if the steel was not sufficiently tough. Technology soon emerged to quantify the steel properties required to arrest such failures. Perhaps motivated by the observation that the early failures involved brittle fracture, initially such methods were based on fracture concepts, with alternative plastic-collapse-based concepts emerging as the limitations of fracture-based methods became evident as the toughness required for arrest increased. What is clear – regardless of which concept is proven relevant – is that the failure process is dynamic, making inertia associated with the 'flaps' that form in the wake of the split a consideration along with related issues such as the length required to affect arrest.

This paper reviews the basis for an effect of flaps weighed in the balance of phenomenology and analyses, working from Smith and Shoemaker's 1974 paper that first asserted the potential role of flaps, on through analytical and numerical work. Due to the complex non-linear interaction that develops between the soil, the pipe flow and failure resistance, and the fluid, recourse is also made to discriminating experiments – with a focus on work involving gaseous detonation. Pressure decay and its role in regard to arrest length is then addressed in light of current models used to quantify arrest. Thereafter, the results are integrated with a view to a more general formulation for arrest.

Key words: flap pressure, arrest length, propagating shear, pipeline failure, backfill conditions

PIPELINES TRANSPORTING GASES or high-vapour-pressure liquids can suffer the rapid axial growth of a split that can run a significant distance. This phenomenon became apparent first in regard to brittle fracture of a natural gas transmission pipeline [1] in which the crack ran axially a total distance of 8.3 miles during a proof-pressure test using natural gas. Had it not encountered a fitting at one end and a joint of tougher ductile pipe at the other, it would have run an even greater distance. The observation that its chance encounter with a ductile joint led to arrest gave rise to the view that long-propagating fractures were a consequence of the brittle nature of the failure. Logically, research

* Corresponding author's contact details:
Email: bleis@columbus.rr.com

This paper was first published in *The Journal of Pipeline Engineering*, December, 2016, and is reproduced here by permission.

Fig.1. Views characteristic of propagating brittle fracture: (a -left) ejected shards (note the Chevron markings); (b - right) near arrest at one end of the failure.

focused on changes to the steel's chemistry and processing to reduce the ductile-to-brittle transition temperature (DBTT) and enhance its toughness. Laboratory heats of steels representative of existing and new linepipe steels were made by systematically varying the chemical composition, the rolling temperature, the amount of hot and cold work, etc. [2]. The effects of those parametric studies were quantified in terms of mechanical properties and fracture toughness. That outcome was then cross-correlated with the results of full-scale fracture-propagation experiments [3] that involved selected mill-produced pipes, with a view to determining the factors that controlled propagating shear failure. Based on the behaviour observed for the in-service failure, wherein arrest occurred when the propagating split encountered a ductile joint of pipe, the expectation was that the propagation would rapidly arrest as it entered ductile joints of pipe, but this did not occur in that testing [4]. Rather, after further study and many tests and related analyses over a period of about 10 years, it was determined that axial propagation could continue if its speed exceeded that of the decompression front (a ductile fracture running at a speed slower than the leading edge of the decompression front, but faster than the trailing edge). Building on that observation, a simple model was formulated that became known as the Battelle two-curve model [5] (BTCM), because it quantified the balance between the speed of the fracture and the speed of the decompression front, and arrest in terms of tangency between these two curves, quantified as functions of the fluid's properties, the linepipe's size and its flow and fracture properties, and the backfill conditions.

Almost coincidental with the release of the BTCM, an alternative hypothesis emerged, in which Smith and Shoemaker [6] asserted that the "driving force for ductile-fracture propagation in a pipe is the pressure acting on the flaps behind the propagating crack tip". Subsequent work has considered the implications of this hypothesis, analytically (for example, Ref.7) and experimentally (for example, Refs 8 and 9), as well as numerically (for example, Ref.9). Work considering the role of flaps continued into the 1990s without a clear consensus on their role, where after work to quantify this aspect diminished.

This paper reviews the basis for an effect of flaps weighed in the balance of phenomenology and analyses, beginning with Smith and Shoemaker's 1974 paper that first considered the potential role of flaps, on through analytical and numerical work by Freund and others. Due to the complex non-linear interaction that develops between the soil, the pipe's flow and failure resistance, and the fluid's expansion behaviour, recourse also will be made to discriminating experiments – with a focus on both the early work at Battelle and recent work developed in the context of gaseous detonation experiments [10]. As crack propagation due to the inertial effects of flap formation under steady-state conditions implies a

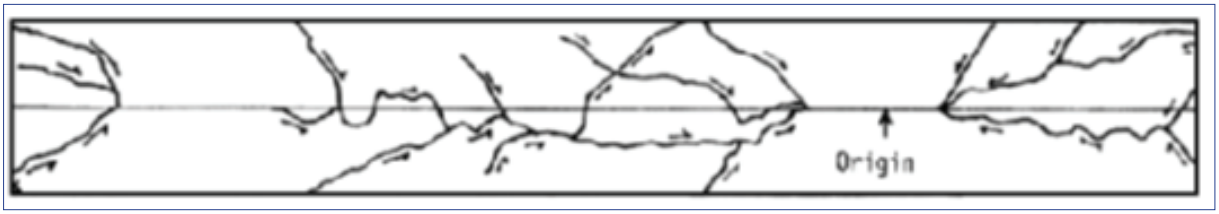

Fig.2. Portion of the image of a reconstructed brittle fracture (not that in Fig.1).

potentially self-sustaining (autocatalytic) process, pressure decay in the wake of cracking is considered in regard to arrest length, whose implications are addressed in the light of current models used to quantify arrest. Thereafter, the results are integrated with a view to a more-comprehensive formulation for arrest, if necessary.

Flap formation, flap pressure, and related inertial effects

Flap formation: contrasting running brittle fracture versus propagating shear

A propagating brittle fracture is typically associated with multiple crack paths due to the limited fracture resistance of a brittle material relative to the energy available to drive the fracture. When such fractures occur on pressurized pipelines, the many shards of pipe formed by this cracking are ejected from the ditch, except for what remains in the ground as the fracture arrests. Figure 1a is typical of the shards ejected, while the image in Fig.1b is representative of what might be found in the ground which, for this view, is approaching the arrest that occurred in a somewhat more ductile joint.

Two observations based on the images shown in Fig.1 are relevant to the role of the flaps in propagating shear. First, as little plastic deformation occurs with brittle fracture because the energy required to create new fracture surface is small, the shards of pipe retain their radial curvature, which is also the case for the pipe that remains in the ditch. Second, the stress waves associated with this failure mechanism led to a characteristic in-plane sinusoidal fracture path. This sinusoidal path, the still pipe-like shape of the shards, and the cracking direction evident from tell-tale chevrons on the fracture surface, facilitate reconstruction of such failures back from either end to locate a common origin, to assist in understanding the cause of such failures. As apparent from Fig.2, which shows the reconstructed crack paths for a portion of one such brittle fracture, such failures can involve tens to hundreds of shards (noting that the origin of the fracture was, as shown in the seam weld, and that some of the crack paths were along the seam). In cases like that shown, the many small shards produced can break-up the characteristic in-plane sinusoidal crack paths, which can complicate reconstruction.

In contrast to the images shown for the propagating brittle fracture in which the pipe-like shape is retained, the outcome for axial failure due to propagating shear is considerably different. Figure 3a, which reflects arrest at one end of a full-scale test, makes this point. While ring-off and pipe-whip might lead to the ejection of the pipe from the ditch in tests involving ductile propagation, there is but one crack. Likewise, while a sinusoidal-like path is apparent in this image, it lies out-of-plane to the pipe wall and is irregular, as it develops due to the axial plastic stretch along the crack path that reflects the large axial strain that runs with the plastic wave that forms with such failures. It is apparent in Fig.3a that the compacted soil covering over the pipe has been ejected, as it was for the brittle failure. However, because the pressure associated with this propagating shear (ductile) failure was much higher, the trench is opened much wider, which then becomes the bed against which the once-round pipe opens against. It is this opening that led to what Smith and Shoemaker first termed flaps, whose formation is illustrated schematically in Fig.3b.

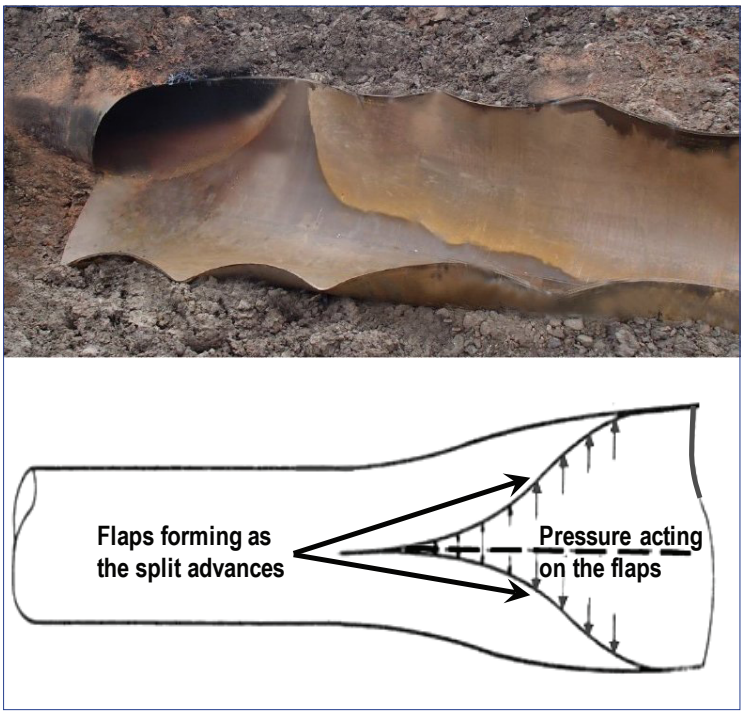

Fig.3. Views characteristic of propagating-shear failure:
(a - top) arrest of ductile shear (cleared of debris);
(b - bottom) schematic illustrating flap formation.

The tendency to form flaps is not unique to propagating-shear failures, but rather reflects the response of a pressurized cylinder (or sphere) in which the energy stored in the compressed media is rapidly released, with that split forming so rapidly that a component of that pressure remains active during its decay as it releases into the atmosphere. As noted earlier, Smith and Shoemaker [6] asserted that it was this pressure acting on the flaps in the wake of the split that was the driving force for a propagating-shear failure in a pipeline. It is appropriate therefore to consider this pressure distribution as the first step in assessing the role of flap formation, and its implications in regard to the distance required for arrest.

Flap pressure in the vicinity of the breach

For an axial split in a pipeline propagating under steady-state conditions the outflow likewise achieves a steady state, which in general depends on the properties of the fluid and the shape of the breach. The pressure field within the propagating breach, which in general varies in three dimensions (3D), reflects the transition from the spatially invariant state within the pipeline well ahead of the breach, and the ambient state developed well beyond the choke point. Measurements of this pressure field adjacent to the pipe wall best quantify the forces acting normal to the flaps, which for the present are based on work by Maxey [8] and by CSM [9], results for which from the latter are shown in Fig.4.

Figure 4 presents the spatial pressure normalized relative to the pressure at the split, which is shown as a function of position downstream of the split where that distance is normalized relative to the pipe diameter (42 in (1067 mm) in this case). Four trends are shown in this figure, being designated in degrees with respect to the plane of the split, each of which diverge from the pressure at the split (which is somewhat less than the line pressure). TDC denotes top-dead-centre, which for present purposes is aligned with the plane of the split, while BDC denotes bottom-dead-centre, which lies 180° off that plane. While well upstream within the pipe the flow is axial and spatially uniform, it is apparent from Fig.4 that the pressure varies spatially and is significantly reduced a short distance beyond the split at locations closest to the plane of the split. Such measurements made under full-scale conditions indicate that the pressure varies in both the circumferential and axial directions, with this variation being associated with the axial and transverse decompression response that develops as the flaps open.

Characterization of the apparently complex 3-D pressure field can be simplified by way of the often-cited suggestion by Baum [11] that the pressure acting on the internal surface of the pipe wall (at any axial location) is determined largely by the pressure gradient normal to the pipe's surface. Studies in that context [9,12] led to the conclusion that an axial (i.e. one-dimensional (1-D)) gas-dynamics' model was well suited to characterize the pressure distribution in the breach for purposes of modelling propagating shear failure. While that conclusion was qualified that it might be necessary to more-generally characterize this

distribution, such a 1-D model eventually was adopted for the engineering model developed by Kanninen *et al.* [12], with this simple model of the pressure response widely used since the BTCM first adopted this approach.

Measured flap-pressure data like those shown in Fig.4 can be used to quantify the role of flap pressure by two approaches. First, if the flap pressure contributed significantly to the driving force for propagation, then empirical models like the BTCM that predicted arrest in terms of the conditions upstream of the breach should err in cases where the pressure distribution in the breach differed from that underlying its empirical calibration. Second, if the flap pressure acting on the upper quadrant of the pipe was significant to flap opening, then it is reasonable to expect that the flap pressure would induce large stresses compared to the linepipe steel's yield stress, thereby contributing to flap opening by plastic bending.

Figure 5 shows pressure distributions measured by Maxey [8] that are presented in the same format used in Fig.4. The distributions shown in Fig.5 represent testing using commercially pure CO2, an N2 mix, and commercially pure N2, with the N2-based gases involving conditions similar to those underlying the BTCM. As evident from this figure, the testing using the CO2 produced normalized pressures that remained rather high as compared to the N2 mix and/or to the commercially pure N2, which can be used to quantify the first approach noted above. As the relative difference between these distributions is reinforced in absolute terms by the much-higher pressure for the CO2 test, if the flap pressure was significant then predictions by the BTCM, which rely only on the upstream conditions, should be clearly in error for this CO2 test. In contrast, as reported by Maxey [13] and discussed further subsequently, no error or pattern in such errors was evident. It follows that, for these cases that involved significantly different flap pressures, the presence of such significant differences in the breach had no apparent effect on the driving force for shear propagation.

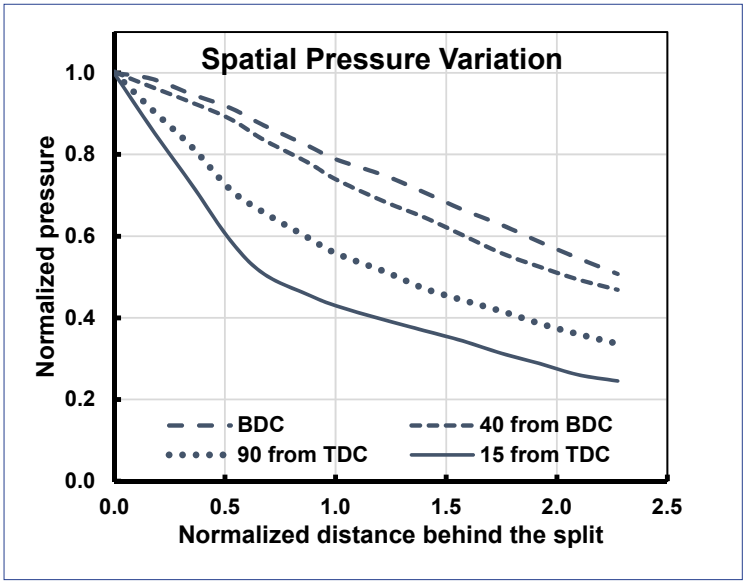

Fig.4. Measured spatial pressure distribution local to a breach (after CSM [9]).

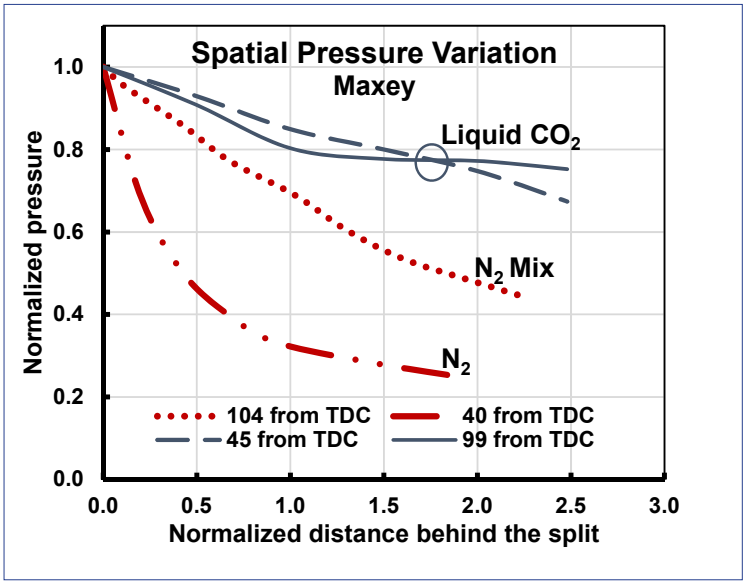

Fig.5. Measured spatial pressure distribution local to a breach (after Maxey [8]).

Insight into flap formation can be drawn from Fig.6, which presents the evolution of the initially round pipe as a function of time before and after the passage of the split, as reconstructed from full-scale test measurements [9].

Sections in this image quantify the pipe shape beginning at 23.3 ms prior to local failure, at which time the pipe remained round, through 10.7 ms after the passage of the split. It is readily apparent from these cross-sections through the pipe that axial failure occurs while the upper

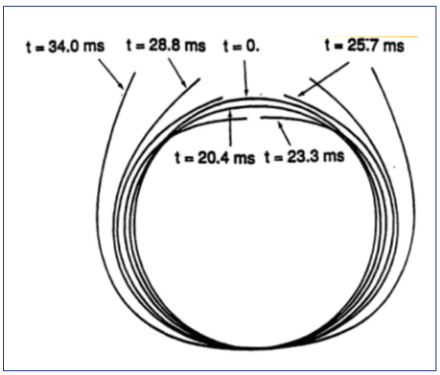

Fig.6. Deformed pipe shapes inferred from measured displacement fields [9].

quadrant of the pipe is ovalized rather than bulged by the pressure, and that this occurs while much of the upper quadrant undergoes circumferential stretch. Further, it is apparent that this ovalization and circumferential stretch lead to flattening of the portion of the pipe that becomes the flaps, which from this image develops over a contained arc of approx. 30°. Once local failure occurs, the plastic flow due to flattening induced by ovalization, and the circumferential stretch leading to failure, is augmented by recovery of the elastic component of the forming strain, which appears from this figure to continue to open the pipe flaps as time passes.

Emery *et al.* [14] have examined the dynamic mechanics of propagating-shear failure that leads to the deformed pipe shapes, such as that shown for example in Fig.6. They idealized this complex pipe deformation, and the evolution of the flaps and axial propagation, through use of a sequence of split rings, as shown schematically in Fig.7a. As evident in this figure, each of the adjacent rings show increasing opening of the split, thereby representing the evolution evident in Fig.6. Although this idealization leads to incompatible displacements between adjacent rings, it was found to reasonably quantify the observed evolution of flap displacement along the axial split – provided that each of the sequential rings had an axial length the order of one-tenth of the pipe's diameter [15]. As is clear from Figs 4 and 5, there is a sharp decay in the pressure acting on the flaps both along and around the breach, which would act to open this sequence of rings.

The results in Figs 4 and 5 indicate that the pressure acting on the flaps decays rapidly beyond the breach. As such, the response over the first one-tenth-diameter-long ring is the worst-case basis to quantify bending due to the pressure acting on the interior face of this sequence of rings, which acts to open the ring and potentially flatten the flaps. Given that flap opening is physically least constrained within the upper quadrant close to the split, it is appropriate to quantify the effects of pressure decay closest to the split in this first ring. In reference to Fig.4, the measured pressure is available within 15° of the split, but not at the split nor otherwise closer to it. Accordingly, the pressure data in Fig.4 covering axial positions up to that for one-tenth diameter were trended circumferentially and axially as the basis to extrapolate to determine pressures adjacent to the split, and thereafter quantify the pressure field acting on the interior of the first split-ring downstream of the split. In turn, this areal distribution was integrated over the region from the split through an arc of 30°, which centrally contains the pressure data measured at 15° from the split. The equivalent point load or pressure resultant, P_R, was then determined, with its centroid found to be approximately 5° off the split in the vicinity of its vertex, which leads to scenario shown schematically in Fig.7b.

As developed in Fig.7b, the tensile stress on the internal surface of the pipe due to the moment caused by this integrated pressure can be approximated[1] for this initially curved pipe section as $(M^*c_i)/(A^*e^*r_i)$, with these symbols defined as noted in the figure. Evaluating this stress

1 This analysis assumes that the strength of the steel under compression is identical to that in tension, reflects pure bending, and considers small displacements. It is a first-order approximation, which is viable for the present purposes provided that the resulting stress is small as compared to SMYS, such that the resulting conclusions would not differ if a more-rigorous approach were used. It is noteworthy that Fig.4 indicates that the initial pipe curvature is lost in the flow process leading to failure, in which case the stress is much reduced as compared to that for the curved section considered here.

due to the circumstances that underlie Fig.4 leads to a tensile stress that is much less than one-tenth of SMYS. Accordingly, the line pressure was assumed in lieu of that just noted to ensure the worst-case scenario, which led to a bending stress the order of 8% of SMYS, which would be reduced substantially if the pipe wall has lost its curvature due to ovalization prior to forming the split as implied by the results shown in Fig.6. That reduced bending stress is approximately 2% of SMYS. Such low stresses indicate that the flap pressure falls far short of that required plastically to open the pipe to flatten it, indicating that the effects of pressure on the driving force for propagation are second order.

The observation that arrest response can be predicted without regard to significant spatial variations in flap pressure indicates that the flaps do not play a critical role in driving propagating-shear failure. Furthermore, it is apparent that flap pressure induces rather small bending stresses as compared to SMYS, and in that context does not plastically open or flatten the flap. It follows that these measurements of flap pressure do not develop compelling support for the role of flaps driving continued shear propagation.

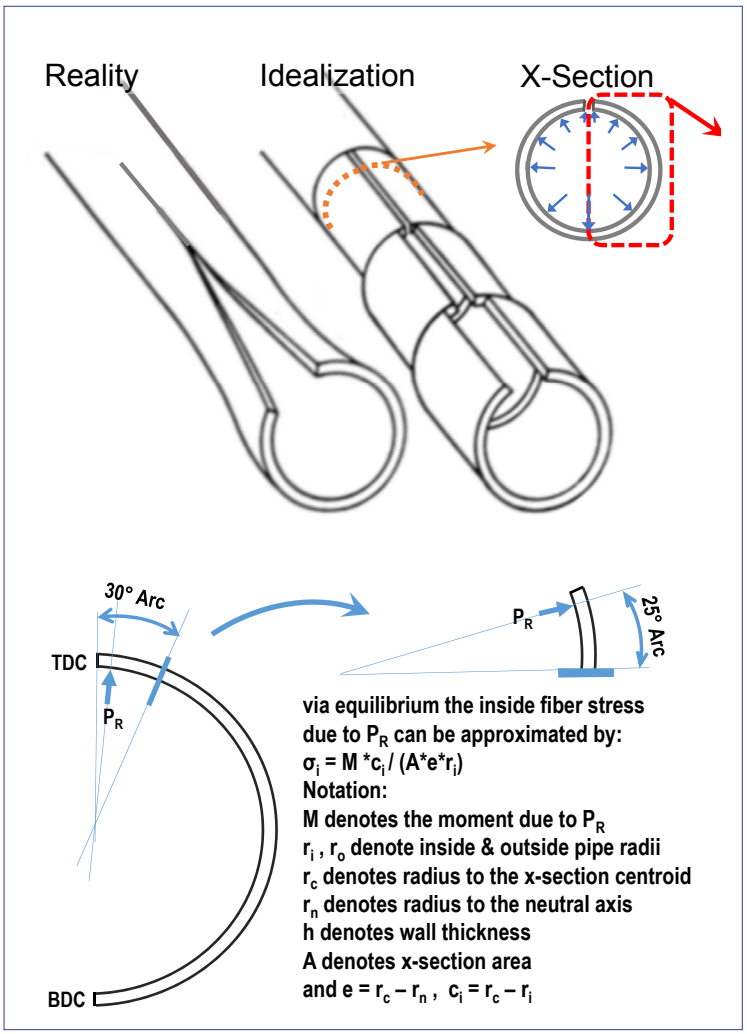
Reality
Idealization
X-Section
30° Arc
TDC
P_R
BDC
P_R
25° Arc
via equilibrium the inside fiber stress
due to P_R can be approximated by:
$\sigma_i = M * c_i / (A * e * r_i)$
Notation:
M denotes the moment due to P_R
r_i , r_o denote inside & outside pipe radii
r_c denotes radius to the x-section centroid
r_n denotes radius to the neutral axis
h denotes wall thickness
A denotes x-section area
and $e = r_c - r_n$, $c_i = r_c - r_i$

Fig.7. Split-ring idealization and related analysis of bending stress: (a - top) split-ring idealization; (b - bottom) schematic of flap bending and analysis.

Inertial effects in flap formation

Flap formation is a highly dynamic process that, based on Fig.6, occurs at a speed of the order of feet or metres per millisecond and in a deformation process that involves correspondingly large accelerations. Thus, it is conceivable that flap inertia could provide, or contribute significantly to, the driving force for continued shear failure in lieu of the asserted role of flap pressure.

Poynton and Fearnehough [16] acknowledged a possible role for flap inertia in summarizing related work by Hahn *et al.* [17]. They concluded that two main factors contribute to continued shear propagation: (1) the radial velocity of the bulging pipe walls (which occurs upstream of flap formation); and (2) the opening displacement at the split, driven by the pressure on the pipe wall. The first of these factors, when taken in conjunction with the mass of the pipe, reflects flap inertia, while the second reflects the just-discussed role of flap-opening pressure.

Freund *et al.* [7] developed a rigid-plastic model of propagating-shear failure in an evaluation of this process done in association with the work undertaken by the American Iron and Steel Institute (AISI) that underlay Smith and Shoemaker's assertion [6]. While based on many assumptions, the paper appears rationally rooted: even so, the authors noted that a complete analysis must await further progress on the fluid dynamics through the breach. Freund *et al.* used their model to trend cause-effect sensitivities:

they considered inertial effects due to the shell walls, which was evaluated via two approaches that led to results quantified in comparative terms in reference to the line pressure in the pipeline and role of the backfill. One approach considered the role of the shell-wall density that initially had been ignored, which led to an estimate of the inertial effects in a form that was expressed relative to the line pressure. This approach determined that the contribution of inertia to the process was trivial in comparison to the line pressure, such that "wall inertia seems to be a minor factor". The second approach used a perturbation analysis of the quasi-static formulation, and determined that – except at very high crack speeds – "the changes due to inertia were typically two orders of magnitude less than their initial values".

In summary, Freund *et al.* stated that both approaches "lead to the conclusion that wall inertia is a small effect over the crack speed range of interest, although there may be significant inertial effects due to backfill". As this conclusion reflects the set of assumptions needed to make their analysis tractable, it is instructive to consider the results of experiments whose design provides direct insight into the role of flaps.

Experimental insight into the potential role of flaps

The prior sections considered the effects of flaps in regard to the role of flap pressure and flap inertia as potential driving forces for propagating-shear failure. The role of flap pressure was addressed in regard to the pressure profile that developed immediately downstream in the wake of a propagating-shear crack, with those results specific to a large-diameter pipeline pressurized with lean gas. Results also were presented in regard to possible inertial effects which, as just noted, relied on assumptions necessary to make the analysis tractable. While, on that basis, the implications were clear, two key questions remain: first, will smaller-diameter transmission-sized pipelines behave similarly, and second, and second would the results for the circumstances considered also be relevant for conditions involving two-phase decompression? Accordingly, this section expands the basis to assess the role of flaps. First, the gas dynamics for two-phase expansion in smaller-diameter pipelines is examined. Thereafter, results for gaseous-detonation testing of tubes is addressed to assess the response of well-developed flaps under conditions where pressure is no longer a factor driving continued propagation.

Quasi-static and dynamic experiments: work by Maxey in 1983

Maxey [8] considered gas dynamics in the wake of a propagating failure using a set-up that involved a rupture-disk upstream of stationary flaps shaped to be consistent with the observations of full-scale tests. Such quasi-static flap experiments serve to quantify the change in pressure acting on the flap affected by a crack-like outlet, free of any upset in this pressure field that might be generated by the propagating failure. Experiments with three N2-based gases were conducted at close to 2000 psig (137.9 bar) and a temperature near 70°F (20°C). The nitrogen-based gases were commercially pure N2, and mixes of N2 involving 3 mole-percent propane and 16 mole-percent propane. Experiments with CO2-based fluids were conducted under conditions that ranged initially from the all-gaseous state through the all-liquid state.

As evident in Fig.5, introduced earlier, these experiments showed that the pressures acting along the stationary crack were higher for the gases exhibiting two-phase behaviour affected by the propane as compared to the single-phase response for the pure nitrogen, which was not a surprise. It was equally evident – in spite of the difference affected by the two-phase behaviour – that the overall trend for the two-phase cases was not unlike that evident in Fig.4 for single-phase cases. In that context, the differences affected by the two-phase response are second-order relative to the axial gradient in pressure affected by the outflow through the

breach. These results thus indicate that two-phase response does not strongly affect the conclusions reached in regard to the lean-gas results considered earlier in Fig.4.

Maxey also obtained data from full-scale experiments involving sand-backfilled, 12.75-in (324-mm) by 0.220-in (5.6-mm) X-65 pipes, whose design was in complement to his rupture-disk set-up. The fluids considered were commercially pure nitrogen, a mix of N2 with 16 mole-percent propane (two-phase expansion), and 100% liquid CO2. Results developed from this work are presented in Fig.5 using the same coordinate system and scales adopted for Fig.4 which, as noted above, involved lean-gas outflow through a breach in a large-diameter pipeline. Except for the break in the trend for the CO2 at 99° from TDC, these results are consistent with those generated in his stationary flap experiments.

Maxey went on to consider the fracture velocity in these tests which, except for the fluid properties, are otherwise comparable, and he noted in that context that the higher pressure acting on the flaps produced in the liquid CO2 test did not lead to a higher fracture velocity as compared to the all nitrogen test. On that basis, and consistent with the earlier consideration of such data, he stated that pressure acting on the flaps was "not the primary factor producing the crack driving force". The fracture speeds were predicted (to within ±13% of the measured values) using the decompressed pressure at the crack tip. Moreover, as reported by Maxey [13], and noted earlier, no error or pattern in such errors was evident. Taken together with the earlier discussion of Figs 4 and 5, it can be concluded that flap pressure is not a major factor, and so can be discarded for the present purposes.

Dynamic experiments: work by Chao in 2004

In view of the work by Freund *et al.* which noted that the effect of backfill inertia to be much larger than that of the flaps, it would be best to experimentally assess the role of flap inertia without any possible effects of backfill. Likewise, since the emergence of the BTCM, line pressure has been long considered the primary driving force for propagating shear, and it would therefore be best to experimentally assess the role of flap inertia without any possible sustaining effects of line pressure. These unique conditions develop in reference to unconstrained gaseous detonation which, if done in a pipeline setting, will generate tremendous flap-opening inertia at the same time as the pressure component falls rapidly to zero as the detonative wave propagates along the pipeline. As this leaves only flap inertia to sustain continued axial propagation, such testing effectively isolates the effects of flap inertia.

Accordingly, data were sought for testing in which the gaseous charge undergoes single-phase decompression as, for this scenario, there is no delay in the pressure decay, which effectively eliminates the role of pressure in the event that propagation continued to some extent during a test. While ideal in concept to assess the contribution of flap inertia as a driving force for propagating-shear failure, gaseous-detonation testing releases a very large amount of uncontrolled energy, and does so very rapidly. Accordingly, such testing is very dangerous at any scale, and becomes increasing so as the scale increases. As it is a dynamic event, capturing the details of this failure process requires specialized equipment and facilities, which tends make such testing as expensive as it is complex and dangerous. Not surprisingly then, the literature dealing with such testing is sparse, and limited to small-scale settings. Fortunately, limited results have been developed for smaller-diameter tubes that reasonably satisfy similitude between the model-scale and full-scale reality, as follows.

Model-scale similitude

Similitude relative to a pipeline or a propagating-shear test site involves parameters such as the thickness-to-diameter ratio and the length of the pipe

being tested relative to its diameter. The flow and fracture properties also pose concern, including possible directionality due to processing. Finally, there is a need to establish steady propagation at high speed such that arrest at a model-scale occurs as it does in a full-scale setting.

Provided that the thickness-to-diameter ratio at the model scale is high, and the test section is long compared to the diameter of tube, then the dimensions of such model-scale tests are analogous to those encountered in full-scale pipe tests that have been designed to reflect pipelines. If, in addition, the tube material evaluated exhibits ductile propagation and is free of directional properties that conspire against axial propagation, and the testing is done under conditions equivalent to a full-scale aboveground test, then the outcome of such testing is a viable worst-case analogue for a buried full-scale pipe test. Under such conditions the results of gaseous-detonation testing provide a viable analogue to assess the role of flap inertia. Data that reasonably satisfy these requirements were found for one comprehensive study that underlies the PhD thesis of Chao [10].

Chao evaluated gaseous detonation in small diameter tubes with D/t of approx.46, which lies toward the lower end of transmission pipeline geometries. One set-up considered end-capped tubes that were 36 in (0.914 m) long that had an outside diameter of 1.65 in (41.3 mm), which leads to a test-section length/tube-diameter ratio of 21.8. This is roughly one-half the length of such full-scale facilities, and so can be said reasonably to represent such test beds (albeit possibly with minor differences in the end restraint). As becomes clear subsequently, reflected waves were not a concern. He tested 6061-T6 (extruded) aluminium tubes that contained a part-through-wall (PTW) axial slit. The 6061 material in that temper has mechanical properties not too different from the lower-end X-Grades and shows reasonable ductility, and as produced would tend to favour axial crack extension rather than constrain it. His work made use of closely-spaced timing wires that showed that initially steady propagation developed and ran at high speed for distance of a few diameters.

Interpretation of Chao's data relative to full-scale tests

The key outcome of a full-scale test is whether or not arrest or propagation occurs. Before arrest can be declared, high-speed propagation must have been established following initiation, which is expected to be sustained over a few diameters. Adopting tube diameter as the metric of the propagation distance in the model-scale tests, propagation must be initiated and a high speed sustained over a distance of several diameters before detonation results can be considered analogous to what occurs in a full-scale test. As indicated above, Chao's detonation tests satisfy this requirement. In that context, his test set-up as well as the tubes he tested reasonably satisfy the requirements of similitude in regard to full-scale tests.

Full-scale tests for which the toughness is insufficient for arrest indicate that as long as a driving force is sustained the failure will run the full length of the test section. By analogy, sustained propagation would be evident in Chao's set-up by propagation over the full length of a tube. With that as a benchmark, one could conclude that a split that ran the full length of a tube was clear evidence that flap inertia could sustain propagating-shear failure. In contrast, the results of some full-scale tests show that arrest has occurred within a diameter or so after entering a pipe joint with sufficient toughness for arrest. By analogy, if propagation was not sustained beyond the few tube diameters needed to establish steady-state propagation, then one could conclude that outcome of a gaseous-detonation test was clear evidence that flap inertia does not sustain propagating-shear failure. Finally, cases that show propagation that lies between these two limiting states would be considered inconclusive.

Results

Figure 8 presents photographs of the outcomes of the many of the gaseous-detonation tests, with enough of the un-failed pipe included for each test as a basis to judge the pipe diameter, and so also the extent of propagation as a function of the pipe diameter for each test. It is apparent that, while the pipe flattens local to the detonation origin, such tests show little to no propagation beyond the few diameters needed to establish a high-rate failure process. In no case is there a hint that flap opening has sustained propagation: arrest ensues rapidly, doing so across the full scope of tests within just a few tube diameters.

It follows that the model-scale gaseous-detonation testing indicates no role for flap inertia under conditions that develop extreme flap-opening loads, which is consistent with the analysis results of Freund *et al.* It is equally clear that, without contained pressure, the crack stops propagating within a few diameters. On this basis it can be concluded that flap inertia is not a major factor in driving propagating-shear failure, and so can be discarded as a consideration for present purposes. It also can be concluded that without pressure driving the split, arrest occurs within a few diameters.

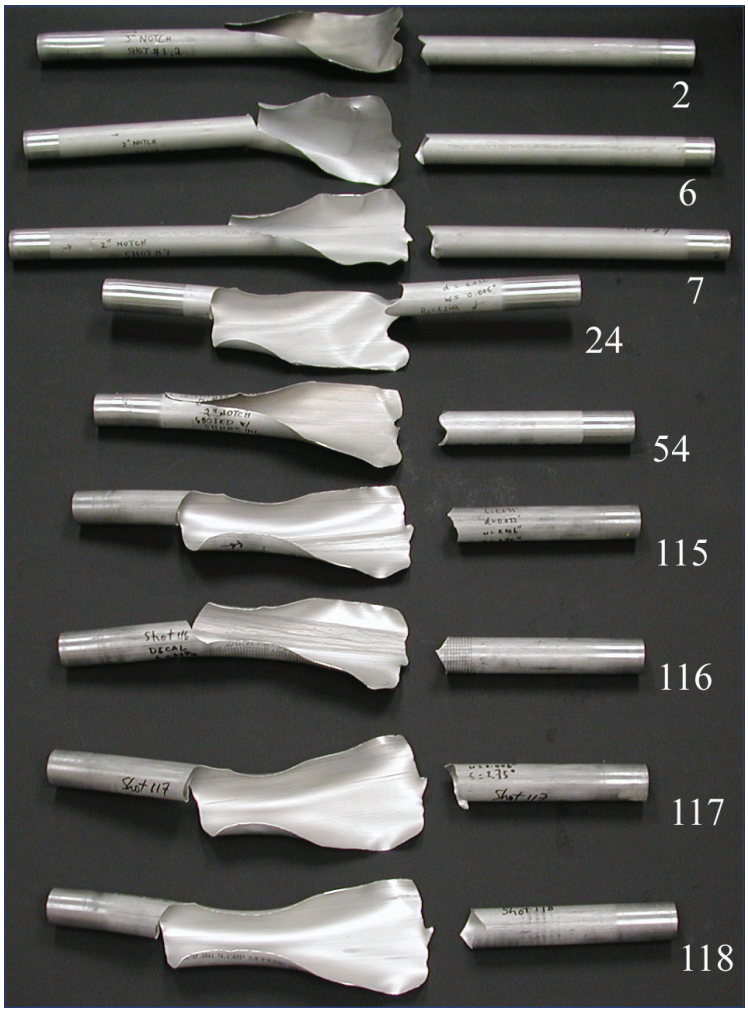

Fig.8. Typical post-test views of gaseous detonation-driven fracture testing of tubes [10].

Distance required for arrest

In defining the basis for interpreting the outcome of the detonation-test data as arrest versus continued propagation, the possibility was noted that results might develop that lay between these otherwise polar extremes, which would limit their utility – as has happened for some full-scale tests. Largely because detonation tests isolate the role of flap inertia, and avoid the complicating effects of two-phase expansion and backfill, that possibility did not materialize. Unfortunately, the circumstances in full-scale tests are not so idealized. Some tests generate large swings in propagation speed, such that steady propagation is not achieved, while in other tests the propagation speed decreases slowly, without clear evidence of arrest. Accordingly, it is useful to quantify the arrest distance, in regard to full-scale tests, and consider its implications in regard to the spacing of crack arresters. Given that local flap pressure coupled with flap inertia has been excluded as a driver for continued shear propagation in the above discussion, this is done relative to line pressure.

Arrest and line pressure

The BTCM determines the energy required for arrest on the premise that arrest occurs when the speed of the decompression front exceeds that of the propagating-shear failure. Recognizing that line pressure exists as the only relevant driving force, one could equally define arrest relative to the instant that the local pressure drops below the arrest pressure.

On that basis, adopting the site where the speed of the decompression front first exceeds that of the propagating failure as the reference point for the onset of arrest, which for the present is determined by the BTCM, continued growth beyond that point prior to full-stop of the failure can only occur over the time required for the pressure to decay below the arrest pressure. Figures 4 and 5 characterize the pressure gradients in the vicinity of the breach, but they provide no insight into the time-rate of pressure decay relative to the speed of the propagating failure.

The pressure in the vicinity of a propagating failure is a function of its speed, the initial line pressure, the speed of the decompression front, and the specific heat ratio of the transported product. The loss of product under choked flow in the wake of the failure results in coupling between the equations governing the shell deformations in the pipe and those for the gas dynamics [18]. In turn, this leads to pressure decay that is exponential in time, as illustrated for example in Fig.9a [19] based on results from computational fluid dynamics (CFD) analysis that, as noted in the figure, is specific to a pipeline transporting pure CO2. The y-axis in this figure is pressure beginning from the operational level, whereas the x-axis indicates its dependence on time. As for Figs 4 and 5, this result is referenced to the split that for purposes of the CFD was considered planar, and so without the complications due to flaps. Figure 9b provides similar results for pressure decay as a function of time that, for this case, reflect experimental measurements obtained for a rich-gas mix, with this data representative of the circumstances on a plane well downstream of the initiating pipe.

Although the CFD results shown in Fig.9a are specific to the pressure decay for a CO2 pipeline, they are instructive more generally because such pipelines operate at high pressure and the product shows two-phase decompression, with a long plateau at the saturation pressure – analogous to hydrocarbon transmission pipelines that experience two-phase response. This CFD prediction indicates that the pressure would show a rapid decay from operational conditions down to the saturation pressure, followed by a much-reduced rate of decay thereafter. The arrest pressure relative to the saturation pressure thus determines whether the pressure will decay rapidly, quickly satisfying the conditions for arrest at a level above the saturation plateau, or much-more slowly to a level below the saturation plateau. The response evident in Fig.9b for the rich-gas scenario represented therein was associated with a predicted arrest stress of approx. 38% of the initial pressure. In the framework of Fig.9b, this arrest pressure falls at a normalized local pressure of about 0.84 which, in light of this figure, would follow shortly after the local passage of the failure. As this arrest stress falls well below the saturation pressure, it follows that propagation would traverse several pipe joints in route to arrest.

While analysis of the rate of decompression that develops in light of Fig.9 indicates that arrest will occur over a quite long distance, arrest – if defined as above – corresponds to the time and location along the pipeline where the decompression front has first outrun the propagating failure, which occurs at the arrest stress. Local flap pressure coupled with flap inertia has not been found to support propagation. So, when the hoop stress falls below the arrest stress, propagation ceases without the energy required to create new surface, and arrest quickly ensues. This expectation follows in view of Fig.8. In this context, although the decompression response is central to quantifying the toughness required for arrest, it does not affect the distance required for arrest as it is defined by the BTCM. Thus, the arrest distance is small – being at most the order of a few diameters in view of Fig.8.

Implications regarding 'fracture arrestors'

The just-discussed interplay between arrest and line pressure has implications in the context of so-called 'fracture arrestors' many of which are asserted to

function by restraining flap opening (for example, Ref.20). Support for this asserted function derives from many full-scale experiments in which propagating shear has been successfully arrested through use of tight-fitting sleeves and wraps. It also follows from the observation that propagation has continued past loose-fitting arrestors, which is asserted to occur because the flap restraint was inadequate. As such observations are contrary to the results presented thus far, it is appropriate to rationalize them independent of the asserted role of flap restraint, as follows from two perspectives.

First, if fracture controls propagating-shear failure and models like the BTCM are applicable, then it is clear from the form of such models that the speed of propagation has a first-order (or higher) dependence on hoop stress. It is equally clear that, as the pipe deforms plastically in advance of the propagating split, a tight-fitting arrestor absorbs a share of the pressure loading, such that the pipe offloads and the hoop stress decreases. Given the stress dependence of propagation speed and the existence of an arrest-stress as discussed above, it is clear that arrest occurs when the hoop-stress driving the failure falls below the pressure corresponding to the arrest stress. Inference based on arrestor sizing indicates that arrest can be simply rationalized in this context without invoking the role of flap restraint. Based on this same logic, continued propagation is anticipated for loose-fitting sleeves, just as has been reported [20].

Second, if through-wall collapse (TWC) in the region ahead of the split controls propagating-shear failure in lieu of fracture, as has been recently argued [21], then the wall-stress dependence of TWC opens to this same rationale. That is, the propensity for continued shear failure via TWC diminishes as the hoop stress driving the failure falls below a critical level, analogous to the arrest stress. Likewise, if TWC controls propagation, then continued propagation is anticipated in cases involving loose-fitting sleeves, just as has been reported.

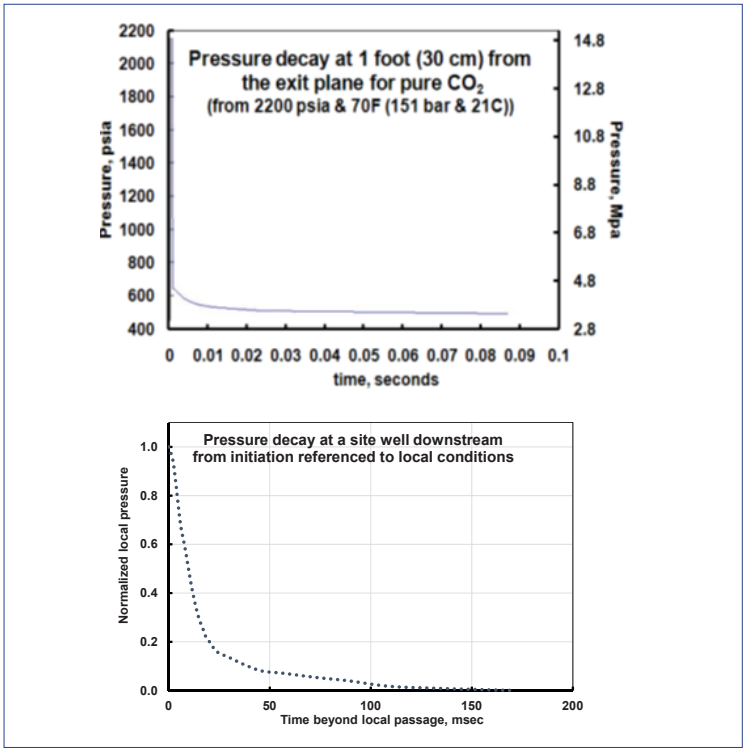
Pressure decay at 1 foot (30 cm) from the exit plane for pure CO_2
(from 2200 psia & 70F (151 bar & 21C))
Pressure, psia
Pressure, Mpa
time, seconds
Pressure decay at a site well downstream from initiation referenced to local conditions
Normalized local pressure
Time beyond local passage, msec

Figure 9. Decompression behaviour for large-diameter pipelines: (a - top) CFD results for a guillotine rupture [19]; (b - bottom) measured response in a full-scale test.

It follows that successful arrest with tight-fitting wraps and sleeves, and continued propagation past loose-fitting arrestors, can be rationalized as a consequence of load-sharing by the arrestor, and reduced wall stress, independent of the asserted role of flap restraint. Accordingly, such observations are not inconsistent with results discussed in regard to Figs 4 through 8, which fail to indicate that flap formation and flap pressure are drivers for propagating-shear failure.

Discussion

Flaps are associated with a running shear failure and the deformation that occurs in the wake of the split, as illustrated in Fig.3. Is a running shear failure a consequence of the opening of the flaps or *vice versa*? Clearly without the split there are no flaps, so the question only applies after some near-steady-state axial propagation ensues, i.e. after the initial opening (rupture) has started to evolve into a running fracture.

Smith and Shoemaker [6] in 1974 identified that the pressure acting on the

flaps is significant in the deformation of the flaps, and asserted that "the driving force for ductile-fracture propagation ... is the pressure acting on the flaps ...". Others in that era formulated models of shear propagation that did not consider flaps or the role of flap pressure. For example, Hahn *et al.* [17] formulated a model that quantified the six processes they postulated underlay shear propagation. These were: "(1) axial decompression; (2) bulging; (3) radial decompression; (4) local stress and strain intensification; (5) plastic deformation; and (6) ductile cracking". Based on the model-schematic in their paper, their "bulge" involved a tight axial split, which opened slightly over a short distance within the bulge, prior to the transition into an opening breach and flap formation. The difference between the bulge with a tight split considered by Hahn *et al.*, and the opened flaps considered by Smith and Shoemaker, might seem subtle to some, but is clearly justified given the very rapid axial pressure decay as a split opens into flaps. As such, the extent of radial opening of a split leads to widely different pressure fields.

Reflecting on a draft of Hahn *et al.*'s then-pending publication, Poynton and Fearnehough [16] reduced the above list of six factors to an energy balance that considered bulging, and fracture energy and kinetic energy, both of which were expressed in reference to the bulge. The schematic adopted by Poynton and Fearnehough to illustrate their model concept was somewhat vague regarding the bulge. A subsequent review of relevant studies written by Fearnehough [22] alludes to the bulge as a split pipe wall, but does not discuss the width or opening of the split. Unfortunately, this leaves the extent of the radial opening for their bulge vague in comparison to the bulge shown by Hahn *et al.*, or the flaps concept of Smith and Shoemaker.

Working in this same era, Maxey recognized that shear propagation occurred in the wake of a plastic wave that was triggered by initiation of the axial split. On that basis he developed an uncoupled model that quantified the balance between the speed of the decompressing gas front and that of the split, and determined arrest in terms of tangency between the two curves representing these speeds. That uncoupled model was formulated in reference to the fluid's properties, the line-pipe's size and its flow and fracture properties, and the backfill conditions upstream of the split. As such, Maxey did not explicitly acknowledge the occurrence of a bulge or flaps. However, by way of his empirical calibration that included backfill effects and containment of the breach, his model implicitly captured the response within the breach – to the extent it was a factor.

Maxey's observation that the speed of propagation in full-scale tests with N2 and CO2 was similar despite the higher pressure measured on the flaps in the liquid CO2 test [8,13] is indicative that the role of flap pressure is secondary. Evidence showing that it is not sufficient to constrain flap opening, but rather that a crack arrestor must be tight enough to constrain the circumferential stretching ahead of the crack tip, is likewise indicative of a secondary role of flaps. Such response has been evident in full-scale propagating shear tests that show the split had propagated under a loose-fitting sleeve [20].

In many ways the just-discussed models reflect the phenomenological understanding of the era they emerged in, with much learned since the above-noted models were formulated. For example, it is apparent in view of Fig.6 that bulging does not occur for propagating-shear failure in the way it is observed in burst tests of short end-capped pups, or might be inferred from the above-discussed model schematics. Rather, the pipe is found to flatten in the vicinity of the split. Likewise, it is evident from the gaseous-detonation-driven failures shown in Fig.8 that in the absence of pressure, an axial split does not propagate, and flap inertia is not a factor. Numerical and analytical models will not discriminate such issues – at least until they can be formulated from first principles in a manner that frees them from assumptions and idealizations

that condition or dictate their outcomes. Unfortunately, while we have learned much, a major gap remains in regard to the data needed to uncouple the physically coupled nonlinearities involving fluid dynamics, structural dynamics, and the foundation/boundary effects of the backfill as the basis for more fundamental models. Well-designed above-ground tests could do much to bridge these gaps, but these remain expensive and of limited value to specific pipeline designs – and as such likely are a pipe dream.

A running-shear failure must typically propagate one to two pipe diameters in each direction before the cross-sectional area of the opening is equal to approximately two pipe diameters [8]. Full-scale tests conducted using natural gas show that the pressure near, but ahead of, the crack tip, is higher than that predicted using a simple isentropic model until the fracture has propagated for about ten pipe diameters in each direction [8]. On this basis a propagating split is a coupled process. In spite of this, a steady-state running shear has been successfully modelled as an uncoupled process. This, too, suggests that the role of the pressure on the flaps is secondary (and/or that it at least approximately scales with the conditions ahead of the split).

The modelling of a running-shear failure is clearly simplified if it is uncoupled. Arrest, in the context of the length required to arrest a steady-state running-shear fracture, is probably a coupled process, but arguably whether a fracture arrests with, say, one, two, or three diameters is secondary to the fact that it arrests.

Summary and conclusions

Two facets of modelling propagating-shear failure have been examined, much of which carried back to the era that the BTCM was developed. As time has passed, and the toughness of the steel needed to ensure arrest of such failures has increased, it is clear that models of that era have limited utility in applications to advanced-design pipelines. Work from the late 1960s and early 1970s also has emerged that indicates propagating shear in that era was due to through-wall collapse [21] rather than fracture, with that work also rationalizing the success of fracture-based models in application to a failure process controlled by collapse.

As consideration is given to formulating alternative approaches to quantify arrest requirements, it will be essential to conclusively know if such formulations can be developed based on conditions upstream of the breach, or whether the breach controls as asserted in regard to the role of the flaps, and/or if these processes are coupled and to what extent. This paper has taken a step toward answering such questions. Important conclusions in that context include:

- If the driving force for ductile-fracture propagation in a pipe is due to, or significantly involves, the pressure acting on the flaps behind the propagating-crack tip, then the gas-dynamics' and fracture-dynamics' processes are not uncoupled during steady-state shear propagation.

- Direct and indirect experimental evidence supports the view that the role of the pressure on the flaps is secondary.

- By its formulation the Battelle two-curve model uncoupled the gas-dynamics' and fracture-dynamics' processes, but by its empirical calibration it implicitly embedded the role of the breach in the steady-state propagating-shear failure process to the extent it was a factor for those circumstances, so the role of the flaps might remain a somewhat open issue for some.

- Alternative approaches to quantify arrest requirements will need to correctly address the role of the flaps and bulging – if any – or empirically embed their effects.

References

1. Anon., Rupture will not delay Transwestern's line. O & G J 58 (17) (Arpil 1960) 105.
2. F.W.Boulger and W.R.Hansen, A study of the effect of manufacturing variables on the properties of line pipe steels. AGA NG-18 Report 9, (March 1963).
3. G.M.McClure, R.J.Eiber, and A.R.Duffy, Investigation of full-scale fracture characteristics of line pipe and correlation with laboratory tests. AGA NG-18 Report 10, (March 1962).
4. W.A.Maxey, J.F. Kiefner,R.J. Eiber, A.R.Duffy, and G.M.McClure, NG-18 full-scale line pipe research data record, Issue II, Vol.II. AGA NG-18 Report 42, (February 1972).
5. W.A.Maxey, Fracture initiation, propagation, and arrest. Paper J, 5th Symposium on Line Pipe Research, PRCI Catalog No. L30174, (November 1974).
6. J.H.Smith and A.K.Shoemaker, Use of pipe wall ductility to characterize ductile fracture in line pipes (12-C-002 (018-4)). United States Steel restricted distribution technical report on the AISI-sponsored line-pipe burst-test program, (March 1975).
7. L.B.Freund, D.M.Parks, and J.R.Rice, Running ductile fracture in a pressurized line pipe. Mechanics of Crack Growth, ASTM STP 590, American Society for Testing and Materials, (1976) 243-262.
8. W.A.Maxey, Gas expansion studies. AGA NG-18 Report 133, (February 1983).
9. G.Buzzichelli, G. Demofonti, L.Rizzi, S.Venzi, M.F.Kanninen, J.W.Cardinal, P.E.O'Donoghue, and T.B.Morrow, The development of a ductile pipe fracture model. CSM-SWRI Joint Interim Report on AGA Contracts PR182-526 and PR15-527, (January 1989).
10. T.W.Chao, Gaseous detonation-driven fracture of tubes. PhD Thesis, California Institute of Technology (2004).
11. M.R. Baum, The relationship between breach development and the depressurization transient during axial rupture of a gas-pressurized steel pipe. J.Press. Vesse.Technol., 104, (1) (1982) 20-24.
12. M.F.Kanninen, P.E.O'Donoghue, J.W.Cardinal, T.B.Morrow, S.T.Green, C.F.Popelar, G.Buzzichelli, G.Demofonti, L.Rizzi, and S.Venzi, Analysis and experimentation on ductile fracture propagation in gas transmission pipelines. PRC NG-18 and HLP Joint Technical Meeting, Chicago, Illinois, March, Paper 3 (1990).
13. W.A.Maxey, Fluid decompression in pipelines. 4th EPRG-PRCI Seminar, Vol I, Duisburg, Germany, Paper 13 (1981).
14. A.F.Emery, M.Perl, A.S.Kobayashi, and W.J.Love, The use of the split ring in modeling ductile axial crack extension in pipes. J.Press. Vess. Technol. 103 (May 1981) 51-154.
15. A.S.Kobayashi, CTOA as a dynamic fracture criterion. 11th International Congress on Fracture, Turin Italy, Paper 3136 (2005).
16. W.A.Poynton and G.D.Fearnehough, An analysis of ductile fracture propagation in gas pipelines. International Conference on Dynamic Crack Propagation, Lehigh University, Bethlehem, PA, (July 1972).
17. G.T.Hahn, M.Sarrate, M.F.Kanninen, and A.R.Rosenfield, A model for unstable shear crack propagation in pipes containing gas pressure. Int. J. of Fracture, 9 (1973) 209-221.
18. H.W.Liepmann and A.Roshko, Elements of gas dynamics. Wiley, New York, (1957) 53-54.
19. B.N.Leis, J.H.Saunders, E.B.Clark, and X.-K.Zhu, Transporting anthropogenic CO2 in contrast to pipelines supporting early EOR. J.Pipe. Eng., 9, (2010) 235-252
20. G.Wilkowski, W.A.Maxey, and P.Scott, Design and optimization of mechanical crack arrestors for pipelines. AGA NG-18 Report 134, (July 1983).
21. B.N.Leis, Arresting propagating shear in pipelines. Microalloyed Steels 2013, Ed. Pascoal Bordignon, Companhia Brasileira de Metalurgia e Mineração, Sao Paulo, *in press*.
22. G.D.Fearnehough, Fracture propagation control in gas pipelines: a survey of relevant studies. Int. J. Press. Vess. & Piping, 2 (1974) 257-382.

Design challenges of steel pipelines in unsteady flow conditions

by Prof. D.G. Pavlou

Department of Mechanical and Structural Engineering and Materials Science, University of Stavanger, Stavanger, Norway

AN APPROXIMATE MODEL for hoop-stress-increase estimation of pipelines subjected to fluid-hammer conditions is developed. The model takes into account the pressure oscillations and the elastic properties of steel. The solution of the derived differential equation is based on finite Fourier and Laplace transforms. The proposed methodology is implemented to a representative example and the results are discussed.

Key words: unsteady flow, hoop stress, fluid hammer, Fourier transform, Laplace transform

WHEN A VALVE IS CLOSED rapidly at the end of a pipeline, a pressure shock is developed and travels with high velocity [1, 2] and this phenomenon, known as 'fluid-hammer', may have catastrophic consequences to the integrity of the pipeline. Fluid-mechanics' models providing the pressure change and pressure-wave velocity have been known since 1898: Joukowsky [3], Frizell [4], and Allievi [5] were among the first researchers who derived formulae for quantitative calculation of pressure surge and velocity. Their formulae are based on one-dimensional mass and momentum equations of fluid-hammer flow and take into account the modulus of elasticity of the pipe's material, the bulk modulus of the contained fluid, the wall thickness, the diameter of the pipe, and the fluid's mass density. Today, many transient-fluid-flow models in one or two dimensions are known [6] providing useful theoretical tools for the estimation of the stress and strain fields of pipelines in fluid-hammer conditions.

Since purpose of the present study is the derivation of a simple tool for dynamic-hoop-stress estimation of steel pipelines in unsteady flow conditions, the Allievi [5] fluid-flow model will be adopted. Taking into account the dynamic load, the theory of axisymmetric shells under axisymmetric loading will be used to simulate the radial displacement equation of the pipeline using the model of a beam on an elastic foundation [7]. Then, an analytic solution based on studies on beams under moving loads [8] will be used for the estimation of radial displacements and hoop stresses for pipelines under fluid-hammer conditions.

Unsteady-fluid-flow model

For the derivation of the governing equation providing the radial deflection of the pipeline's wall, Allievi's unsteady-flow formula [5] will be adopted. According to Allievi's study, the pressure change due to a sudden reduction of the flow in a pipeline is:

$$\Delta p^* = \pm \rho u \alpha \qquad (1)$$

where ρ is the fluid's mass density, u is the flow speed before the rapid reduction, and α is the velocity of the pressure wave due to fluid hammer, given by the following equation:

$$\alpha = \sqrt{\frac{K/\rho}{1+(2RK)/(hE)}} \qquad (2)$$

Author's contact details:
Email: dimitrios.g.pavlou@uis.no

This paper was first published in *The Journal of Pipeline Engineering*, September 2015, and is reproduced here by permission.

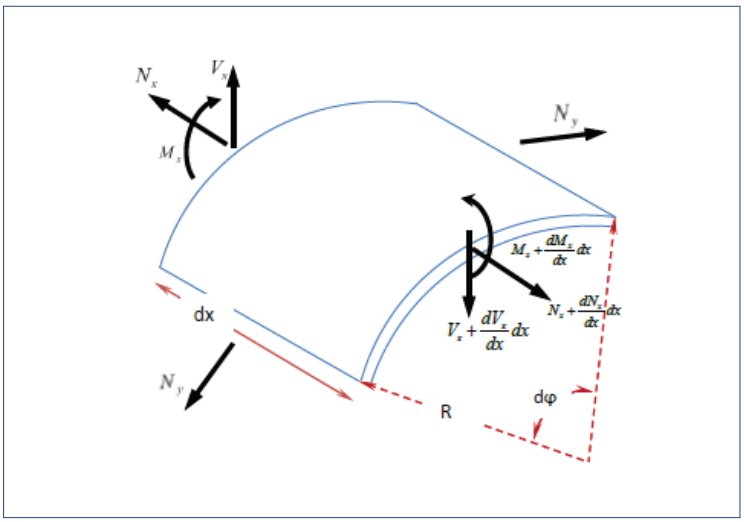

Fig.1. Equilibrium of a pipe-wall element.

In Equn 2 K is the bulk modulus of elasticity of the fluid, E is the modulus of elasticity of the pipeline's material, and R and h are its internal radius and wall thickness, respectively. If pst is the static pressure (during steady-state flow), the total pressure due to fluid hammer is:

$$P_{tot} = p_{st} \pm \Delta p^* \qquad (3)$$

The required time T for the shock wave to travel back to the point where the sudden stopping of flow occurred is:

$$T = \frac{2L}{\alpha} \qquad (4)$$

where L is the length of the pipe as far as the valve which stops the flow.

In the case where the time T_v of closure of the valve is not zero, and in the specific case where $T_v > T$, the maximum overpressure can be obtained from the following formula:

$$\Delta p^* = \pm \rho u \frac{2L}{T_v} \qquad (5)$$

In the case where $T_v < T$, the rapid closure is considered as being equivalent to instantaneous closure, and the shock wave will reach its maximum value given by Equn 1.

Hoop-stress model

The equilibrium equations [9] (containing translational inertia effects) of a wall element of a cylindrical shell (Fig.1) under pressure $p(x,t)$ are given by:

$$\frac{\partial N_x}{\partial x} R dx d\phi - \rho h \frac{\partial^2 u}{\partial t^2} = 0 \qquad (6)$$

$$\frac{N_y}{R} + \frac{\partial V_x}{\partial x} + \rho h \frac{\partial^2 w}{\partial t^2} = p(x,t) \qquad (7)$$

$$\frac{\partial M_x}{\partial x} + V_x = 0 \qquad (8)$$

In Equns 6-8, N_x, N_y, V_x, and M_x are the force resultants shown in Fig.1, h is the wall thickness, t is time, and w and u are the radial and longitudinal displacements, respectively. For long, axially restrained, pipelines the assumption that the longitudinal displacement u is zero can be adopted. By taking into account the above assumption, combining Equns 6-8 yields:

$$N_x = const \qquad (9)$$

$$\frac{N_y}{R} - \frac{\partial^2 M_x}{\partial x^2} + \rho h \frac{\partial^2 w}{\partial t^2} = p(x,t) \qquad (10)$$

According to the general theory of cylindrical shells [9], the following formulae are valid:

$$N_y = \frac{Eh}{R} w \qquad (11)$$

$$M_x = D \frac{\partial^2 w}{\partial x^2} \qquad (12)$$

where D is the flexural rigidity of the shell, and is given by:

$$D = \frac{Eh^3}{12(1-\nu^2)} \qquad (13)$$

and ν is the Poisson's ratio.

Then, with the aid of Equns 11 and 12, Equn 10 yields:

$$D \frac{\partial^4 w}{\partial x^4} + \frac{Eh}{R^2} w + \rho h \frac{\partial^2 w}{\partial t^2} = p(x,t) \qquad (14)$$

The radial strain ε_{yy} is given by the following [7] equation:

$$\varepsilon_{yy} = \frac{w}{R} \tag{15}$$

and the hoop stress is:

$$\sigma_{yy} = E\,\varepsilon_{yy} \tag{16}$$

The radial displacement w can be correlated to σ_{yy} by the following equation:

$$w = \frac{R}{E}\sigma_{yy} \tag{17}$$

And with the aid of Equn 17, Equn 14 can be rewritten as:

$$\frac{\partial^4 \sigma_{yy}}{\partial x^4} + \frac{Eh}{R^2 D}\sigma_{yy} + \frac{\rho h}{D}\frac{\partial^2 \sigma_{yy}}{\partial t^2} = \frac{E}{RD}p(x,t) \tag{18}$$

In fluid-hammer conditions the pressure $p(x,y)$ can be derived with the aid of Equns 1 and 2. Since the pressure shock Δp^* travels with velocity α, the function $p(x,y)$ can be derived as:

$$p(x,y) = \Delta p^* \delta\{x - \alpha t\} \tag{19}$$

where $\delta\{x-\alpha t\}$ is the Dirac Delta function, and t denotes time. Using the notation

$$P_o = \frac{E}{RD}\rho u\sqrt{\frac{K/\rho}{1+(2RK)/(hE)}} \tag{20}$$

and taking into account Equns 1, 2, and 19, Equn 18 can be rewritten as follows:

$$\frac{\partial^4 \sigma_{yy}}{\partial x^4} + \frac{Eh}{R^2 D}\sigma_{yy} + \frac{\rho h}{D}\frac{\partial^2 \sigma_{yy}}{\partial t^2} = P_o\,\delta\{x - \alpha t\} \tag{21}$$

Analytic solution of the dynamic model

Assuming that the ends of the pipeline are simply supported on their perimeters, the following boundary conditions are valid:

$$w(0,t) = 0 \qquad \left.\frac{\partial^2 w(x,t)}{\partial x^2}\right|_{x=0} = 0 \tag{22}$$

$$w(L,t) = 0 \qquad \left.\frac{\partial^2 w(x,t)}{\partial x^2}\right|_{x=L} = 0 \tag{23}$$

Considering that the pipe is un-deformed at $t = 0$, the following initial conditions can be used:

$$w(x,0) = 0 \;and\; \left.\frac{\partial w(x,t)}{\partial t}\right|_{t=0} = 0 \tag{24}$$

Taking into account Equn 17, Equns 22-24 can be rewritten as follows:

$$\sigma_{yy}(0,t) = 0 \qquad \left.\frac{\partial^2 \sigma_{yy}(x,t)}{\partial x^2}\right|_{x=0} = 0 \tag{25}$$

$$\sigma_{yy}(x,0) = 0 \;and\; \left.\frac{\partial \sigma_{yy}(x,t)}{\partial t}\right|_{t=0} = 0 \tag{26}$$

and

$$\sigma_{yy}(x,0) = 0 \;and\; \left.\frac{\partial \sigma_{yy}(x,t)}{\partial t}\right|_{t=0} = 0 \tag{27}$$

With the aid of the following finite sine Fourier transform and its inverse form:

$$S(j,t) = \int_0^L \sigma_{yy}(x,t)\sin\frac{j\pi x}{L}\,dx \qquad j = 1, 2, 3, \cdots \tag{28}$$

$$\sigma_{yy}(x,t) = \frac{2}{L}\sum_{j=1}^{\infty} S(j,t)\sin\frac{j\pi x}{L} \tag{29}$$

and taking into account the following properties:

$$\int_0^L \frac{d^4 \sigma_{yy}(x,t)}{dx^4}\sin\left(\frac{j\pi x}{L}\right)dx = \frac{j^4\pi^4}{L^4}S(j,t) \tag{30}$$

$$\int_0^L \delta(x-at)\sin\frac{j\pi x}{L}dx = \sin\frac{j\pi a t}{L} \tag{31}$$

the finite sine Fourier transform can be applied to Equn 21 yielding:

$$\frac{j^4\pi^4}{L^4}S(j,t)+\frac{Eh}{R^2D}S(j,t)+\frac{\rho h}{D}\ddot{S}(j,t)=P_o\sin\frac{j\pi a\,t}{L} \tag{32}$$

Using the following notations:

$$\omega_{(j)}^2=\frac{j^4\pi^4}{L^4}\frac{D}{\rho h} \tag{33}$$

$$\Omega_{(j)}^2=\omega_{(j)}^2+\frac{E}{\rho R^2} \tag{34}$$

and

$$\omega=\frac{\pi a}{L} \tag{35}$$

Equn 32 can be rewritten as:

$$\ddot{S}(j,t)+\Omega_{(j)}^2S(j,t)=\frac{P_oD}{\rho h}\sin j\omega t \tag{36}$$

If we use the notation:

$$P^*=\frac{P_oD}{\rho h} \tag{37}$$

and taking into account Equn 20, the parameter P^* can be written as:

$$P^*=\frac{Eu}{\rho h}\sqrt{\frac{K/\rho}{1+(2RK)/(hE)}} \tag{38}$$

To solve Equn 36, a Laplace transform in the domain of time t will be applied. The definition of the Laplace transform and its inverse form employed in this solution is:

$$L\{S(j,t);t\to\xi\}=$$
$$\bar{S}(j,\xi)=\xi\int_0^\infty S(j,t)e^{-\xi t}dt \tag{39}$$

$$S(j,t)=L^{-1}\{\bar{S}(j,\xi);\xi\to t\}=$$
$$\frac{1}{2\pi i}\int_{\varepsilon-i\infty}^{\varepsilon+i\infty}\frac{\bar{S}(j,\xi)}{\xi}e^{t\xi}d\xi \tag{40}$$

Applying the operator L to Equn 36, the following formula can be obtained:

$$L\left\{\frac{\partial^2S(j,t)}{\partial t^2};t\to\xi\right\}$$
$$+\Omega_{(j)}^2L\{S(j,t);t\to\xi\}=$$
$$P^*L\{\sin(j\omega t);t\to\xi\} \tag{41}$$

Taking into account the following properties of Laplace transform:

$$L\left\{\frac{\partial^2S(j,t)}{\partial t^2};t\to\xi\right\}= \tag{42}$$
$$\xi^2\bar{S}(j,\xi)-\xi^2S(j,0)-\xi\frac{\partial S(j,t)}{\partial t}\bigg|_{t=0}$$

$$L\{\sin(j\omega t);t\to\xi\}=\frac{j\omega}{\xi^2+j^2\omega^2} \tag{43}$$

as well as the following conditions derived from Equn 27:

$$S(j,0)=0,\qquad\frac{\partial S(j,t)}{\partial t}\bigg|_{t=0}=0 \tag{44}$$

Equn 41 then yields:

$$\xi^2\bar{S}(j,\xi)+\Omega_{(j)}^2\bar{S}(j,\xi)=P^*\frac{j\omega}{\xi^2+j^2\omega^2} \tag{45}$$

Equation 45 is an algebraic equation with respect to the transformed variable $\bar{S}(j,\xi)$. The solution of Equn 45 yields:

$$\bar{S}(j,\xi)=P^*\frac{j\omega}{\left(\xi^2+j^2\omega^2\right)\left(\xi^2+\Omega_{(j)}^2\right)} \tag{46}$$

Taking into account the following property [10] of an inverse Laplace transform:

$$L^{-1}\left\{\frac{1}{\left(\xi^2+j^2\omega^2\right)\left(\xi^2+\Omega_{(j)}^2\right)};\xi\to t\right\}=$$
$$\frac{1-\cos j\omega t}{j^2\omega^2}-\frac{1-\cos\left(\Omega_{(j)}t\right)}{\Omega_{(j)}^2} \tag{47}$$

the variable $\bar{S}(j,\xi)$ in Equn 46 can be inversed, yielding:

$$S(j,t)=P^*\left[\frac{1-\cos j\omega t}{j^2\omega^2}-\frac{1-\cos\left(\Omega_{(j)}t\right)}{\Omega_{(j)}^2}\right] \tag{48}$$

Then, with the aid of Equn 29, the hoop stress $\sigma_{yy}(x,t)$ can be derived as follows:

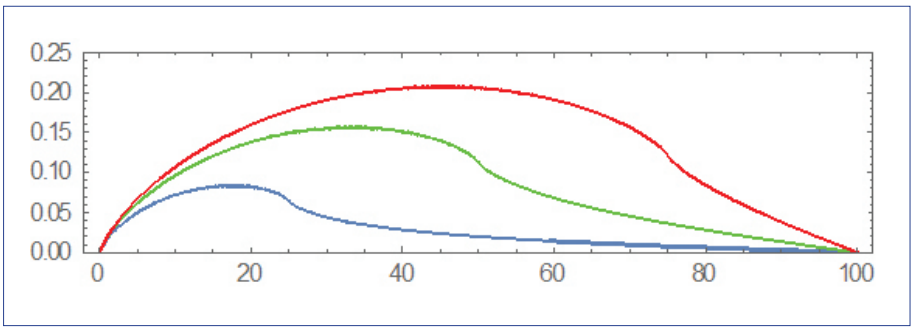

Fig.2. Dynamic radial displacement of the pipe's wall for three time instants after a sudden close of the end valve (blue: $t_o/4$ = 0.02535 sec; green: $t_o/2$ = 0.0507 sec; red: $3t_o/4$ = 0.07605 sec).

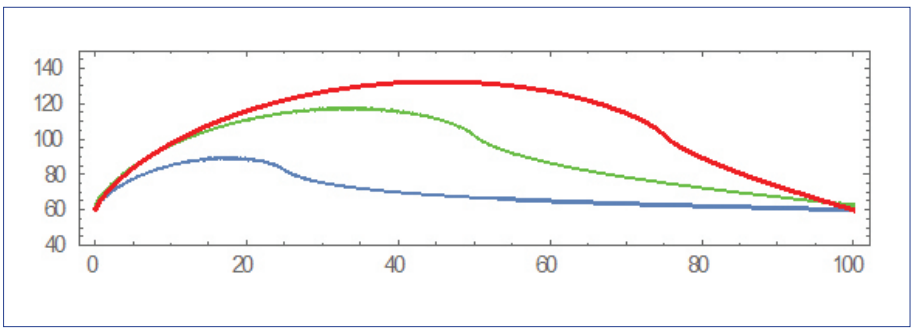

Fig.3. Hoop stresses on the pipe wall for three time instants after a sudden closure of the end valve (blue: $t_o/4$ = 0.02535 sec; green: $t_o/2$ = 0.0507 sec; red: $3t_o/4$ = 0.07605 sec).

$$\sigma_{yy}(x,t) = \frac{2P^*}{L}\sum_{j=1}^{\infty}\left\{\frac{1-\cos j\omega t}{j^2\omega^2} - \frac{1-\cos\left(\Omega_{(j)}t\right)}{\Omega_{(j)}^2}\right\}\sin\frac{j\pi x}{L} \quad (49)$$

Implementation of the model

A short steel pipeline with length L = 100 m, diameter $2R$ = 1.20 m, and wall thickness h = 10 mm, is used to convey water with density ρ = 1000 kg/m^3, bulk modulus of elasticity K = 219 x 10^7 N/m^2, and static pressure p_{st} = 60 MPa. Assuming that the steady-state flow speed is u = 0.1 m/s, a sudden stop of the flow happens. Taking into account that the modulus of elasticity of the steel is E = 210 GPa and the Poisson's ratio is ν = 0.3, the flexural rigidity D and the parameter P^* can be calculated from Equns 13 and 38 respectively, yielding D = 19,232 Nm and P^* = 2.07115 x 10^{12} N^2/m^6. Using Equns 33-35, the functions $\omega(j)$ and $\Omega(j)$, and the parameter ω, can be derived as:

$$\omega_{(j)} = 0.0432811\, j^2 \quad (50)$$

$$\Omega_{(j)} = \sqrt{5.8333x10^8 + 0.00187325\, j^4} \quad (51)$$

and

$$\omega = 30.9844 \text{ sec}^{-1} \quad (52)$$

The velocity α of the pressure-wave travel is calculated from Equn 2 yielding α = 986 m/s. Taking into account Equn 17, Equn 49 can be used for the derivation of the dynamic radial displacement $w(x,t)$ for several time instants, namely $t = t_o/4$, $t = t_o/2$, and $t = 3t_o/4$, where to is the time required the pressure wave to travel the length of the pipe, i.e. to = L/α = 0.1014 sec. Graphical representation of the modes of radial deformation for the above time instants is demonstrated in Fig.2, showing that a radial dilatation of the pipe's cross section is moving from its right-hand end towards to the left.

Figure 3 demonstrates the distribution of the hoop stresses along the pipe's length, and from Figs 2 and 3 it can be shown that the maximum hoop stress (dynamic plus static) is 133 MPa, and the maximum dynamic radial displacement is 0.26 mm. Both maximum values are located at the middle of the pipeline when $t = 3t_o/4$ = 0.07605 sec.

Figure 4 demonstrates the hoop-stress distribution along the pipeline for three

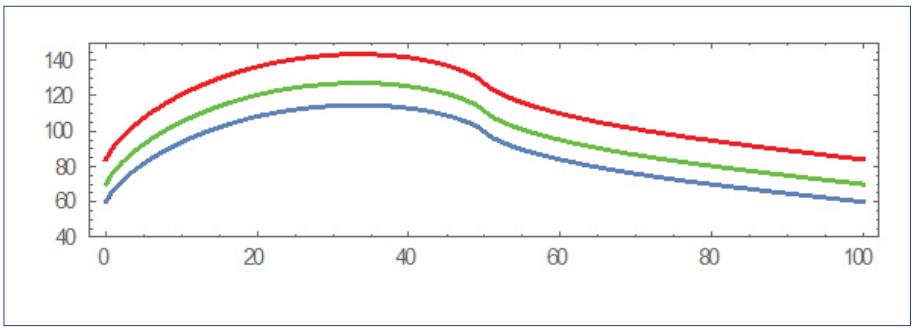

Fig.4. Hoop-stress distribution for three different diameters when the pressure wave front is located in the middle of the pipe (blue: 2R = 1.2 m; green: 2R = 1.4 m; red: 2R = 1.6 m).

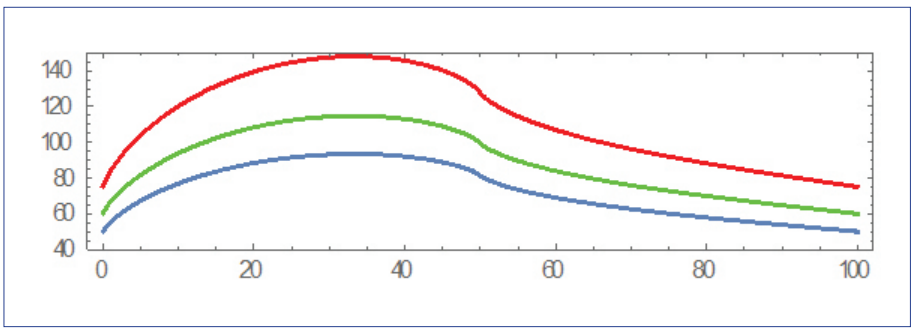

Fig.5. Hoop-stress distribution for three different wall thicknesses when the pressure wave front is located in the middle of the pipe (blue: h = 120 mm; green: h = 10 mm; red: h = 8 mm).

values of the diameter, namely 1.2 m, 1.4 m, and 1.6 m, when $t = t_o/2 = 0.0507$ sec, while Fig.5 shows the results of the effect of the wall thickness on the dynamic hoop stress. It should be noticed that since σ_{yy} depends on $1/j^2$, the convergence of the series given in Equn 49 is rapid. For more than 100 members of the series, the change in the results is negligible; therefore, the value j =100 is adopted. Note that all the mathematical calculations and graphics in this paper have been performed using Mathematica [11].

Conclusions

1. An analytic model for approximate estimation of the hoop-stress increase in pipelines subjected to fluid-hammer conditions has been derived.

2. The model takes into account the pressure oscillations and the elastic properties of steel. The solution of the derived differential equation has been based on finite Fourier and Laplace transforms.

3. Implementation of the model in a representative example has been provided. The results indicated that:

(a) The location of the maximum radial displacement and maximum hoop stress is different from the location of the pressure-wave front. In the example given, the maximum values of the total hoop stress and radial displacements are 133 MPa and 0.26 mm, respectively. The above values have been calculated for $t = 3t_o/4 = 0.07605$ sec.

(b) The increase of the pipe diameter yields an increase of the dynamic hoop stress. For an increase of the diameter by a factor of 1.6/1.2 = 1.33, the corresponding factor of increase of the maximum hoop stress is 145/155 = 1.26.

(c) The increase of the wall thickness yields a rapid decrease in the dynamic hoop stress because the flexural rigidity D depends on h^3. For an increase of the thickness by a factor 1.2/0.8 = 1.5,

the corresponding factor of decrease of the maximum hoop stress is 93/150 = 0.6.

References

1. D.G.Pavlou, Pressure-wave propagation in multi-layered fibre-reinforced polymeric pipelines due to hydraulic hammer. J.Pipe. Eng., 13, (1) (2014).
2. Idem, Composite materials in piping applications. Destech Publications, (2013).
3. N.Joukowsky, Über den hydraulischen stoss in wasserleitungsröhren, Mémoires de Académie Impériale des Sciences de St.-Pétersbourg, Series 8, 9, (5) (1990) 1-71.
4. J.P.Frizell, Pressures resulting from changes of velocity of water in pipes, Trans ASCE, 39, Paper 819, (1898) 1-18.
5. L.Allievi, Teoria generale del moto perturbato dell' acqua nei tubi in pressione (colpo d' ariete). Annali della Societá degli Ingegneri ed Architetti Italiani, 17, (5) (1902) 283-325.
6. M.S.Ghidaoui, M.Zhao, D.A.McInnis, and A.H.Axworthy, A review of water hammer theory and practice. App. Mech. Revs, 58, (2005) 49-76.
7. A.P.Boresi and R.J.Schmidt, Advanced mechanics of materials, John Wiley & Sons, (2003).
8. L.Frýba, Vibration of solids and structures under moving loads, Thomas Telford Publications, (1999).
9. S.P.Timoshenko and S.Voinowsky-Krieger, Theory of plates and shells, McGraw-Hill, (1959).
10. A.P.Prudnikov, Y.A.Brychkov, and O.I.Marichev, Integrals and Series, Vol. 5: Inverse Laplace transforms, Chapter 2. Taylor & Francis, London, (2002).
11. www.wolfram.com/mathematica/?source=nav

Listing of forthcoming industry events *(continued from p24)*

IoT in Oil and Gas
13-14 September 2017
Houston, TX, USA
iotinoilandgas.com
Exploring the latest developments of IoT in oil and gas.

CANWELD EXPO&CONFERENCE 2017
13-14 September 2017
Montréal, QC, Canada
canweldexpo.com
It's annual event for the welding, fabricating and finishing industry.

Pipeline-Pipe-Sewer Technology Conference and Exhibition (PPST)
17-19 September 2017
Egypt
www.pipelinepipesewer.com
The Pipeline-Pipe-Sewer-Technology Conference and Exhibition (PPST), organised by the EITEP, is a conference and exhibition on oil, gas water and wastewater transportation in Africa and the Middle East.

14th Beijing International Construction Machinery Exhibition & Seminar
20-23 September 2017
Beijing, China
www.e-bices.org
BICES/IVEX is a world leading exhibition in fields of construction machinery, building material machinery, mining machinery and commercial vehicles. The BICES show has a glorious history of 20 years and is held every 2 years. It endeavors to show the latest equipments, products, services and technologies in the industry.

Intersolar Middle East
25-27 September 2017
Dubai World Trade Centre, UAE
www.intersolar.ae
It is the key event in the Middle East dedicated to the solar industry. The conference is a premier networking platform and has a focus on established, emerging and the 'untapped' markets in the MENA region, PV Power Plants, Best Practices, Financing and Business Models. Since being founded, Intersolar has become the most important platform for the global solar industry.

Future Oil & Gas Agenda
27 September 2017
UK
www.futureoilgas.com
The business conference that brings together oil majors and technology innovators with financiers and investors at a high level conference with formal meetings and network sessions.

continued on p64

Structural analysis of vertical storage tanks using new approaches to determine their safe operational life

by D.A. Neganov

Centre for Steel, Strength Calculations, Welding, and Metals, Pipeline Transport Institute, Moscow, Russian Federation

THIS PAPER PRESENTS Transneft PJSC's requirements for carrying out technical evaluation and numerical calculation of the stress-strain state in vertical steel tanks as a fundamental constituent part of establishing their technical condition. Basic methods are discussed for conducting testing and studies of metals and corrosion-protection coatings in tanks. The main directions for developing the system for evaluating the condition vertical steel tanks are described.

Key words: vertical steel tanks, evaluation of technical condition, technical assessment, stress-strain state, laser scanning.

GUARANTEEING RELIABLE, SAFE, AND accident-free tank operations is considered one of the most important constituent parts of the pipeline transportation system, and requirements for this are stipulated in the Russian Federation's legislation 116 - FZ (Federal Law) *On the industrial safety of hazardous production facilities*. These requirements are met by maintaining the safety of tanks' operation, which is in turn strengthened by the requirements of federal laws, technical regulations, and national and industry standards. The requirements of these regulatory documents can be combined in one system: evaluating the technical condition of vertical steel tanks.

The constant improvement to instruments and methods of carrying out technical assessments, and the use of computer modelling, are essential components for evaluating the technical condition of vertical steel tanks (hereafter VST) in order to ensure their necessary reliability is maintained, and the costs for inspection, reconstruction, and repair are optimized.

Evaluating a VST's technical condition

The evaluation of the technical condition involves a set of measures including technical assessment and the determination of safe service life, both for tank elements with defects and for the tank as a whole; a general diagram showing how the evaluation of a VST's technical condition is carried out is shown in Fig.1.

Technical assessment of VSTs

The basis for evaluating a tank's technical condition is the initial data which are obtained from the results of technical inspections and analyses. The technical assessment is a combination of measures to determine the tank's technical condition, character, and the location and causes of any defects found; and to provide data

Author's contact details
Email: neganovda@niitnn.transneft.ru

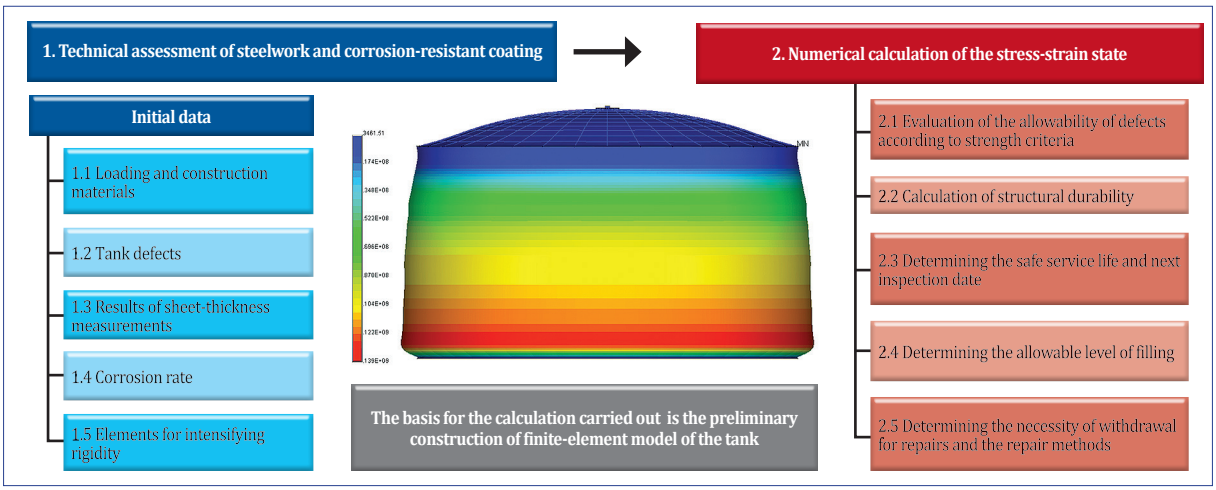
1. Technical assessment of steelwork and corrosion-resistant coating
2. Numerical calculation of the stress-strain state
Initial data
1.1 Loading and construction materials
1.2 Tank defects
1.3 Results of sheet-thickness measurements
1.4 Corrosion rate
1.5 Elements for intensifying rigidity
The basis for the calculation carried out is the preliminary construction of finite-element model of the tank
2.1 Evaluation of the allowability of defects according to strength criteria
2.2 Calculation of structural durability
2.3 Determining the safe service life and next inspection date
2.4 Determining the allowable level of filling
2.5 Determining the necessity of withdrawal for repairs and the repair methods

Fig.1. Evaluating the technical condition of VSTs.

for subsequent analysis, with the aim of allocating repairs and/or establishing the tank's safe service life until the next time such measures are conducted.

The technical assessment of tanks (Fig.2) can be divided into partial technical assessment – where the tank is not withdrawn from operation – and full technical assessment, where the tank is withdrawn from operation for a period from 137 to 254 days, and the tank is cleansed from oil and oil products.

The main methods of conducting the assessments are:

-
- studying the design and technical documentation for the tank;
- external examination of the structure and the corrosion-protection coating;
- geodesic survey, in order to determine any discrepancies between the tank's structure and its design;
- acoustic-emission inspection;
- visual inspection;
- ultrasonic thickness gauging;
- non-destructive testing (NDT) of the parent metal using ultrasonic testing (UT) with phased-array technology (PAT), and magnetic testing (MT);
- NDT of welds using radiographic testing, UT, leak-detection testing, and dye-penetrant testing;
- checking the condition of the corrosion-protection coating;
- inspection of the foundation and substructure of the tank.

These methods are constantly being improved. One example of this improvement can be seen in the introduction of an ultrasonic testing system equipped with a roller PAT sensor by Transneft PJSC (Public Joint Stock Co). This system is used to measure the remaining thickness of the bottom plate sections with corrosion damage, detected as a result of MT, as well as to inspect areas which cannot be reached by MT. This substantially increases the probability of corrosion defects being detected.

The use of laser scanning is another of the more-recent trends in carrying out inspections and in creating computer models of tanks using real geometry, and with subsequent calculation of the stress-strain state. This has several advantages in comparison to other techniques. The main advantages of laser scanning are high automation, which avoids errors connected with human factors; a high level of accuracy and productivity in surveying; and the possibility of conducting work in low lighting with a high level of detail and three-dimensional visualization.

Laser scanning can be conducted during partial as well as during full technical assessments of VSTs in order to obtain the spatial coordinates of the bottom, wall, and top surfaces of the tank. This

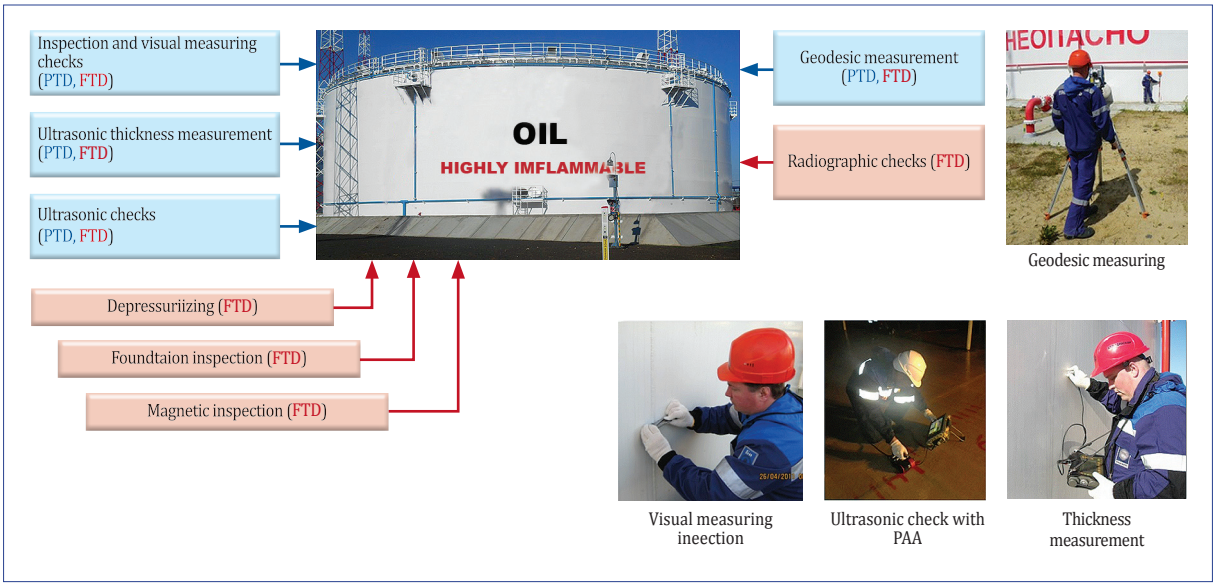

Fig.2. Technical assessment for VSTs.

forms the data set which can be used to measure deviation from the vertical, the level of the annular bottom plate, and to make stress-strain state calculations, among other attributes.

Laser scanning (Fig.3) is performed using laser stations which record separate scans that are subsequently combined to form an integrated point cluster. After recording, this cluster is exported into a polygonal model, which is in turn processed by software tools and transformed into a surface on which contours and borders of curvature are marked out. A NURBS surface is then built and generated, and saved in formats used by the software for modelling structures' stress-strain state (IGS, IGES, CATIA, etc.).

The regulatory documentation governing technical assessment is constantly being improved. The guideline document *Trunk pipeline transportation of oil and oil products: rules for technical assessment of tanks* came into force in Transneft PJSC in 2016, and contains the following basic innovations:

- The interval between a tank's technical assessment is increased, on the condition that additional non-destructive tests are performed during construction. This allows the cost of diagnostic work during a tank's operation to be reduced.
- The document takes into account modern inspection methods, including ultrasonic testing of metal structures UT with PAT.
- Assessment requirements are established for tanks equipped with heat-insulating systems.

Fig.3. VST laser scanning.

1. Laser scanning

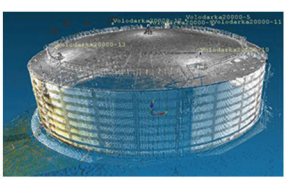

2. Point cluster of the stationary roof

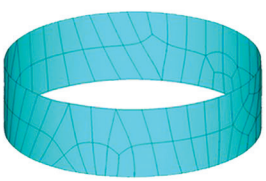

3. Geomentc model of the wall of tank VSTP-20000

4. Finite-element model of tank wall

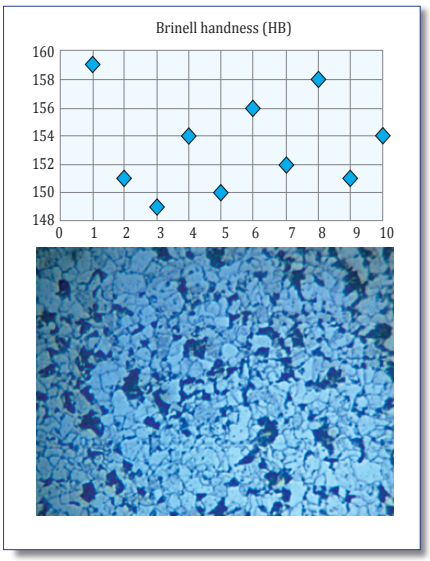

Fig.4. Evaluating the hardness and other parameters of the structure.

Determining the mechanical properties of materials in a tank's structure

One of the requirements for evaluating a tank's technical condition is for the inspection crew to determine the mechanical properties of the steels in the tank's structure, and their chemical composition, without cutting-out samples.

Determining the chemical composition and steel grade of metal structures under field conditions is performed using mobile spectrum analysers.

Fig.5. and studies of sections of tank metalwork.

The strength characteristics of a tank's metal structure are non-destructively determined by the Brinell hardness test (using mobile dynamic hardness testers).

Determining quantitative structural parameters (grain size, pearlite volume content, etc.) is performed using both portable and stationary optical microscopes (Fig.4), as well as the replica method.

Based on data for the metal's chemical composition, hardness, grain size, and dispersed particle parameters, the mechanical characteristics of a tank's metal structures are determined. Data for the mechanical properties obtained in these ways are used as initial data in evaluating the tank's technical condition.

In addition to evaluating the tank's metal structure without cutting-out samples, tests and studies of metal structural elements using cut-out samples are carried out in the Pipeline Transport Institute's materials'-testing laboratory during full technical assessments. The characteristics thus determined include: strength and ductility of the parent metal in the structure and of the metal in welded joints, through tensile testing according to GOST 1497 and GOST 6996; impact toughness, through impact bending tests according to GOST 9454 and GOST 6996 [1-3] with subsequent evaluation of the proportion of the ductile component in the fracture; and quantitative metallographic micro-structure analysis and electron-microprobe analysis of dispersed particles (Fig.5).

The mechanical characteristics of steels in tank metal structures obtained in this way are used for subsequent calculations of strength, stress-strain state, and service life.

Determination of the mechanical and chemical characteristics is conducted as part of the innovative work entitled *Fundamental research into improving the theory and practical calculations of durability and safe service life for pipelines, tanks, and metal structures in Transneft PJSC's facilities.*

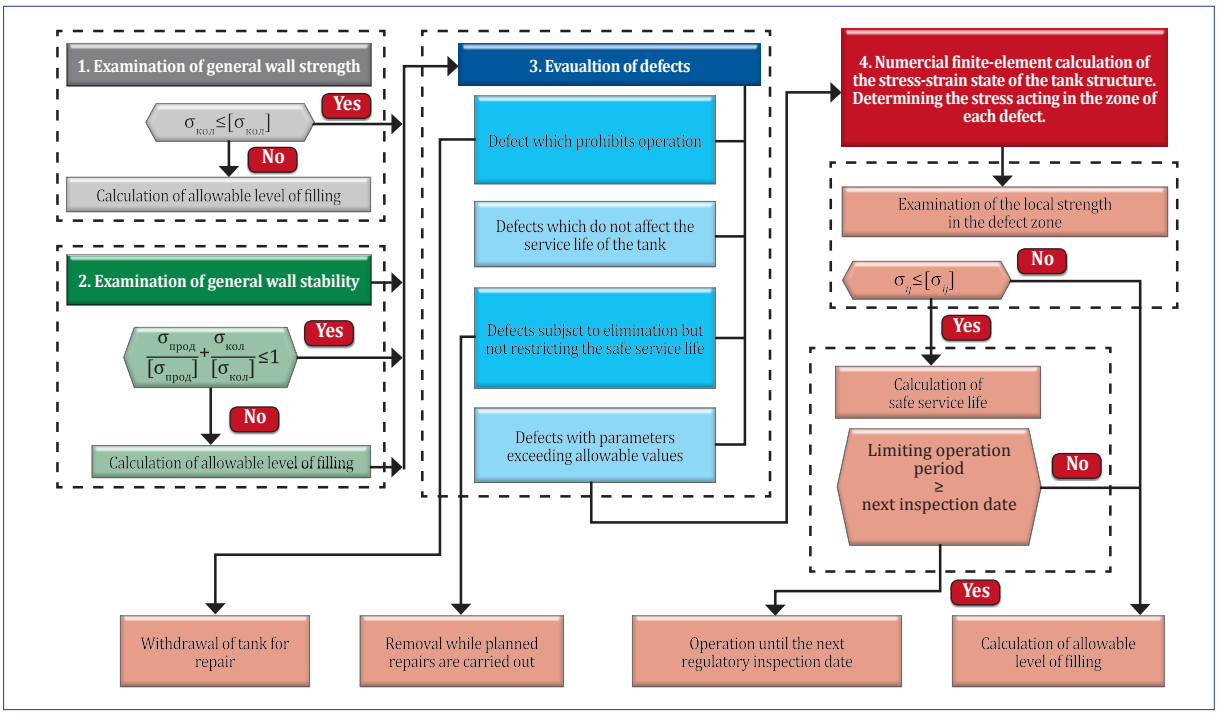
1. Examination of general wall strength
$\sigma_{кол} \le [\sigma_{кол}]$
Yes
No
Calculation of allowable level of filling
2. Examination of general wall stability
$\frac{\sigma_{прод}}{[\sigma_{прод}]} + \frac{\sigma_{кол}}{[\sigma_{кол}]} \le 1$
Yes
No
Calculation of allowable level of filling
3. Evaualtion of defects
Defect which prohibits operation
Defects which do not affect the service life of the tank
Defects subjsct to elimination but not restricting the safe service life
Defects with parameters exceeding allowable values
4. Numercial finite-element calculation of the stress-strain state of the tank structure. Determining the stress acting in the zone of each defect.
Examination of the local strength in the defect zone
$\sigma_{ij} \le [\sigma_{ij}]$
No
Yes
Calculation of safe service life
Limiting operation period ≥ next inspection date
No
Yes
Withdrawal of tank for repair
Removal while planned repairs are carried out
Operation until the next regulatory inspection date
Calculation of allowable level of filling

Fig.6. Diagram of how safe service life and conditions for safe operation are calculated for VSTs.

The selection of equipment and methodology development to study tank metal structures material is conducted as part of the design and development work under the project *Design and development of laboratory facilities for studying steels used to manufacture pipe products, tanks, and metal structures for the Transneft organizations' systems*.

Numerical calculation of the stress-strain state in a VST

Where there are deviations from design geometry, formed during long-term operation due to the influence of climate or foundation settlement under cyclic loading, the stress-strain state of tank walls cannot be reliably calculated using analytical methods in accordance with current building rules and regulations.

To determine the stress-strain state of tank walls in these cases, calculations are performed using the finite-element methods using, for example, the software packages Ansys and SCAD Office.

The Ansys software package used by Pipeline Transport Institute is the most-effective tool for computer modelling and tank-strength calculations, as it allows the use of results from the data processing of high-precision laser scanning in a wide spectrum of data formats, thus forming a link between assessment of the technical condition and the definition of conditions for subsequent safe tank operation.

The results of stress-strain state calculation of a tank wall are used:

- to determine the maximum allowable level of filling, with the aim of extending the tank's safe service life (according to the results of partial technical assessment);
- to calculate the subsequent safe service life of a tank with defects in the parent metal and in the welded joints, taking into account actual stress-strain state (according to the results of the full technical assessment).

The algorithm for conducting a technical condition evaluation on a tank enables the safe service life to be calculated and safe operating conditions to be

determined. The numerical calculation of the stress-strain state, strength and stability testing of the tank walls, and the evaluation of the acceptability of any defects revealed during the technical assessment, are conducted according to the diagram presented in Fig.6.

As a result of the stress-strain state calculation, the stresses acting in the area of any detected defects are determined, and a prognostic calculation is made for the safe service life of the tank wall with these defects. Where it is not possible immediately to withdraw the tank from operation, restrictions are established for permissible operation until scheduled repair work can be carried out.

After the calculations are made in accordance with the rules for tank repair and reconstruction, the components which are to be repaired, and the methods of their repair, are identified. The main goal is to identify the repair locations and their minimum extent, or to provide for the replacement of defective components, guaranteeing defect-free future tank operation with minimal cost.

A clear example is the calculation of the actual load-bearing capacity of stationary roofs in vertical steel tanks with pontoons: 20,000 tanks exist with deviations from their design geometry, as a result of long-term operation, identified in the course of inspection of their technical conditions. According to calculated results, the possibility and method of repair have been determined (for example, by strengthening individual elements of the load-bearing frame, or replacing roof shields) in order to restore the roofs' load-bearing capacity (Fig.7) and the tanks' future safe operation within their design parameters.

Methods of evaluating the technical condition of tanks are constantly being improved. In organizations in the Transneft group, tanks with stationary domed aluminium roofs are used, and are subject to the influence of climatic factors, such as drops in temperature and uneven snow loading. In order to determine the conditions for the safe operation of these roofs, an appropriate procedure has been developed by the Pipeline Transport Institute which is defined in the document *Trunk pipeline transport of oil and oil products: evaluating the technical condition of domed aluminium roofs in vertical steel tanks for the storage of oil and oil products*.

In order to ensure that the conditions are met for the safe operation of domed aluminium roofs, annual monitoring and evaluation of their technical condition are performed, with recommendations being made for safe operating conditions in winter.

At present, the Pipeline Transport Institute is conducting research into two methodologies for calculating the effect of geometric defects on a tank's metal structure, namely:

- Computer modelling, development of a calculation procedure, and recommendations for ensuring the stability of tank walls during the cutting-out of sections and replacement with repair panels, taking into account the actual geometry and the impacts of wind and snow loading.

- The development of a procedure for calculating tank-wall stability, taking into account its actual geometry and evaluating the technical condition.

Up to now these procedures for calculating the integrity of tank metalwork do not exist in Russian or foreign regulatory documents, including at a federal level.

Study of corrosion-protection and thermal-insulation coatings

A research laboratory has been established at the Pipeline Transport Institute, furnished with modern testing equipment capable of carrying out both standard and special tests. The laboratory guarantees quality control for

1. Load-bearing capacity of a stationary roof with deviation from design geometry before repairs are carried out

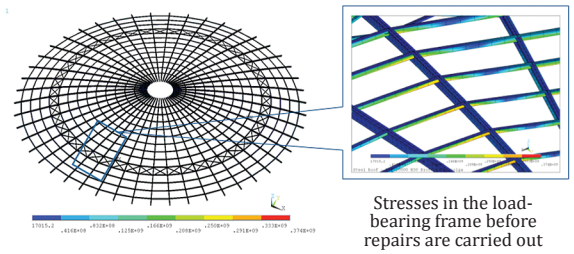

Stresses in the load-bearing frame before repairs are carried out

Parameter	Value/limit value	Conclusion: load-bearing capacity
Maximum height difference between adjacent radial beams in the load-bearing frame	131 mm	Not guaranteed. A 20% decrease in snow load or repair is required.
Maximum stresses in the load-bearing frame	374 MPa / 259 MPa	
Criteria for ensuring the strength of the beams in the load-bearing frame	1.74 / 1.00	

2. Load-bearing capacity of a stationary roof after repairs are carried out

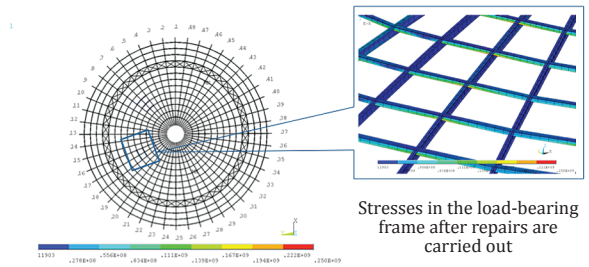

Stresses in the load-bearing frame after repairs are carried out

Parameter	Value/limit value	Conclusion: load-bearing capacity
Maximum height difference between adjacent radial beams in the load-bearing frame	41 mm	Guaranteed
Maximum stresses in the load-bearing frame	250 MPa/ 259 MPa	
Criteria for ensuring the strength of the beams in the load-bearing frame	0.90 / 1.00	

Fig.7. Calculating the actual carrying capacity of stationary roofs and an example of roofs in VSTP-20000 tanks.

the corrosion-protection and thermal-insulation coatings – of various types and from various manufacturers – by conducting independent tests to confirm the actual characteristics of products used in the Transneft PJSC system.

In addition, the laboratory is supplied with qualified corrosion-protection coating (CPC) and thermal-insulation coating (TIC) inspectors and specialists who, as members of the inspection crews, carry out comprehensive assessments of the condition of tanks' corrosion-protection coatings, entering details of any detected defects into a single coordinate system.

In the period from 2013 to 2015, the technical condition of the corrosion-protection coating in 122 tanks was evaluated, and this revealed discrepancies between their qualitative indicators and the regulatory requirements. Repairs of the defects found in the corrosion-protection coatings of the tanks that were under guarantee were made at the expense of contractors who had carried out the painting. Further tests are planned for 30-40 tanks annually with corrosion-protection coatings.

The main indicators controlling the quality of the corrosion-protection coatings for tanks in operation are appearance, thickness, adhesion, and dielectric integrity. The expert evaluation currently being conducted allows the following results to be obtained in the short term:

- identification of CPC defects in tanks under guarantee and elimination of the defects at the contractor's expense;
- monitoring the formation and development of defects, and undertaking effective remedial work;

Fig.8. Distribution of samples in OPSs in various climatic regions in GOST 16350 [4].

Distribution of aamples in oil-pumping stations (OPSs) in various climatic regions for GOST16350							
Moderate	Moderately humind	Moderately warm	Moderately warm with a mild winter	Very cold	Cold	Moderately cold	Maritime
4	1	2	3	2	4	5	7

- developing an algorithm for CPC selection during tank construction and extensive repairs, and introducing new materials.

In the course of research into corrosion at Transneft PJSC's facilities, the problem of determining the actual rate of atmospheric corrosion, depending on the geographical location of the operating facilities, is being investigated (Fig.8). Over a period of five years, surveys will be conducted at 28 oil-pumping stations with tank farms, and measurements corrosion rates will be made, taking into account both the natural and climatic factors. In this way, a correlation will be made between the environmental impact on the CPC and the laboratory tests, in order to ensure that the test characteristics simulate, both in duration and intensity, the impact of various corrosive conditions on the coated samples. Ultimately, a well-founded choice of external CPC will be able to be made based on atmospheric corrosion activity.

Proposals for areas of co-operation in evaluating the technical condition of VSTs

Various proposals for evaluating the technical condition of vertical steel tanks have been prepared by the Pipeline Transport Institute which could be used in organizations operating VSTs:

- to develop a programme of technical assessment, aimed at evaluating VSTs technical condition in order to determine the length and conditions of safe future operation;

- to develop the necessary regulatory documentation for conducting the following work:
  - rules for technical assessment;
  - procedure for laser scanning;
  - procedure for evaluating technical conditions;
  - procedure for testing the technical conditions in order to extend the period of operation until the next planned technical inspection.

- to support the technical assessment and the technical-condition evaluation (TCE);

- to prepare reports of the TCE based on results of technical assessment and technical condition testing;

- to develop rules for the reconstruction and repair, taking into account the results of the technical assessment.

Conclusions

The approaches to evaluating the technical conditions of the tanks used at all Transneft PJSC's facilities are examined, as well as the approaches requited to determining their safe service lives. The standards developed for evaluating the tanks' technical condition, and laboratory testing of samples from tanks' metal structures, corrosion-protection, and thermal-insulation coatings, have allowed Transneft PJSC to reduce the frequency of ttank inspections, as well as reducing the amount of materials used for vertical steel tank construction. For future work, proposals for modernizing the evaluation process for vertical steel tanks have been prepared.

References

1. GOST 1497-84. Metals. Tensile test methods.
2. GOST 6996-66. Welded joints. Mechanical properties testing methods.
3. GOST 9454-78. Metals. Impact bending test method under reduced, room and elevated temperature.
4. GOST 16350-80. Climate of the USSR. Regionalism and statistical parameters of climatic factors for technical purposes.

A study of the impact of low ambient temperatures on weld technology and the properties of welded joints in trunk pipelines

by N.G. Goncharov*[1], O.I. Kolesnikov[1], A.A. Yushin[1], and O.I. Filippov[2]

1 Laboratory of Welding, Pipeline Transport Institute, Moscow, Russian Federation

2 Transneft PJSC, Moscow, Russian Federation

AT LOW TEMPERATURES the operating capability of welded joints in pipe steels deteriorates: hardness and ultimate tensile strength increase; ductility and impact toughness decrease. The implementation of welding technologies at low temperatures requires additional measures. This article presents the results of research into solutions to the problem of reliability enhancement in welded joints, operating at low temperatures, in the JSC Transneft pipeline system in the Far North of the Russian Federation.

As a result of this work, revised temperatures and their rates of change have been established and substantiated, in the form of optimized thermal welding cycles. It has been found that the properties required of welded joints are ensured by achieving a specific structure, eliminating the martensite component. Numerical values for the cooling rate are substantiated within the martensite-decomposition temperature range.

Key words: welding, welded joint, low temperatures, mechanical properties, thermal welding cycle, strain capacity, heat-affected zone, martensite.

OVER THE PAST TWO DECADES, Transneft JSC has constructed a number of pipelines in the Far North of the Russian Federation, including the Eastern Siberia – Pacific Ocean pipeline, and the Zapolyarie – Purpe oil pumping station pipeline. The total length of these lines is over 3,000 km; installation and welding has been carried out at ambient temperatures as low as -40°C [1, 2, 6]. For the construction of these oil pipelines, pipes of K56-K60 grade steel have mainly been used, with diameters of 1020-1220 mm (40-48 in) and wall thicknesses of 11-27 mm.

Currently, for work taking place in sub-zero temperatures, the approach to welding technology commonly used assumes that preheating the pipe ends to temperatures in the range of 100-150°C is sufficient to provide the correct temperature conditions for welding. However, as practice has shown, welding technology in low-temperature conditions differs from the existing methods.

Domestic and foreign experience in pipeline construction and repair in the Far North has shown that at low temperatures (below 0°C), the metallurgical processes in welding have a number of peculiarities,

*Lead author's contact information
Email: goncharovng@niitnn.transneft.ru

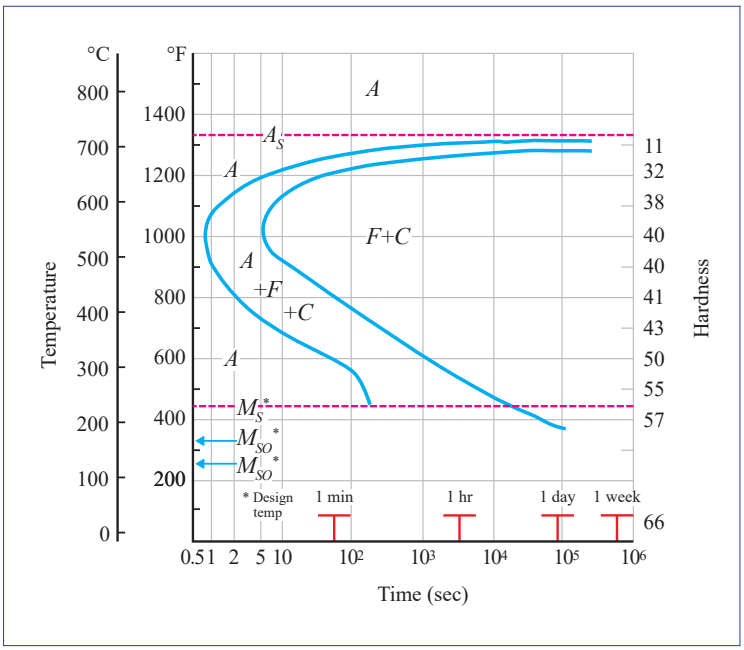

Fig.1. Isothermal diagram of transformation during cooling of steel with an S-curve at the start and end of austenite decomposition.

both in weld-pool crystallization, and in selecting the welding parameters, which determine the mechanical properties of the welded joint as a whole. Therefore, in order to obtain a good welded joint, it is very important to select the correct thermal welding cycle, so as to ensure that an optimal structure is obtained in the welded joint [1, 2].

At low temperatures, the operating capability of welded joints in pipe steels deteriorates: hardness and ultimate tensile strength increase; ductility and impact toughness decrease. The main indicator of the operating capability of welded joints is the ductile-to-brittle-transition temperature – the temperature at which the impact toughness sharply decreases. The lower this temperature is, the more reliable the welded joint becomes.

During crystallization of the weld-pool metal and the base metal at low temperatures, an increased cooling rate is observed in the heat-affected zone (HAZ). As a result, the migration of gases and oxides from the molten metal to the surface is impeded, which increases the content of hydrogen, oxygen, nitrogen, and non-metallic inclusions in the weld metal, and can lead to the formation of pores and hot cracks.

During welding at low temperatures, the possibility of hot cracks forming in welded joints is further increased with the increase in the speed of elastic-plastic deformation in the critical temperature range, where the heated metal is already in a brittle state. The probability of cold cracks forming in the HAZ is particularly high in pipe joints with wall thicknesses of 16 mm and above.

In winter conditions, the welding and technological properties of the electrodes deteriorate, mainly because of moisture intrusion, leading to additional porosity in the joint metal. Increased heat removal during welding of thick-walled pipes worsens weld penetration in the base metal, which leads to incomplete penetration [1, 3-5, 8].

As the ambient air temperature decreases, the weld joint metal's ductility and its crystallization crack resistance fall. The working conditions of the equipment deteriorate, which increases the probability of joint defect formation. The probability of brittle fracture at butt joint during its welding or repair increases [2, 8].

The main problem in low-temperature pipeline welding is the reliability assessment for the welding operation, and a most effective solution has been the development of additional operations to compensate for the effects of low temperatures. Specialists from the Pipeline Transport Institute and the Bauman Moscow State Technical University have conducted research analysing the effect of thermal welding cycle parameters on the metallurgical processes in the weld joint during its crystallization and, correspondingly, on the mechanical properties of the metal in the high-temperature zone at welding.

The object of the study was ring-type weld joints in K56-grade steel pipes, made using two technologies [8]:

- manual arc welding using basic coated stick electrodes, and the 'uphill' method;

- automatic FCAW-GS (flux-cored arc wire gas-shield) welding with the root weld made using GMAW (gas metal arc welding) and surface-tension-transfer technology.

The following sequence was used in carrying out this work:

- A review of regulatory requirements was conducted for the mechanical properties of welded joints (ultimate tensile strength, yield strength, elongation, impact toughness, and hardness level in the weld-joint zones).

- Based on these requirements for the mechanical properties, the requirements for the optimum structure of the welded joint were experimentally determined. The calculation of the temperature range for austenite decomposition was made using an S-curve (Fig.1). Different structures were experimentally obtained for a wide range of cooling rates in the decomposition temperature range from 0.1 to 300°C/s.

- Improved curves for non-isothermal austenite decomposition were plotted for three pipe-steel options (Fig.2). On the basis of these charts, an optimum heat cycle was formed for single-pass (Fig.3) and multi-pass welding (Fig.4) of K56 (K60) grade pipe steels.

- An analysis of structural transformations in weld joints was carried out for K56-grade steels with CE contents ranging from 0.29 to 0.43. The permissible martensite content was established for the HAZ, dependent on the carbon content of the steel and its maximum allowable hardness (Fig.5).

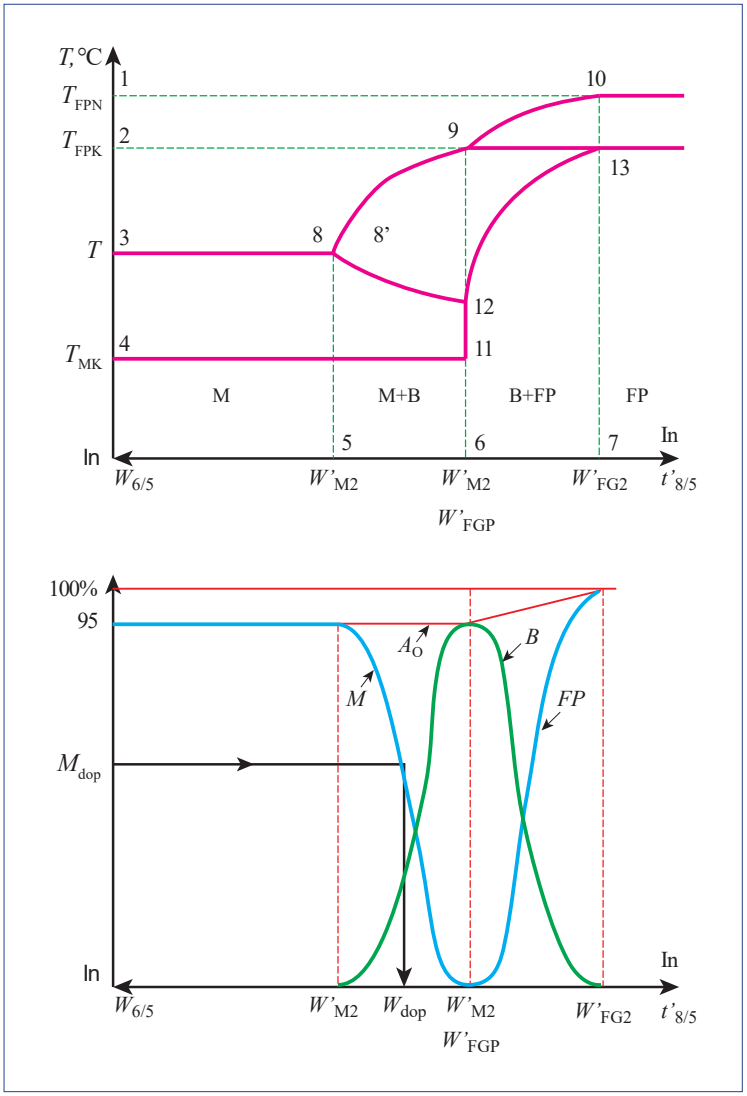

Fig.2. Standard schematic AAD (an-isothermal austenite decomposition) diagram for low-carbon low-alloyed steels.

T_{FP}, T_{FK}, T_{MN}, and T_{MK} — temperatures at the start and end of ferritic-perlitic (FP) and martensite (M) transformations;

W_{FP1}, W_{FP2}, W_{M1} and W_{M2} — critical cooling rates ($W_{6/5}$), at which 1 and 100% FP and 1 and 95% M are formed.

- A physico-mathematical model of the thermal processes during welding was developed to calculate the optimum thermal cycles.

- Key criteria were identified for developing a ranking system for these measures.

Studies have established that:

- The strength, plastic, and toughness properties of the metal at the joint and in the near-weld area directly depend on the structure of the metal. The best structure for the pipe and weld joint metal is a fine-

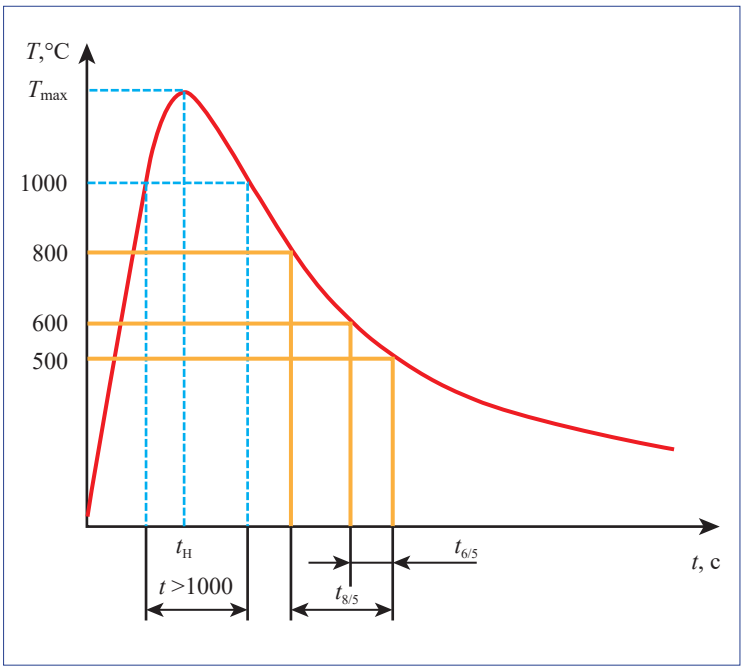

Fig.3. Welding thermal cycle in the heat-affected zone during single pass welding and its main parameters.

T_{max} — maximum heating temperature
T_n — time to reach maximum heating temperature
t >1000 — duration of stay at T > 1000
$t_{8/5}$ — time of cooling from 800 to 500°C
$t_{6/5}$ — time of cooling from 600 to 500°C;
$t_{6/5}$ — time of cooling from 600 to 500°C;
$w_{6/5} = 100/t_{6/5}$ — speed of cooling from 600 to 500°C ($w_{6/5} = 225/t_{8/5}$)

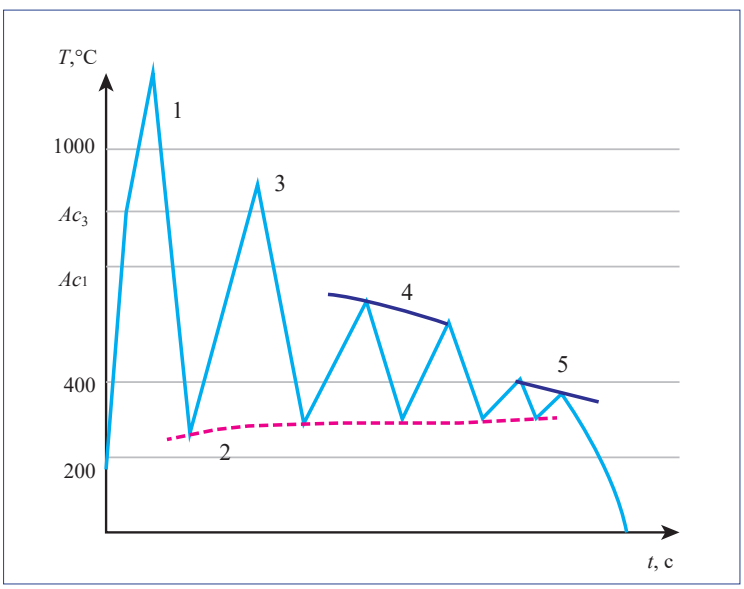

Fig.4. Thermal cycles in the heat-affected zone during multi-pass welding.

1 — tempering
2 — autoheating
3 — recrystallization and refinement of austenite grain
4 — annealing
5 — repeated heating

grained uniform ferritic-bainitic microstructure.

- The structure's impact on specific mechanical properties is determined by its morphology. The main characteristics which determine the morphology of the structure are: the carbon content in the metal, basic alloying and complex microalloying, the content of harmful impurities, the amount of quenching, the hardness of the metal, and the thermal welding cycle parameters.

- Analysis of structural transformations in welded joints for K56-grade steels with different chemical compositions (CE 0.29-0.43) showed that martensitic structure formation in the steel with higher carbon equivalent starts at lower cooling rates than in the steel with a higher carbon equivalent. Steel with higher carbon equivalent is more prone to quenching (Fig.5).

- The most effective technique of affecting the structure – and, accordingly, the properties of the metal – is the control of heat input by choosing the optimum thermal welding cycle, and the parameters that enable development this were determined. It was shown that the optimum thermal cycle shall provide the cooling rates 10-40°C/s within the temperature range 600-500°C. Also, the calculations showed that at hardnesses up to 240 HV10, the probability of quenched structures forming decreases sharply.

- The main criterion for the operating capability of welded joints functioning in low temperatures is impact toughness. When the pipe

metal grade increases, the requirements for impact toughness also increases.

- The calculated and experimental justification for temperature in the welding process, based on the permissible structural transformations in the welded joints and on the required mechanical properties, allowed the optimum (theoretical) thermal welding cycle which meets the requirements of structural transformations and welded joint properties to be obtained. In the case of a maximum CE content (up to 0.43) in the pipe steel, repeated heat treatment in the range of 600-500°C produces a decomposition of residual martensite. With a minimal CE content (from 0.29), the absence of martensitic structures is evident right after the first pass of the weld.

- It was experimentally confirmed that a ferritic-bainitic metal structure is formed when cooling rates of up to 40°C/s are observed, and quenched (martensitic) structures are absent, which gives impact-toughness levels not lower than 62 kJ/cm^2.

- It was also experimentally confirmed that the inter-layer temperature (inter-layer heating) not only affects the restricted cooling rate, but also ensures proper hydrogen diffusion, thereby lowering the probability of cold cracking [7].

- The criterion for brittle component content in the welded joint was established to be no more than 40%. Critical cooling rates were determined for the brittle component content, depending on the CE in the metal, the metal thickness, the welding method, and the ambient temperature.

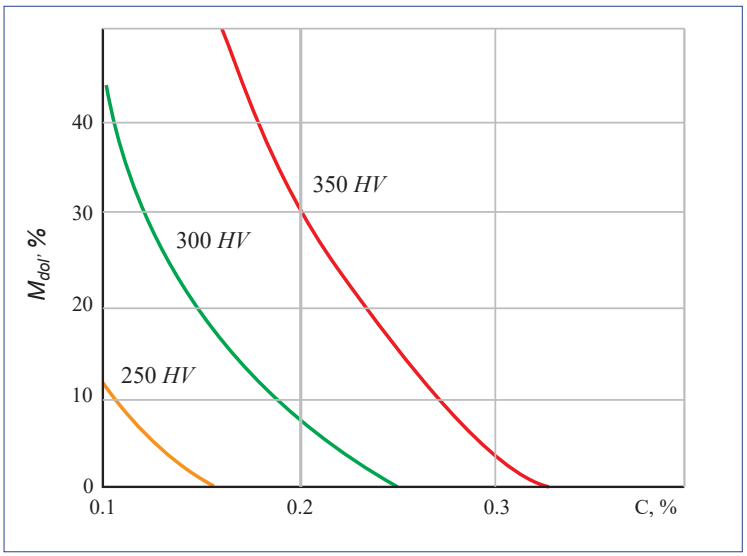

Fig.5. Allowable martensite content in the heat-affected zone dependent on the carbon content in steel and the maximum allowable hardness.

Main results

1 The results of this research show that the implementation of welding technologies at low temperatures in the range of 0°C to -50°C requires additional operations to regulate heat input to the metal. This is relevant for welding technologies such as manual arc welding and GMAW + FCAW-GS.

2 The calculated and experimental evidence for the temperatures required in the welding process were established based on analysis of the regulatory requirements for the properties of welded joints and of structural transformations in welded joints with a view to guaranteeing the required metal properties.

Data analysis showed that the strength, plastic, and toughness properties of the metal at the joint, in the HAZ, and in the near-weld area, directly depend on the metal's structure. The structure's effect on specific mechanical properties is determined by its morphology. The most effective technique for affecting the structure – and, accordingly the properties of the metal – is the control of heat input

Ambient air temperature, °C	Welding method	Thickness of pipe wall, mm	Compensatory measures at CE		
			up to 0.34 inclusive	from 0.35 to 0.41 inclusive	from 0.41 to 0.43 inclusive
From 0 and above	MAW [Manual arc welding]	up to 30	Preheating to 50°C		
	MW [Mechanised welding] + AFCW [Automatic flux-cored welding]				
From 0 to -10	MAW	up to 30	Preheating to 100°C		
	MW + AFCW				
From -10 to -20	MAW	up to 30	Preheating to 150°C and holding for no less than 10 mins		
	MW + AFCW				
From -20 to -30	MAW	up to 30	Preheating to 150°C and holding for no less than 10 mins		
	MW + AFCW	up to 30	Preheating to 150°C and holding for no less than 15 mins		
From -30 to -40	MAW	up to 12	Preheating to 150°C and holding for 20 mins + concurrent (inter-layer) heating to 50°C		
		from 12 to 21	Preheating to 150°C and holding for 20 mins + concurrent (inter-layer) heating to 50°C	Preheating to 150°C and holding for 25 mins + concurrent heating to 150°C	
		from 21 to 30	Preheating to 150°C and holding for 25 mins + concurrent heating to 150°C		
	MW + AFCW	up to 12	Preheating to 150°C and holding for 20 mins + concurrent (inter-layer) heating to 50°C		
		from 12 to 21	Preheating to 150°C and holding for 25 mins + concurrent heating to 150°C		
		from 21 to 30			

Table 1. The impact of low temperatures on welding thermal cycle parameters for various methods of welding.

by choosing the optimum thermal welding cycle.

It is established that ensuring a cooling rate of no more than 40°C/sec in the range 600-500 °C allows a ferritic-bainitic structure in the welded joint to be obtained, which guarantees impact toughness values at the required level.

3. A mathematical calculation model of thermal processes was developed for welding technologies such as manual arc welding and GMAW + FCAW-GS. The model was designed to obtain, by calculation, the numerical values for the main parameters for welding in low-temperature conditions.

4. The measures for obtaining optimum heat input into the metal were defined

From -40 to -50	MAW	up to 12	Preheating to 150°C and holding for 20 mins + concurrent heating to 50°C	Preheating to 150°C and holding for 25 mins + concurrent heating to 150°C
		from 12 to 21	Preheating to 150°C and holding for 25 mins + concurrent heating to a temperature of 150°C	*
		from 21 to 30	Preheating to 150°C and holding for 25 mins + concurrent heating to 150°C	*
	MW + AFCW	up to 12	Preheating to 150°C and holding for 25 mins + concurrent heating to 150°C	*
		from 12 to 21	Preheating to 150°C and holding for25mins + concurrent heating to 150°C	*
		from 21 to 30	*	
Note: * Welding is recommended to be carried out in shelters with control of the ambient temperature.				

Table 1 (*continued****).***

and ranked, taking into account ambient air temperature, welding method, weld-metal thickness, and carbon equivalent. A list of these is given in Table 1.

References

1. Zh.A. Poluzyan, A.G Mazel, Welding of main lines at low air temperatures. Construction of main lines and installation of gas and oil fields. VNIIST Works 30 Part 1 (1974) 262-331.
2. O.I.Kolesnikov, N.G. Goncharov, Welding of pipelines at low temperatures. Sci. and Technol. of Oil and Oil Product Pipeline Transport 2 (2011) 14–16.
3. O.I. Sleptsov *et al.*, Increasing welded structure strength for the North. Novosibirsk, Science. Siberian branch (1989) 223.
4. Yu.Ya.Meshkov, Physical aspects of the steel part cold brittleness issue. Strength of materials and elements of metal structures at low temperatures. Yakutsk, Publishing House of the Yakut Branch of the AS of the USSR, (1985) 66–74.
5. Welding Process Theory. Ed. by V.V. Frolov, Moscow, Higher School, (1988) 559.
6. I.E.Oskin, N.G.Goncharov, I.O.Kolesnikov, Requirements for welding materials for construction and repair of oil pipelines. Sci. and Technol. of Oil and Oil Product Pipeline Transport 4 (2011) 33–35.
7. E.L.Makarov, Cold cracks during welding of steel alloys. Moscow, Machine-Building (1981) 246.
8. Assessment of the impact of low ambient temperatures on welded joints of main pipelines. Report on research and development by Federal State Autonomous Institution Scientific and Training Center Welding and Testing of N.E. Bauman MSTU, Contract No. 743P/NIR/02-41/2014 dated 4/11/2014, Stage 2.

Listing of forthcoming industry events *(continued from p48)*

PetroChem Canada
27-28 September 2017
Sarnia, ON, Canada
petrochemcanada.com
Petrochem Canada brings together senior leaders in the petrochemical industry along with government officials, investors, regional development representatives and more. The industry experts will gather to discuss how to attract global capital investment to the region, current incentives to build, and the need for government policies to support diversification in the market.

IPLOCA 2017 Convention
25-29 September 2017
Mexico City, Mexico
www.iploca.com
IPLOCA's mission is to provide value to members through a forum for sharing ideas, engaging the industry and its stakeholders, facilitating business opportunities and promoting the highest standards in the pipeline industry.

SCHWEISSEN & SCHNEIDEN 2017
25-29 September 2017
Messe Düsseldorf Fairgrounds, Dusseldorf, Germany
www.schweissen-schneiden.com
SCHWEISSEN & SCHNEIDEN is the meeting place for experts and top decision makers of the joining, cutting and surfacing technology industry.

KUWAIT OIL & GAS SHOW
15-18 October, 2017
Mishref, Kuwait
kogs2017.com/
KOGS 2017 incorporates an international exhibition of oil and gas hardware and services and a broad spectrum technical conference programme. It serves all areas of the oil and gas industry; including petroleum geosciences, exploration & production and refining & petrochemical products and services.

LAGCOE 2017
24-26 October 2017
Lafayette, LA, USA
www.lagcoe.com
LAGCOE 2017 provides an access to state-of-the-art equipment, service, and technologies as well as technical presentations from worldwide leaders in the onshore and offshore oil and gas exploration and production industry.

Rio Pipeline Conference
24-26 October 2017
Rio de Janeiro, Brazil
www.ibp.org.br
Rio Pipeline Conference and Exposition aims at gathering professionals of technical and managerial level in search for knowledge on cutting-edge technologies and the best management practices in the area.

continued on p80

Geomechanical modelling of construction conditions for trunk pipeline underwater crossings

by D.R. Vafin*[1], D.A. Shatalov[1], and Z.Z. Sharafutdinov[2]

1 Linear Pipeline and Underwater Line Laboratory, Pipeline Transport Institute, Moscow, Russian Federation

2 Center for Construction Methods, Inspection of Buildings and Facilities, Pipeline Transport Institute, Moscow, Russian Federation

THIS PAPER EXAMINES issues of predicting technical and technological complications in the process of constructing trunk pipeline for underwater crossings using the directional drilling (also called directional boring) method, depending on the properties of the soils forming the underwater crossing. The prediction is made on the basis of geomechanical modelling of the underwater crossing, taking into account of the soil stresses arising during construction of the crossing. Basic criteria are formulated for predicting the stability of the soils along the bore during the construction of underwater crossings.

Key words: directional drilling, river crossing, geomechanical modelling, soil strength, soil stability, drilling mud

ONE OF THE TECHNICAL challenges which arises when designing an underwater crossing and selecting the construction method is the assessment of possible complications in the construction process, and the economic evaluation of attainable technical results. In the absence of a method to evaluate the potential for complications, difficulties can arise in developing appropriate solutions. As a consequence of these difficulties, mistakes can be made in the design, or existing and successfully applied modern technologies for underwater-crossing construction can be ignored.

The main complications in the process of constructing underwater crossings for trunk pipelines using the directional-drilling method in unstable soils are:

- the loss of the bore, when the soil forming the walls of the bore collapses;
- the deviation of the design profile from actually achieved by in the drilling process;
- loss of circulation of drilling fluid (mud);
- 'balling' of the drilling bit;
- increased wear and damage to the drilling tool;
- conditions preventing the pull-out of the drilling tool from the bore, or the pipeline while it is being pulled through.

These complications and the accidents arising from them are dictated by the geological conditions for the work, and eliminating their consequences would involve significant additional labour and financial expenditure, to the extent that the results achieved by this type of construction would be lost.

*Corresponding author's contact details:
Email: vafindr@niitnn.transneft.ru

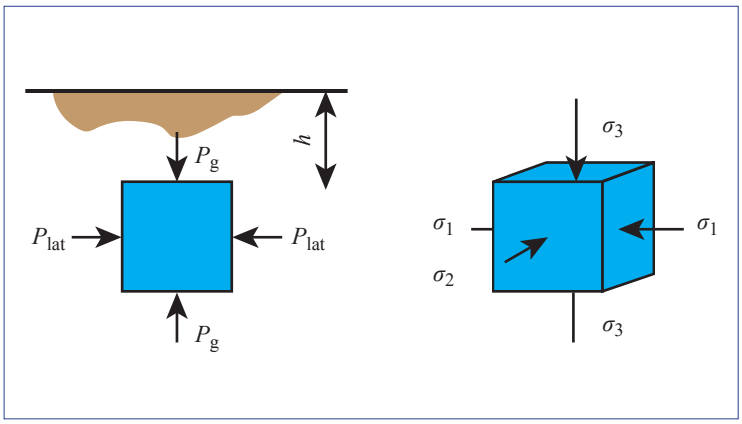

Fig.1. Diagram for determining main normal stresses on rectangular and cylindrical bodies: (a) distribution of normal stresses in monolithic rock; (b) distribution of normal stresses in porous rock.

A geomechanical model is being developed for forecasting and modelling the construction process for directional and horizontal oil and gas wells. The model includes research into the properties of the rocks near the wellbore profile, and uses geophysical and other engineering and technical methods [1,2]. It describes the loads acting on the rocks in the near-wellbore zone and the stresses arising as a result, and also determines the condition of the wellbore walls and predicts possible complications in the process of well drilling and operation. During construction of an underwater crossing using the directional-drilling method, geomechanical models are not currently used for the process of the crossing construction, pipeline pulling, or crossing operation. To a significant extent, this limits the effectiveness of the engineering and technical methods and evaluations used in the directional-drilling method.

In connection with this, the challenge is to formulate the basic criteria for building a geomechanical model that can be applied to the construction of underwater crossings using the directional-drilling method. This would allow the technology for constructing the crossing to be chosen, and the pipeline's operating conditions to be assessed. Building a geomechanical model would help in drawing-up strict requirements for carrying out engineering and geological surveying and for their results, which are used to make design solutions in the construction of underwater crossings.

Loads and stresses acting on the bore walls of an underwater crossing

Studies of the stress state of the rocks surrounding the wellbore, and the methods of evaluating them, have been carried out by many specialists [1, 3, 4]. As a basis for calculating the stress state of the soils along the underwater crossing bore in trunk pipelines, we have used the methodology developed by A. N. Popov [2].

In their natural state, soils are in equilibrium, and the strength of the soils counterbalances the effect of gravity and tectonic forces. The stress state in the soils will appear as their strains which, in the plastic conditions, are determined by the degree to which overburden pressure exceeds strength, or by the soils' yield strength.

Rock pressure can be subdivided into geostatic P_g and lateral pressure P_{lat} (Fig.1a). Geostatic pressure is the pressure caused by the weight of the overlying rock, and is given by Equn 1:

$$P_g = \rho_{av} g H \qquad (1)$$

where g is gravitational acceleration, equalling 9.81 cm/sec^2; ρ_{ov} is the average density of the overlying rock in kg/m^3; and H is the depositional depth of the rock in metres.

Reference 2 shows the load transfer applied vertically to the rock, in a horizontal direction:

$$P_{lat} = P_g \lambda \qquad (2)$$

where λ is the lateral-earth-pressure factor.

During the drilling process, part of the drilled-out rock is detached from the bed and is carried out by the drilling mud to the surface. Consequently, a free surface arises, on which strains can appear and, as a result, stresses are redistributed along the bore. The acting pressure of the drilling mud in the bore begins to counteract the lateral pressure of the rock.

The parameter which determines the possibility and extent of rock strain is the lateral-earth-pressure factor. As solids with atomic structures, monolithic rocks have high strengths which ensures a lateral-earth-pressure factor value of λ = 0.1-0.2 and a low capability for transferring rock pressure onto the walls of the borehole. These values of λ provide a stable condition in the bore. As rock ductility increases, the lateral-earth-pressure factor also increases, and the soils become unstable because rock pressure is more vigorously transferred onto the walls of the borehole.

The value of the lateral-earth-pressure factor depends on the rock properties and, when the Poisson's ratio values for the rock μ = 0.13 - 0.25, is calculated according to the formula proposed by Dinnik (Equn 3); when the value of the internal friction angle φ = 38 - 58°, the lateral-earth-pressure factor is determined according to Krupennik's formula (Equn 4):

$$\lambda = \frac{\mu}{1-\mu} \tag{3}$$

$$\lambda = \frac{1-\sin\varphi}{1+\sin\varphi} \tag{4}$$

Thus, for example, the lateral-earth-pressure factor for high-ductile clays is around 0.7, while for sands it is 0.3–0.4.

The pressure of the drilling fluid in the borehole P_b (Equn 5) is governed by the static P_{stat} (Equn 6) and the dynamic P_{dyn} pressures. The static pressure depends on the density of the initial drilling fluid and the equivalent circulation density of the fluid, and thus depends on the amount and density of drilled-out rocks. The dynamic pressure depends on the change in drilling-fluid pressure in the borehole during pump work or tripping operations.

$$P_b = P_{stat} + P_{dyn} \tag{5}$$

$$P_{stat} = \rho g H \tag{6}$$

The density of drilling mud with drilling-cuttings' content (Equn 7) increases compared to the density of the initial fluid pumped in:

$$\rho = (1-c_s)\rho_{dm} + \rho_{rp} c_s \tag{7}$$

where:

ρ_{rp} is the average density of rock particles in kg/m^3;
ρ_{dm} is the density of drilling mud in kg/m^3;
c_s is the proportion of cuttings in the drilling mud, as a unit-less fraction.

An increase in drilling-mud pressure such that it exceeds lateral rock pressure can lead to an increase in tensile stresses on the wellbore walls. As a result of their impact, fractures form in the surrounding soil, which may lead to hydro-fracturing of the rock, i.e. mud spring initiation, or to the simple loss of circulation of the drilling mud. In small-diameter wellbores, the mud pressure also exceeds the lateral rock pressure because of the impact of dynamic pressure and the presence of cuttings in the well. In large-diameter wells, i.e. when they are reamed, the dynamic pressure has almost no impact on hydro-fracturing in the rock.

The pressure of liquid in the fractures and pores of the soil is known as the formation pressure (Equn 8) and is determined by:

$$P_{fm} = K_{an} \rho_w g H \tag{8}$$

where:

K_{an} is the formation pressure anomaly factor;
ρ_w is the water density, equal to 1000 kg/m^3.

The values of P_g and P_{lat} as components of rock pressure characterize the natural stresses in rock as if it were monolithic, while the values σ_1 and σ_3 are the natural stresses in the body of the porous rock model [2]. The orientation of normal stresses is presented in Fig.1b.

The horizontal stress (Equn 9) is equal to:

$$\sigma_1 = \lambda P_g + P_{fm}(1-c)(1-\lambda) \tag{9}$$

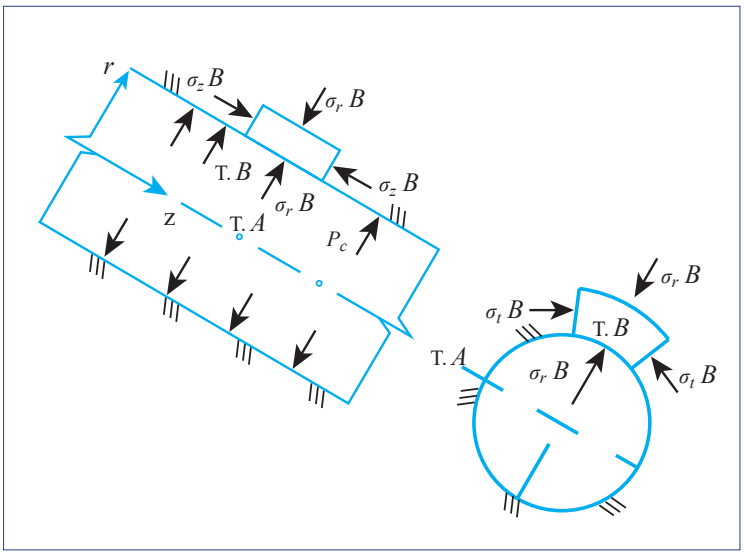

Fig.2. Stress distribution in a directional borehole.

where:

P_g is the geostatic pressure in MPa;
P_{fm} is the formation pressure in MPa;
c is the proportion of unit area (Equn 10) in the dangerous (under examination) cross-section:

$$c = \exp\left(-19.16m^2\right) \qquad (10)$$

The vertical stress (Equn 11) is given by:

$$\sigma_3 = P_{fm} + \frac{P_g - P_{fm}}{c} \qquad (11)$$

The stress state of a wellbore is calculated in a cylindrical coordinate system, where the *z*-axis is superimposed onto the axis of the wellbore and the normal stress is denoted as σ_z; the radial stress σ_r is in the direction of the radius vector; the tangential stress σ_t is perpendicular to the radial stress. The stresses in directional and horizontal wells are determined by two points: in the lateral part of the wellbore by point A and in the top zone by point B.

In directional wells, the distribution of stress at points A (Equn 12) and B (Equn 13) is shown in Fig.2 and takes the following form shown in Equns 12 and 13 (*see right*) where α is the angle of the wellbore curvature in degrees.

The pressure of hydro-fracturing in a directional well at point A (Equn 14) and at point B (Equn 15) is determined by the formulae:

$$P_{frA} = c\left(3\sigma_3 - \sigma_1\right) + P_{fm}\left(1 - c\right) + c\tau_u \qquad (14)$$

$$P_{frB} = 0.5c\left(3\sigma_3 + \sigma_1\right) + P_{fm}\left(1 - c\right) + c\tau_u \qquad (15)$$

The stresses around a horizontal well are shown in Fig.3 and come to:

– at point A

$$\begin{cases} \sigma_z = \sigma_1 + 2\mu\left(\sigma_3 - \sigma_1\right) \\ \sigma_r = P_{fm} + \dfrac{P_g - P_{fm}}{c} \\ \sigma_t = \sigma_3 + \sigma_1 + 2\left(\sigma_3 - \sigma_1\right) - \sigma_r \end{cases} \qquad (16)$$

– at point B where $\varphi = 90^\circ$

$$\begin{cases} \sigma_z = \sigma_1 - 2\mu\left(\sigma_3 - \sigma_1\right) \\ \sigma_r = P_{fm} + \dfrac{P_b - P_{fm}}{c} \\ \sigma_t = \sigma_3 + \sigma_1 - 2\left(\sigma_3 - \sigma_1\right) - \sigma_r \end{cases} \qquad (17)$$

The pressure of hydro-fracturing at points A (Equn 18) and B (Equn 19) is given by:

$$P_{frA} = c\left(3\sigma_3 - \sigma_1\right) + P_{fm}\left(1 - c\right) \qquad (18)$$

$$P_{frB} = 0.5c\left(\sigma_3 + 3\sigma_1\right) + P_{fm}\left(1 - c\right) \qquad (19)$$

The difference between tangential stress in the vicinity of the well and natural stress is governed by disparities in natural stress and drilling mud pressure in the well. Admittedly, the ratio of their values is unknown. The calculation is therefore based on conditions of non-equation for every point - see Equn 20 (*see right*).

The use of this methodology allows the loads acting on the rock to be determined for the near-well zone of directional and horizontal wells, as well as the stresses and hydro-fracturing pressures which thus arise in the rock. Calculating the lateral-earth-pressure factor using Dinnik's and

Kruppenik's formulae is limited by the values of the Poisson's ratio and the soil's internal friction angle and does not cover all possible values. Therefore, this problem requires its own additional solution.

Soil characteristics and elastic-state conditions

The primary geological factor determining the stability of the wellbore walls is the soil strength. The soil strength is dictated by the nature and force of the bonds between the minerals and particles from which it is formed. Depending on the type of chemical bond and on the parameters determining the soil strength, soils can be classified as:

- rocky;
- disperse consolidated;
- disperse non-consolidated.

Rocky soils are characterized by covalent and polar-covalent bonds, which provide high strength and properties of solids.

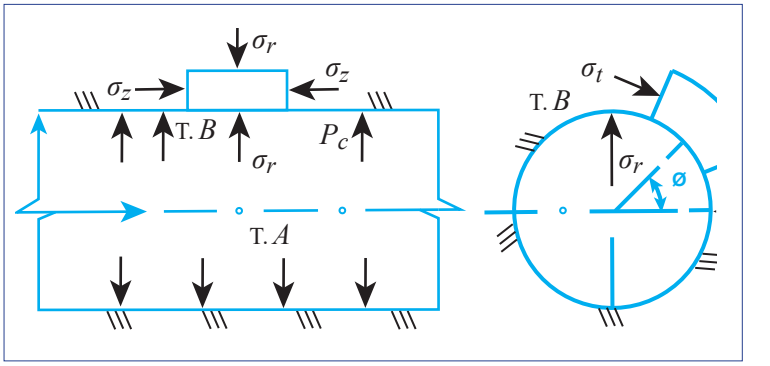

Fig.3. Stress distribution in a horizontal borehole.

The internal friction forces, which arise in the rock from the external load, have secondary significance in rocky soils when compared to structural cohesion, and this means that the internal friction force can be ignored. These soils include granite, calcium, limestone, mica, etc. The rocky soil strength may be determined in uniaxial compression tests (Equn 21) or by punch indentation (Equn 22):

$$\tau_u = \frac{\sigma_{ck}}{2}, \sigma_{cp} = \frac{\sigma_{ck}}{2} \qquad (21)$$

$$\tau_u = K_1 p_{av}, \sigma_{cp} = K_2 p_{av} \qquad (22)$$

at Point A:

$$\begin{cases} \sigma_z = \sigma_3\left(\cos^2\alpha - 2\mu\sin^2\alpha\right) + \sigma_1\left(1+2\mu\right)\sin^2\alpha \\ \sigma_t = \left(3\sigma_1 - \sigma_3\right)\sin^2\alpha + 2\sigma_1\cos^2\alpha - \sigma_r \\ \sigma_r = P_{fm} + \dfrac{P_b - P_{fm}}{c} \end{cases} \qquad (12)$$

at Point B:

$$\begin{cases} \sigma_z = \sigma_3\cos^2\alpha + \left(\sigma_1 + 2\mu\left(\sigma_3 - \sigma_1\right)\right)\sin^2\alpha \\ \sigma_t = \left(3\sigma_3 - \sigma_1\right)\sin^2\alpha + 2\sigma_1\cos^2\alpha - \sigma_r \\ \sigma_r = P_{fm}\dfrac{P_b - P_{fm}}{c} \end{cases} \qquad (13)$$

$$\begin{aligned} &if\ |\sigma_z| > |\sigma_t| > |\sigma_r|\ then\ \tau_{\max}\frac{\left(\sigma_z - \sigma_r\right)}{2}, \sigma_{cp} = \frac{\left(\sigma_z + \sigma_r\right)}{2} \\ &if\ |\sigma_t| > |\sigma_z| > |\sigma_r|\ then\ \tau_{\max}\frac{\left(\sigma_t - \sigma_r\right)}{2}, \sigma_{cp} = \frac{\left(\sigma_t + \sigma_r\right)}{2} \\ &if\ |\sigma_z| > |\sigma_r| > |\sigma_t|\ then\ \tau_{\max}\frac{\left(\sigma_z - \sigma_t\right)}{2}, \sigma_{cp} = \frac{\left(\sigma_z + \sigma_t\right)}{2} \end{aligned} \qquad (20)$$

where K_1 and K_2 are proportionality factors, which are dependent on the Poisson's ratio:

$$K_1 = 0.346 - 0.109\mu$$
$$K_2 = 0.509 - 0.020\mu$$

Consolidated soils are represented by argillite, siltstone, clay, loam, and loamy sand in various consistencies in which the natural agglomerates are bound together by hydrogen bonds. The strength of the hydrogen bonds in their volume depends on the water-cut in argillaceous components. Argillaceous soils can be subdivided into solid and ductile, depending on the water-cut.

Solid clays are characterized by higher strength. In these clays, water is absent, giving the clay the ductile properties, since clay particles are bound by hydrate bonds. At low geostatic pressure, clay with particles bound by hydrate bonds behaves like a solid with atomic structure: it has strength, sometimes slowly and weakly reacting with water. The ultimate strength of solid clays is described by Equn 23.

The shear strength of ductile clays will be determined by the water content in the composition of the silica gel membrane of the clay particles, and by the condition of the hydrogen bonds in the membrane. The hydrate membrane, at the moment the load is applied, acquires a water-repellent property due to the significant induction period of bond formation, and the triaxial bond between the clay particles disappears. They become non-oriented in relation to one another and react weakly with each other.

In order to determine the design strength and evaluate the stability of consolidated soils, such characteristics as the degree of ductility and the magnitude of specific cohesion are used. Ductility indicates the clay's capacity to absorb water without dispersing: the lower a clay's ductility, the faster it will disperse. The ductility index itself is informative for the drilling process as an indicator evaluating the clay's absorbing capacity and its mechanical impurity content. The disadvantage of this indicator is that, in order to determine ductility, an initial sample of clay must be dried. The advantage is that drilled-out rock cuttings are used to determine its value. Yielding characterizes the initial state of the clay due to its ductility. Physically, this is reflected as an indicator demonstrating how close the clay in its initial state is to its ductile state, and its capacity for dispersion. Where the yield index $I_l > 0$, argillaceous soils are considered to be ductile.

The process of ductile clays destruction is characterized by swelling of clays without any loss of bond between particles, and by their subsequent dispersion in the volume of the fluid. Where the yield index $I_l < 0$, argillaceous soils belong to the solid group, and the process of destruction under the impact of arising stresses occurs with a minimal quantity of water absorbed. In clays with varied degrees of ductility, porosity will be equal to zero; this is connected with the fact that the water structured in it forms part of the clay structure and is its continuation [5].

The ultimate shear stress in soils is calculated according to the Mohr-Coulomb strength theory:

$$\tau_n = \tau_{c0} + \sigma_n tg\varphi \qquad (23)$$

$$\sigma_n = \sigma_{cp} - \tau_{\max} tg\varphi \qquad (24)$$

where τ_{c0} is the cohesion factor, corresponding to the ultimate shear-stress value at $\sigma_n = 0$, MPa;

- φ is the internal friction angle, degrees;
- σ_n is the normal stress (Equn 24), MPa.

The condition (Equn 25) corresponds to the soil's elastic state, taking into account long-term strength k_{lt}:

$$\left|\tau_{\max}\right| \le k_{lt}\tau_n \qquad (25)$$

The safety margin of wellbore walls at the point under examination is given by Equn 26:

$$n = \frac{\tau_n}{\tau_{\max}} \qquad (26)$$

if $n > 1$ then the solid is in an elastic state;
if $n < 1$ then the solid may deform plastically or collapse.

During the construction of underwater crossings using the directional-drilling method, passing through non-consolidated soils (such as sands, gravel, and shingle) is complicated by the unstable state of the borehole shaft, and by constant collapses. Furthermore, coarse fractions are not carried out of the well, but accumulate on the lower surface of the borehole. Maintaining stability in these soils for directional boreholes with large diameters is a challenging technical task. The nature of these collapses depends on the particle-interaction processes. Interaction between soil particles is characterized by internal friction forces and structural cohesion. The shear strength of non-consolidated soils grows in proportion to the increase of intergranular contact area, which is expressed in parameters such as porosity and density.

For dense soils, the structural cohesion is ranges from 0.03 to 0.05 MPa, and for loose soils it is 0 MPa. The relationship between shear resistance S in non-consolidated soils and load p given their different density (per porosity metres: m_1 indicates a limited loose state, and m_4 a dense state), and the relationship between the angle of internal friction of a medium-grained sand and its porosity m are presented in Figs 4 and 5 [6]. Structural bonds have elastic character, determining the extent of rock deformability and its compaction. This accounts for a sand friability on the surface of the earth. In the subsurface, the soil is in a compacted state; however, when the stratum is drilled, decompaction occurs, i.e. the grains of rock become loosened, ruining the structural strength of the soil.

During the drilling process, the drilling fluid vigorously reacts with penetrated soils. Clay dispersion, having a low content of clay particles, seeps into the soil and wets its particles, thus leading to its disintegration. The structural bonds between the particles ruptures, and the soil begins to flow. Up to a certain soil-moisture level, the angle of internal friction hardly changes. However, the angle of internal friction tends towards rapid reduction with oversaturation of the rock with water. This is a direct consequence of the increased water content in non-consolidated soil, accompanied by the reduction in the number of contacts between soil particles [6].

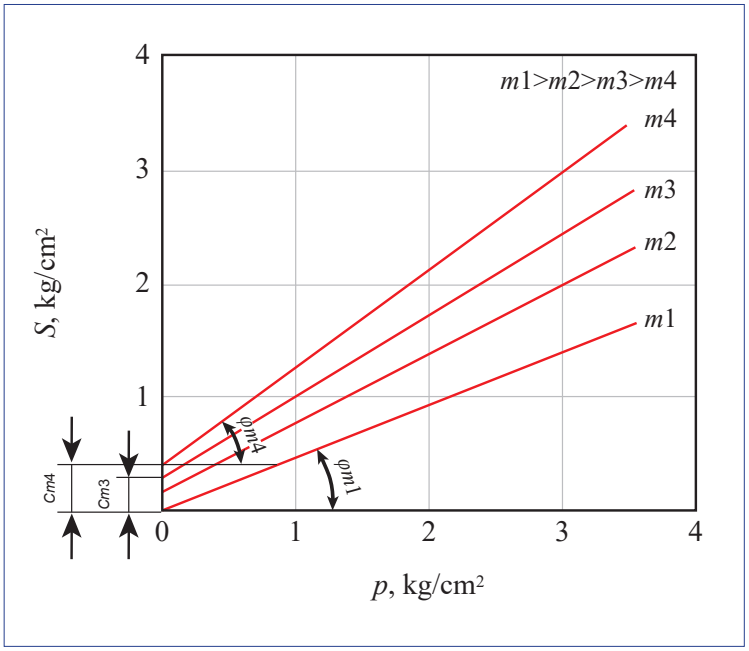

Fig.4. The relationship between shear resistance in uncemented soils and loads at different densities (by porosity).

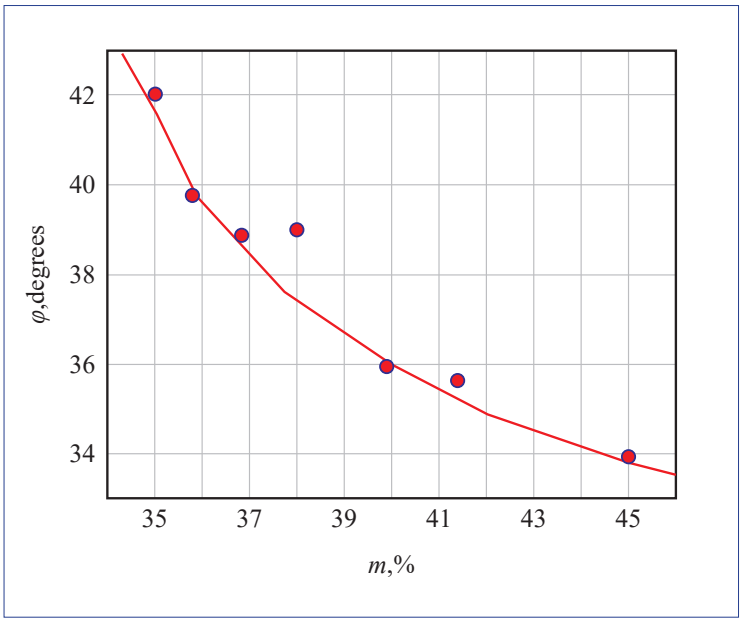

Fig.5. The relationship between angle of internal friction in a medium-grained sand and its porosity.

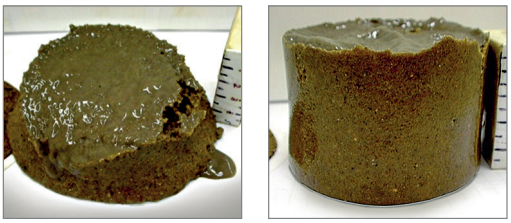

Fig.6. The physical condition of samples and their appearance.

The maximum safety margin for non-consolidated soil in a dense condition is the relationship between τ_u and s_n, which is given by Equns 23 and 26.

Rocky soils have sufficient strength to support a borehole in a stable state. The strength condition is determined by uniaxial compression and punch indentation tests. A stable state in argillaceous soils is achieved when clay is in a solid or semi-solid state, while where it is in a plastic state, the clay will be extruded into the borehole. The clay's state is determined according to its yield strength and structural cohesion value. The stability of non-consolidated soils is determined by the degree of their compaction *in situ*, and by its structural cohesion and the angle of internal friction.

On the basis of the calculations presented here and their comparison according to Equn 26, it is possible to predict the stability of soils along a borehole. Where the condition $n > 1$ is not fulfilled for a particular interval, the borehole walls are liable to collapse and the will be unstable.

The interaction of dispersed non-consolidated soils with drilling fluid

Drilling fluid (mud) is a poly-dispersed structure linked by hydrogen bonds, which are created by the chemical properties of its constituents. Therefore, the behaviour of the drilling fluid is determined by the strength of these hydrogen bonds and their degree of distribution throughout the fluid. The strength of the drilling-fluid structure, in turn, depends on the level of polarity and concentration of constituents in the fluid. Where there is a uniform distribution of bonds' strength in the fluid, the mud will display clearly manifested pseudo-plastic properties. Where there is a less-uniform level of distribution of hydrogen bonds' strength throughout the fluid, the drilling mud will acquire the properties of a visco-plastic liquid.

Drilling fluid is filtered through permeable channels in a non-consolidated soil, whose size is much bigger than the particles of the mud's solid phase. Filtration takes place until the moment when the differential pressure and pressure losses for the mud movement are equalized; at that point, the mud structure does not disintegrate. Where the depth of the drilling mud penetration into the permeable bed is achieved, and depending on the energy input leading to its structural collapse, part of the water is removed from the mud's disintegrated structure, and is accompanied by accumulation of the solid particles into the mud.

The solid particles either form a united structure or simply accumulate as the solid phase (Fig.6), depending on the state of the water around them, and the quality of the bonds within it. When permeable channels become smaller than the size of the solid-phase particles, the structure of the mud disintegrates under the impact of differential pressure and it separates into its constituents, which clog the permeable channels, forming a barrier in the near-borehole zone.

The seepage depth of the fluid depends on the following conditions: the seepage depth will decrease at constant differential pressure, with higher shear stress in the liquid, while the seepage depth will increase at a constant effective shear stress and higher differential pressure. That is, the uniformity of distribution and the seepage depth of the drilling mud are affected by its pressure at pumping and by the strength of the bonds in the mud volume, i.e., if the mud

constitutes a single structured system, and is not broken into separate structured clusters, then filtration will take place. A significant role in the filtration process belongs to the strength of the bonds in the liquid's volume, and this can be seen especially clearly where components of the liquid satisfy Abrams' criteria [7], i.e. the effective diameter of particles is less than one-third of the diameter of the permeable channel. The results of well-known studies into filtration processes were analysed on the basis of a similar approach to drilling-mud filtration in non-consolidated soils.

Supported by the data [9] for determining the fractional content of clayey suspensions and muds, and also by the results of their filtration through non-consolidated soils of various fractional content [8], results were studied for the process of drilling-mud filtration through clayey suspensions and muds (Fig.7). It was understood from this that the possibility of successful drilling-mud filtration into a porous medium is determined by the ratio of the permeable channel size (D_w) to the drilling mud particles size (D_T) and by the pressure gradient between the well and the bed. This can be achieved given the following conditions:

- where $D_w/D_T < 1$, drilling-mud filtration does not occur, and the solid phase of the mud accumulates on the surface of the filter;
- where $1 < D_w/D_T < 6$, drilling-mud filtration occurs with infilling of the pore space in the non-consolidated soil, i.e. with forming a clogged zone;
- where $D_w/D_T \geq 6$, the filtration depth is determined by the condition of the bonds in the mud structure and by the pressure gradient between the mud volume and the filter.

An analysis of the results of research [8] into the process of muds filtration in sand samples of various grain-particle size showed that at shear stresses from 0.2 to 0.7 MPa, filtration of the mud extends to the full length of the sample while keeping its geometrical dimensions where ductility factor values are 800-3000 s^{-1} (Fig.7). In order to guarantee the process of the drilling-mud filtration through samples based on fine sand with an effective particle diameter of 0.142 mm, the necessary DSS (dynamic shear stress) value should be 120 dPa. In order to guarantee the process of filtration

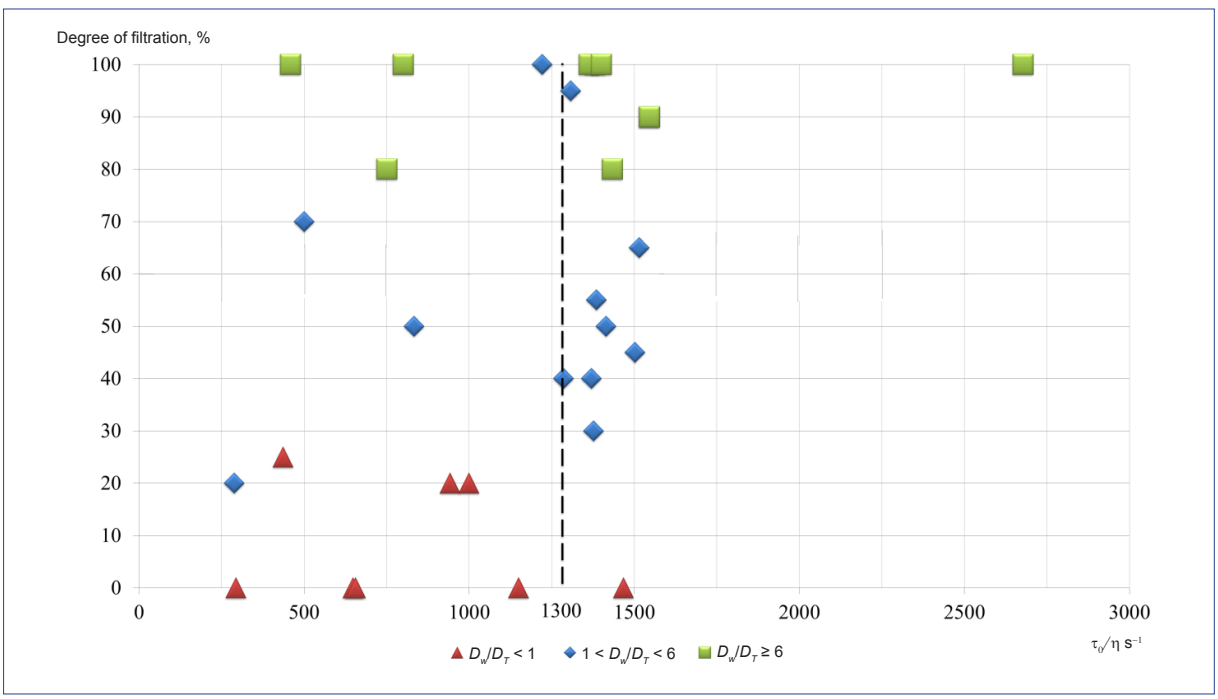

Fig.7. The impact of the ductility factor on the dispersal of various fractions on the degree of their filtration through samples of uncemented soil.

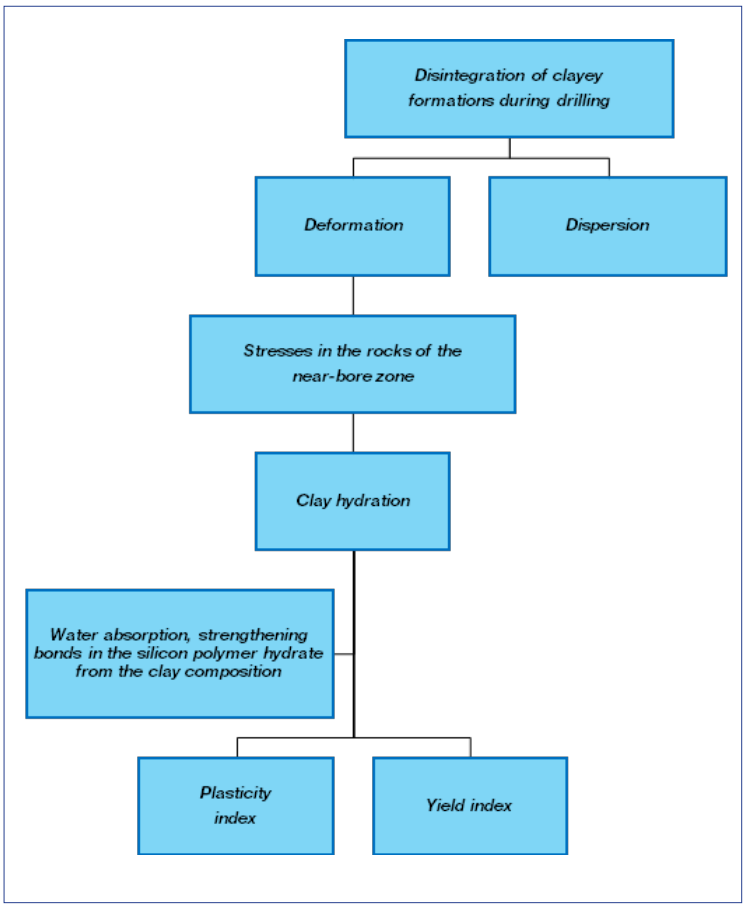
Disintegration of clayey formations during drilling
Deformation
Dispersion
Stresses in the rocks of the near-bore zone
Clay hydration
Water absorption, strengthening bonds in the silicon polymer hydrate from the clay composition
Plasticity index
Yield index

Fig.8. Factors determining the process of borehole wall collapse, where it is formed of argillaceous sediment.

through a porous medium with large effective particle diameter, the DSS value of the drilling mud must be increased. Where a value of τ_0/η >1300 was guaranteed, not only was drilling-mud filtration successful, but non-consolidated soil samples were also strengthened due to the strength of bonds between the drilling mud's constituents and the soil particles.

Limiting values were thus determined for successful drilling-mud filtration with strengthening of the porous medium, based on studies and experience of constructing large-diameter directional boreholes. These limiting values are: the ratio of permeable channel size to drilling mud particle size (D_w/D_T) > 6; dynamic shear stress ≥ 300 dPa; the ductility factor ≥ 1300 s^{-1}. These values for the ductility factor allow control of the condition for non-consolidated soils to improve their strength in order to form stable borehole walls when passing through unstable soils during the borehole drilling.

Interaction of argillaceous soil with drilling mud

The process of clay disintegration in a borehole where there is a reaction with water includes two stages. In the first stage, the clay absorbs water; and in the second, which limits the process of clay disintegration, hydrated particles of clay disperse. The factors which determine the process of clay disintegration are presented in Fig.8.

The disintegration of clay can occur during hydration and swelling of solid non-ductile clays. The increase in clay volume during the hydration process, i.e. the appearance of strains, contributes to the occurrence of stresses in the rock at the borehole walls, leading to its collapse. All these processes are characteristic, above all, for clays with high ductilities and low yield indicators. For a clay capable of absorbing a large quantity of water, the process of its disintegration is characteristically accompanied by a significant increase in volume.

With an increase of water content in the clay and the consequent increase in its yield indicator, the role of the degree of clay volume increase will decline, and there will be a drop in the magnitude of stresses capable of leading to the occurrence of the forces which disintegrate the clay at the borehole wall. At the same time, there will be an increase in the possibility complications with key seals, wall-packing rings and other technical components. It will also be necessary to prevent dispersion of argillaceous cuttings in the high-velocity flow of the drilling mud.

Where a moisture-content indicator characterizing the reduction of its strength characteristics is reached, the clay will tend towards flowing under the impact of geostatic pressure (quick clay). However, it must be understood that where clay is significantly diluted by inert components (fragments of rock, sand, etc.), it is these components that will make up the structural body of the argillaceous sediments and determine their behaviour under the impact of geostatic pressure. In

this case, the stability of the borehole walls will be determined by the by the inert components of argillaceous sediments.

Clays which have a low ductility index values will be characterized by another behaviour *in situ*, i.e. in the case when their hydro-silicate membrane has low absorbing capacity relative to water. For the separate minerals of clay, the ductility number is determined by the value of I_p approx.10-30 [9] according to Grim's data. It is the boundary value characterising the reduced moisture retention capacity of clay (i.e. its hydrophily).

Where there is contact with water and absorption of a small quantity of water, similar clays, increasing in volume, will destroy the borehole walls. But their relatively low hydrophily forces this clay immediately to disperse, regardless of their moisture-retention state, i.e. the yield indicator. The role of a factor such as an increase in volume will be less significant for these clays due to the speed of their hydration process and the low quantity of water absorbed by them. The dilution of these clays with filler material only accelerates and aggravates their disintegration process.

A similar speed for processes of hydration softening and disintegration is dictated by the fact that the hydro-silicate membrane of clay undergoes significant changes during the bleeding processes, and has low ductility and flexibility. Therefore, it is not capable of absorbing a significant quantity of water. The drilling process in such a clay is characterized by intensive clay dispersion, borehole collapse, higher recovery of cuttings, etc. In order to stabilize the borehole in similar argillaceous sediments, technical actions should be taken, depending on the impact on clays and their ductility indicators.

Geomechanical model of an underwater crossing for a trunk pipeline

When constructing a geomechanical model for a trunk pipeline underwater crossing using directional drilling, the following points need to be considered:

- analysis of the conditions in which work is to be carried out (acquisition of geological, geophysical, and petro-physical data; analysis of drilling and reaming the boreholes for underwater crossing, together with analysis of the drilling muds used in similar geological conditions; analysis of complications which might arise during the construction of underwater crossings; identification of any additional data required for modelling; summarizing the analysis results);
- analysis of the initial stress-strain state of the soils making up the borehole walls (calculation of the loads acting on the rock in the near-borehole zone, and the stresses thereby arising; assessment of the condition of the borehole walls; prediction of possible complications);
- hydrodynamic modelling with the impact of drilling mud, or other fluid, on the state of the rock and its strength characteristics (choice of rheological parameters for drilling mud; calculation for filtration of drilling or fluid into the bed; borehole flushing)
- analysis of the stress state of the soils making up the borehole wall, taking into account data from hydrodynamic modelling;
- summing-up and making recommendations for improvement to the technology for constructing underwater crossings, drilling trajectory, drilling-fluid formulation, the basis for using the directional-drilling method regarding the conditions of crossing construction.

Based on the methodology presented above, geomechanical models have been constructed for the underwater crossings of trunk oil pipelines in differing geological conditions across the Suvoroshch and

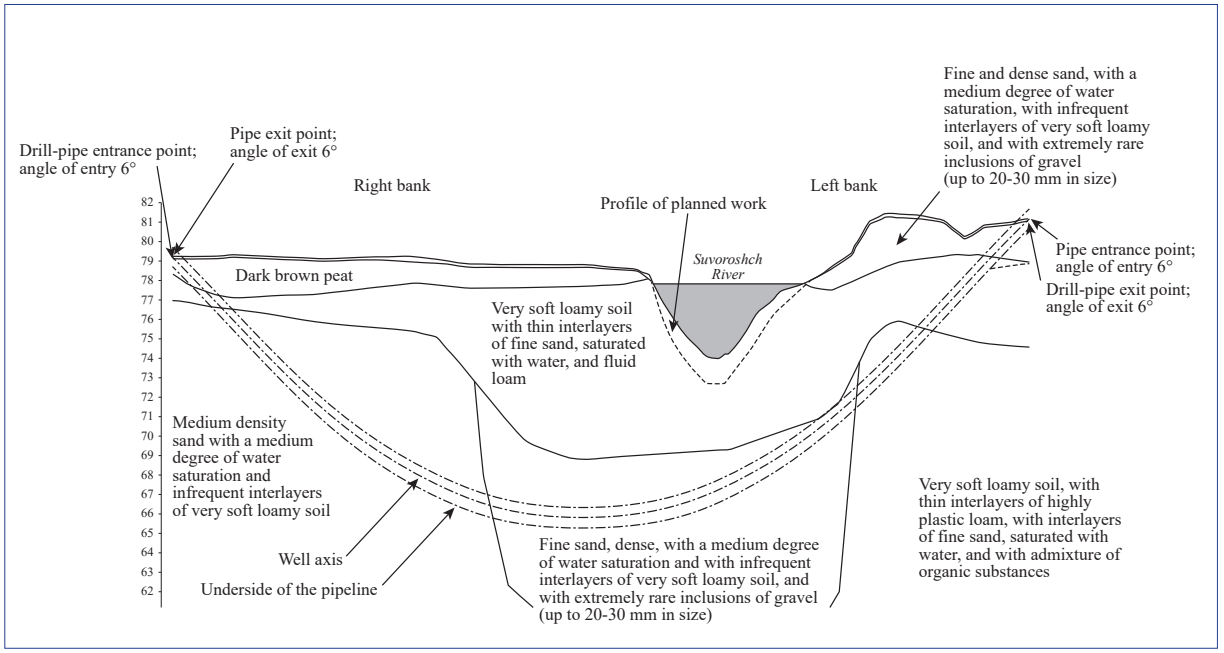
Drill-pipe entrance point; angle of entry 6°
Pipe exit point; angle of exit 6°
Right bank
Profile of planned work
Left bank
Fine and dense sand, with a medium degree of water saturation, with infrequent interlayers of very soft loamy soil, and with extremely rare inclusions of gravel (up to 20-30 mm in size)
Suvoroshch River
Pipe entrance point; angle of entry 6°
Drill-pipe exit point; angle of exit 6°
Dark brown peat
Very soft loamy soil with thin interlayers of fine sand, saturated with water, and fluid loam
Medium density sand with a medium degree of water saturation and infrequent interlayers of very soft loamy soil
Well axis
Underside of the pipeline
Fine sand, dense, with a medium degree of water saturation and with infrequent interlayers of very soft loamy soil, and with extremely rare inclusions of gravel (up to 20-30 mm in size)
Very soft loamy soil, with thin interlayers of highly plastic loam, with interlayers of fine sand, saturated with water, and with admixture of organic substances
82
81
80
79
78
77
76
75
74
73
72
71
70
69
68
67
66
65
64
63
62

Fig.9. Borehole profile for the Suvoroshch River crossing.

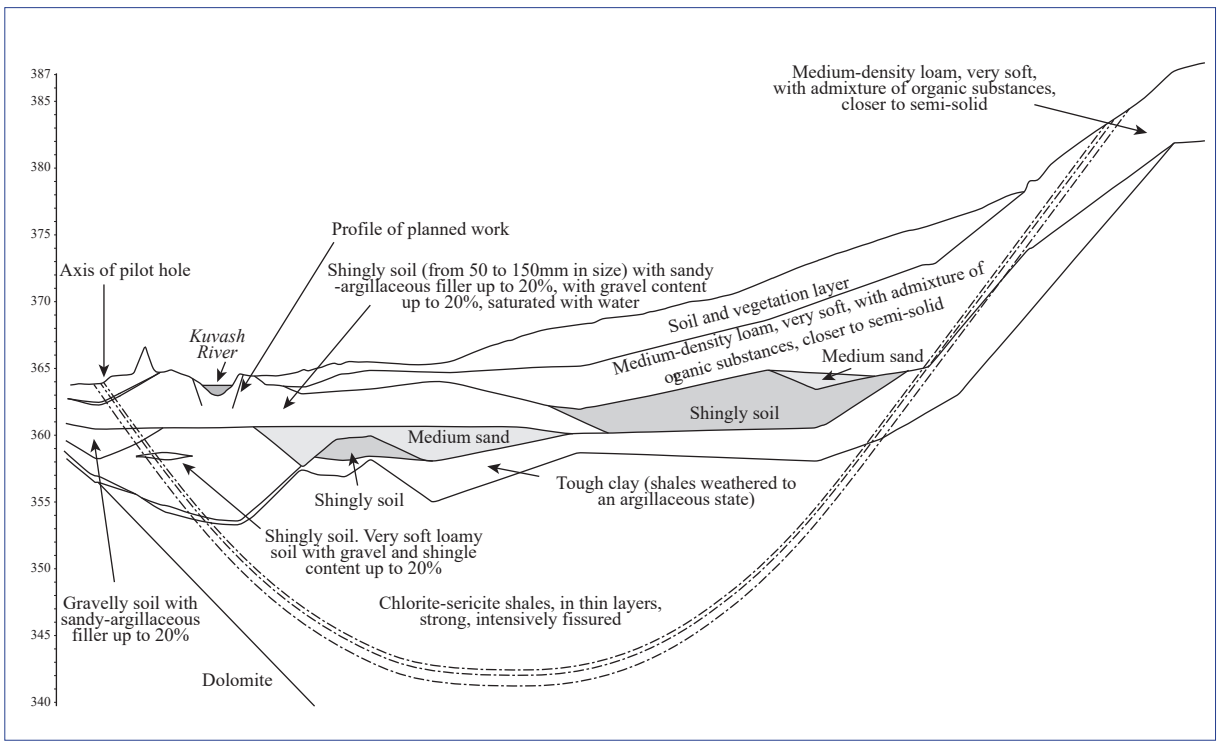
Medium-density loam, very soft, with admixture of organic substances, closer to semi-solid
Profile of planned work
Axis of pilot hole
Shingly soil (from 50 to 150mm in size) with sandy -argillaceous filler up to 20%, with gravel content up to 20%, saturated with water
Soil and vegetation layer
Medium-density loam, very soft, with admixture of oganic substances, closer to semi-solid
Kuvash River
Medium sand
Shingly soil
Medium sand
Tough clay (shales weathered to an argillaceous state)
Shingly soil
Shingly soil. Very soft loamy soil with gravel and shingle content up to 20%
Gravelly soil with sandy-argillaceous filler up to 20%
Chlorite-sericite shales, in thin layers, strong, intensively fissured
Dolomite
387
385
380
375
370
365
360
355
350
345
340

Fig.10. Borhehole profile for the Kuvash River trunk crossing.

Kuvash Rivers. Profiles of the boreholes and the geological conditions are shown in Figs 9 and 10.

An analysis of the works carried out at the Suvoroshch and Kuvash Rivers showed that the greatest difficulties during borehole drilling and reaming will be due to to the following complications: instability of the borehole walls, lost circulation of the drilling mud, insufficient cuttings recovery from the borehole, narrowing of the borehole, and absorption of the clay into the mud.

A preliminary analysis of the stressed

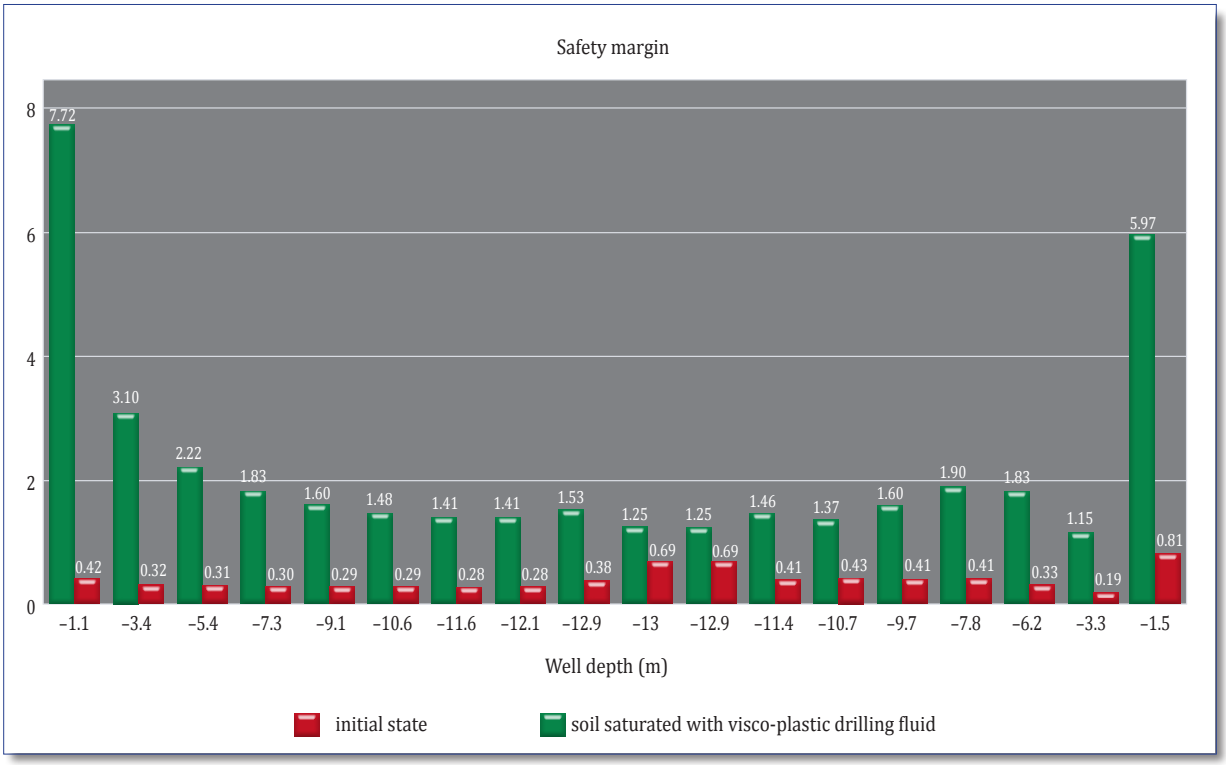

Fig.11. Soil safety margin for the Suvoroshch River crossing.

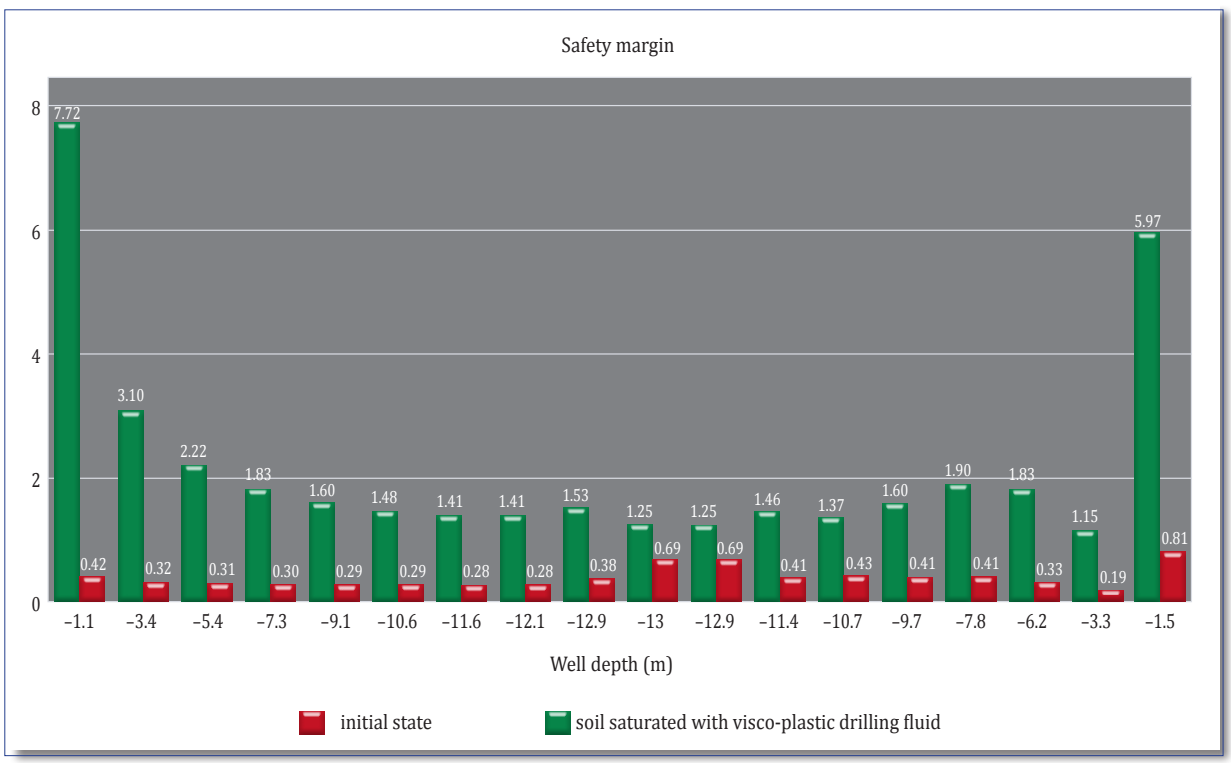

Fig.12. Soil safety margin for the Kuvash River crossing.

condition of soils making up the borehole walls in the Suvoroshch River crossing revealed two dangerous areas with very high active pressures: sandy silts at a depth of up to 12 m (compressive stresses were up to 6 MPa, and tensile stress up to 0.08 MPa) and very soft loamy soil at a depth of 5 m (tensile stresses were up

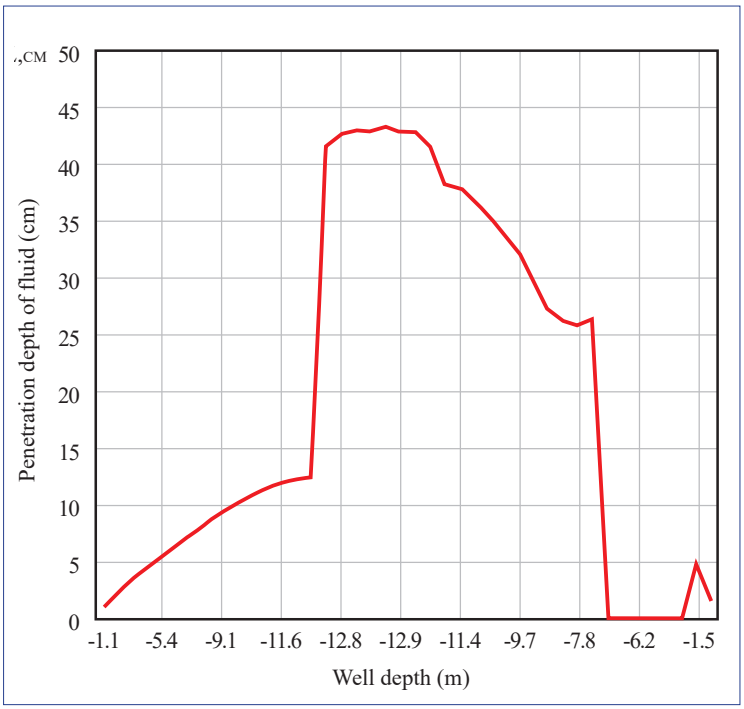

Fig.13. Penetration depth of drilling fluid in uncemented soil.

to 0.04 MPa and compressive stresses up to 2.5 MPa). Throughout the length of the entire borehole, the maximum shear stresses are two times higher than the ultimate strength of the soils forming the borehole.

At the Kuvash River crossing, the highest tensile stresses were found in the borehole wall during drilling through shales at a depth below 17 m. However, the ultimate strength of shales is very high, at more than 50 MPa, and thus complications do not arise when they are drilled. The greatest challenge is presented by shingle and gravel soils: where they occur, at a shallow depth of up to 7 m, the resulting stresses are not great, but the ultimate strength of such soils is minimal.

Data were thus obtained concerning the stability of the boreholes at the Suvoroshch River (Fig.11) and the Kuvash River (Fig.12) crossings which indicate that the boreholes must be strengthened.

Boreholes can be strengthened using structured drilling muds or spacing-strengthening mud formulations. Preventing disintegration in argillaceous sediments is possible with the addition into the fluid of a special stabilizing chemical. The drilling-mud parameters which regulate bond strength in the mud and the filtration process into the permeable channels were as follows: dynamic shear stress of 30-40 Pa and density of 1050 kg/m^3. A curve describing the seeping depth of the drilling fluid into the permeable channels of the soil forming the underwater crossing of the Suvoroshch River is presented in Fig.13.

An analysis of the stress state of the soils forming the borehole wall, considering the data from hydrodynamic modelling, showed that as a result of the work carried out, the safety margin of the soils forming the borehole walls was tripled along the entire length of the underwater crossing of the Suvoroshch River. The minimum safety margin during drilling of sandy silts was 1.41 at a depth of 12 m, in fine sand it was 1.25, and in the area passing through very soft clays it was 1.04.

At the Kuvash River crossing, the safety margin was more than 1.5 when drilling consolidated soils, more than 88 for constituting shales, and more than 1 for gravel and shingle soils.

The geomechanical models which were constructed for the Suvoroshch and Kuvash River crossings thus revealed the necessity of strengthening the soils which form the borehole walls. Soil strengthening should be carried out by using drilling mud with increased structural strength. Regarding the conditions when drilling through gravel and shingle sediments for the crossing under the Kuvash River, additional strengthening with special formulations is advisable.

Conclusions

Based on the results of the work completed, basic criteria were formulated for geomechanical modelling of the conditions for constructing underwater river crossings for trunk pipelines.

The methodology presented here of calculating the stressed condition of

soils allows loads acting on the soils to be determined for the wellbore zone of directional and horizontal boreholes, taking into account the impact of the drilling mud. The stresses thus arising can also be determined, where they may be capable of leading to hydro-fracturing in the soils.

The ultimate strength of the soils can be determined using the Mohr-Coulomb strength theory, which takes into account the nature and bond strength of the minerals and particles making up the soil.

The model's reliability is increased by the presence of experimental data for strength and strain properties in soils and research into the influence of drilling muds on them.

An analysis of the stress state of the soils, and hydro-dynamic modelling of the impact of drilling mud on the state of the soils and their strength characteristics, must be carried out jointly in view of the redistribution of stresses within the soil when pores and fractures areas are filled with drilling fluid. This will also improve the quality of geomechanical modelling.

Within the framework of the geomechanical model developed for conditions in the construction of underwater crossings, we plan further to model the stress-strain state of the pipeline in the contact zone with soil and at its pulling-through the borehole.

References

1. V.S.Voytenko, Applied geomechanics in drilling process, Moscow, Nedra, (1990) 252
2. A.N.Popov, N.N.Golovkina, Strength analysis of wellbores in porous rocks, Ufa UGNTU, (2001) 70.
3. S.G.Lekhnitsky, Stress analysis in elastic isotropic mass near vertical cylindrical circular excavation, AS USSR, ESD. 7 (1938).
4. L.A.Shreyner *et al.*, Rock deformation behavior at high pressures and temperatures, Moscow, Nedra, (1968) 358.
5. V.M.Goldberg, N.P.Skvortsov, Permeability and filtering in clay, Moscow, Nedra, (1986) 160.
6. N.N.Maslov, Fundamentals of soil mechanics and geological engineering, Moscow, Higher School, (1968) 629.
7. N.Makovei, Drilling Hydraulics. M.Nedra, (1986) 600.
8. Z.Z.Sharafutdinov, et al., Construction of main pipeline crossings through natural and artificial obstructions, Novosibirsk, Nauka, (2013) 339.
9. R.E.Grim, Mineralogy and practical use of clay, Moscow, Mir,(1967) 510.

Listing of forthcoming industry events (*continued from p64*)

Gas Asia Summit & Exhibition (GAS)
25-27 October 2017
Singapore
www.gasasiasummit.com/
The event aims to address all aspect of the gas and LNG value chain from the upstream to the downstream and power sector as well as highlight new dynamics that are revolutionizing the Asia gas market today.

European Autumn Gas Conference
6-8 November 2017
Milan, Italy
www.theeagc.com/
EAGC is Europe's commercial and strategic gas conference, used by the most senior executives from the world's largest gas companies to network with peers and customers, review trends, question policy and agree future strategy.

2017 Pipeline Leadership Conference
8-9 November 2017
Dallas, TX, USA
plconference.com
The Pipeline Leadership Conference is a new event directed toward top executives involved with building and operating oil and gas pipelines throughout North America. The event will attract thought leaders to discuss innovative approaches and best practices for managing new construction, ensuring safety, improving efficiency and overcoming challenges from inside and outside the industry

Abu Dhabi International Petroleum Exhibition and Conference (ADIPEC)
13-16 November 2017
Abu Dhabi, UAE
www.adipec.com
The Abu Dhabi International Petroleum Exhibition and Conference (ADIPEC) is one of the world's most influential events for the oil and gas industry. As a premium exhibition platform ADIPEC enables professionals from around the world to do business and grow.

PPIM 2018: 30th Pipeline Pigging & Integrity Management Conf. and Exhibition
29 January – 1 February 2018
Marriott Marquis Hotel, Houston, TX, USA
Organized by Clarion Technical Conferences and Tiratsoo Technical. For details, see www.clarion.org.

Technology for Future and Ageing Pipelines
11-12 April 2018
Het Pand Conference Centre, Gent, Belgium
Organized by Clarion Technical Conferences and Tiratsoo Technical in association with Lab. Soete of the Universteit Gent. For details, contact jtiratsoo@gs-press.com.

POMME 2018: Pipeline Operations & Management – Middle East Conference
23-26 April 2018
Gulf Convention Centre, Manama, Bahrain
Organized by Clarion Technical Conferences and Tiratsoo Technical. For details, see www.clarion.org.

PIPELINE
TRANSPORT INSTITUTE

Pipeline Transport Institute is a research and development center of the Transneft, PJSC, for carrying out of research-and-development and design-and-experimental operations, as well as development of new technologies, equipment, materials, and regulatory documentation in the field of design, construction, operation, and repair of the pipelines for transportation of oil and petroleum products.

Areas of activities:

- carrying out of research-and-development, design-and-experimental, and technological operations, as well as development of technical solutions, ensuring safe and reliable operation of main and technological pipelines, buildings, and structures (facilities) of Transneft, PJSC, and Transneft system organizations (TSO);
- development of interstate, national, and industry standards, as well as other normative documents, in the field of construction and operation of main and technological pipelines, as well as pipeline transportation facilities;
- formation and maintenance of an information system for assessing the conformity of equipment and materials; carrying out of technical documentation examination and laboratory tests for compliance with the requirements of national, interstate, and foreign standards, as well as with the requirements of normative documents of Transneft, PJSC; development of standard programs, organization and/or participation in the activities for addition (extension of certification) of the products into the Core products register;
- provision of expert-consulting and engineering services in the field of design, construction, and operation of main, field, distribution, technological pipelines, and other facilities of the fuel and energy complex;
- scientific and technological support for construction of the facilities of Transneft, PJSC;
- assessment of the technical state of pipelines, development of the methods for increasing the transmission capacity of main pipelines;
- control, coordination, and provision of implementation of the activities on realization of the innovative development program of Transneft, PJSC, including search, development, approbation and introduction of innovative products and technologies;
- development of the documents in the field of industrial and fire safety, as well as the documents for prevention and elimination of emergencies in the field of environmental protection;
- assurance of the status of Pipeline Transport Institute, in the external market as a national research center, carrying out a wide range of operations in the field of hydrocarbons pipeline transportation.
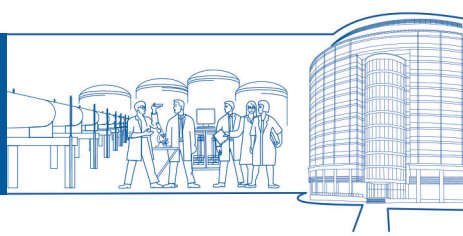
Pipeline Transport Institute
47a, Sevastopolskiy prospekt St.,Moscow, 117186
Tel.: (495) 950-8295, Records Management: (499) 799-8285, fax: (495) 950-8297
www.niitnn.transneft.ru, e-mail: niitnn@niitnn.transneft.ru